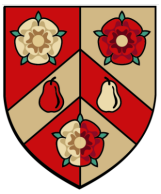


Sympathetic-neuron-derived neuropeptide Y (NPY) regulates adipose tissue immunometabolic homeostasis

Yitao Zhu



Wolfson College

University of Oxford

A thesis presented for the degree of

Doctor of Philosophy

Trinity 2024

Acknowledgements

Pursuing a DPhil degree has been described as a long and tough journey full of stress, uncertainties, and tiredness. During the past four years, I have indeed experienced moments of struggling to optimise experimental protocols, trying to figure out reasonable hypotheses and future directions, worrying about results and outcomes, and staying up late in front of microscopes. On the other hand, there have also been eureka moments when I saw the specific innervation of NPY^+ axons in arterioles (Figure 3.5), the perfect labelling showing $UCP1^+$ adipocytes can be lineage traced to $NPY1R^+$ cells (Figure 4.5), and the significant phenotypes of the NPY-cKO animals. All these discoveries finally established an unprecedented working model that explains the role of NPY^+ sympathetic nervous system in regulating the immunometabolic and energy homeostasis of adipose tissue.

So many people and things have supported me throughout this journey, without which I would not have been able to achieve the accomplishments and complete the long tough journey. Therefore, I would like to express my overwhelming gratitude to them.

I would like to thank my supervisor Professor Ana Domingos for inspiring me and providing resources that helped me make progress in my research while giving me enough freedom to make my own schedules and develop my own project. I would like to thank Professor Shingo Kajimura who shared his insights and expertise concerning thermogenic adipocytes, which are very important for my research. I am grateful to my transfer and confirmation of status examiners Robin Klemm, Neil Herring, and Oliver Neely, who assessed my project from different aspects, and their criticism and advice helped my research become more convincing and complete. Professor Neil Herring became my second supervisor after the transfer

of status, and his advice concerning the cardiovascular system helped me characterise the vessels innervated by NPY^+ sympathetic axons.

I would like to thank Dr Yao Lu who assisted me with the *in vitro* culturing experiments, and we worked so hard together to try to find out the impact of NPY on mural cell differentiation. Without her, we would not have been so successful in publishing this research.

I would like to thank Dr Noelia Martinez-Sanchez, Dr Samuel Malone, and Dr Gitalee Sarker for teaching me the experimental techniques necessary for my research. I really appreciate their devotion and patience.

I would like to thank (now Dr) Emma Habermann and Conan O'Brien, who are always willing to discuss our research and things happening around us. They gave me so much advice on both science and life as a DPhil student, and it was my great pleasure to work in the same lab with you for four years.

I would like to thank all the supporting staff at DPAG, Dunn School, Kennedy Institute, and the Biomedical Services for their support to keep everything on track and make sure the facilities are available for researchers. I would especially like to thank Robert Hedley at Dunn School and Cristofer at Kennedy Institute for their technical support.

I would like to thank all my friend in Oxford for always being around to listen to my worries and complaints and sharing their ideas to help me solve the problems I came across or provide emotional support. Having nice meals with you was always a pleasure for me.

I would like to thank Wolfson College and Oxford for such a lovely community where I can always find someone with the same interests and a nice natural environment where I can surprisingly come across a fox or a badger. It was a great

experience to walk with friends in the parks and meadows and punt along the beautiful River Cherwell.

Finally, I would like to thank my family: my parents Ling Tao and Jiahao Zhu, and my Grandma Jiaying Qiu for always protecting my curiosity towards the world when raising me and for their warmest and steadiest support that encouraged me to start my career as a scientist. They have always tried to provide the best resource for me in terms of my life and education.

Declaration

I, Yitao Zhu, declare that the work presented in this thesis is completely my own. Unless otherwise stated, I designed and performed all experiments with guidance from Professor Ana I. Domingos. Where necessary, I also received help from colleagues, collaborators and peers, as detailed here:

The ideas underlying this work were generated by myself after reading literature and talking with Professor Ana I. Domingos. Dr Gitalee Sarker also shared her scRNA-Seq dataset of the sympathetic ganglia with me and provided information useful for conceiving this project. I got help from Dr Yao Lu in cell-culturing experiments and qPCR; I collaborated with Professor Licio A. Velloso and got help in measuring energy expenditure; I collaborated with Professor Cheng Zhan and got help in knocking out NPY from mouse hindbrain. Professor Shingo Kajimura helped me measure the oxygen consumption of adipocytes *in vitro*.

I learned the skill of adipose tissue clearing from Dr Samuel Malone; I received advice on flow cytometry from Dr Emma Habermann; I learnt how to use the thermo-camera from Dr Sean Wilcox. Other techniques including isolating primary mural cells, differentiating mural cells or SVF into thermogenic adipocytes, cell proliferation assay, and cold-challenge experiment were self-taught based on lab protocols or previous publications.

A manuscript was derived from this research and published in Nature titled "Sympathetic neuropeptide Y protects from obesity by sustaining thermogenic fat" (Y. Zhu et al., 2024).

Signature *Date*

Abstract

Neuropeptide Y (NPY) is secreted by sympathetic nerves (LUNDBERG et al., 1982; Lundberg, Franco-Cereceda, Hemsen, Lacroix, & Pernow, 1990), but its direct impact on thermogenic adipocytes is unknown. Here we uncover the mechanism by which peripheral NPY protects from obesity. Our imaging of cleared murine brown and white adipose tissue (BAT and WAT) established that NPY^+ sympathetic axons are only a minority that mostly maps to the peri-vasculature; our analysis of single-cell RNA-sequencing datasets identifies mural cells as the main NPY-responsive cells in adipose tissues. We show that NPY sustains mural cells, known as a source of beige cells in both BAT and WAT (Long et al., 2014; Shamsi et al., 2021) and that NPY facilitates the differentiation to thermogenic adipocytes. We found that diet-induced obesity leads to neuropathy of NPY^+ axons and concomitant depletion of the mural cell pool of beige fat progenitors. This defect is replicated in conditional knockout (cKO) mice with NPY specifically abrogated from sympathetic neurons. These cKO mice have whitened BAT with reduced thermogenic ability and lower energy expenditure even before the onset of obesity; they develop adult-onset obesity on a regular chow diet and are more susceptible to diet-induced obesity without increasing food consumption. Our results indicate that relative to central NPY, peripheral NPY produced by the sympathetic nerves has the opposite effect on body weight homeostasis by sustaining the proliferation of the mural cell progenitors of thermogenic adipocytes.

Keywords— Sympathetic nervous system - Obesity - Neuropeptide Y - Mural Cells

Table of Contents

1 Introduction **1**

1.1 Adipose tissue 1

1.1.1 The component of adipose tissue 1

1.1.2 Adipocytes 4

1.1.2.1 The progenitors of adipocytes 4

1.1.2.2 Adipogenesis and lipolysis 4

1.1.2.3 Beige adipocytes and thermogenesis 7

1.1.3 Immune cells and adipose metabolism 8

1.1.3.1 Myeloid cells 9

1.1.3.2 Lymphocytes 11

1.1.3.3 Cytokines and thermogenesis 12

1.1.4 Non-immune stromal-vascular fraction 12

1.1.4.1 Fibroblasts 12

1.1.4.2 Mural cells 13

1.1.4.3 Vasculature and adipose tissue metabolism . . . 16

1.2 Sympathetic nervous system and its function in adipose metabolism 17

1.2.1 The structure of sympathetic nervous system 17

1.2.2 Sympathetic regulation of adipose tissue 18

1.3 Neuropeptide Y 20

1.3.1 Central Neuropeptide Y and feeding behaviour 20

1.3.2 Peripheral NPY in adipose tissue 21

1.3.3 NPY receptors and their downstream pathways 22

1.4 Aim and Hypotheses 24

2 Methodology **25**

2.1 Animals . . . 25
2.1.1 Animal models for studying obesity . . . 25
2.1.2 Reporting and lineage-tracing animal models . . . 26
2.1.3 Sypathetic neuron-specific NPY-knockout model . . . 26
2.2 Animal dissection . . . 26
2.2.1 Dissection of sympathetic ganglia . . . 27
2.2.2 Dissection of brown and white adipose tissues . . . 28
2.2.3 Dissection of sympathetic axons . . . 28
2.3 Immunofluorescent Imaging (IF) . . . 29
2.3.1 Tissue Fixation . . . 29
2.3.2 Whole-mount IF . . . 29
2.3.3 Cryosection and IF . . . 30
2.3.4 Paraffin embedding and IF . . . 30
2.3.5 Adipo-Clear . . . 31
2.3.6 Antibodies for IF staining . . . 32
2.4 Microscopy . . . 32
2.4.1 Confocal microscopy . . . 32
2.4.2 Light-sheet microscopy . . . 33
2.4.3 Dextran-70kDA injection and intravital microscopy . . . 33
2.4.4 Image analysis . . . 34
2.5 Primary cell culture . . . 35
2.5.1 Isolation of the adipose stromal-vascular faction (SVF) . . . 35
2.5.2 Purification of mural cells from the adipose SVF . . . 36
2.5.3 *In vitro* differentiation of adipocytes . . . 36
2.5.3.1 White adipocytes . . . 36
2.5.3.2 Beige-like adipocytes . . . 37
2.5.4 Proliferation assay with EdU . . . 37

2.5.5 Oxygen consumption assay . . . 38
2.6 Quantitative real-time qPCR . . . 38
2.6.1 Isolation of mRNA . . . 38
2.6.2 First-strand synthesis of cDNA . . . 40
2.6.3 qPCR and the list of primers . . . 41
2.6.4 Data analysis . . . 41
2.7 Flow cytometry and cell sorting . . . 41
2.7.1 Single-cell suspension . . . 41
2.7.2 Staining . . . 41
2.7.3 Antibodies for flow cytometry or cell sorting . . . 43
2.8 Enzyme-linked immunosorbent assay (ELISA) . . . 43
2.8.1 Sample preparation . . . 43
2.8.1.1 Blood plasma . . . 43
2.8.1.2 Protein extraction from adipose tissue . . . 44
2.8.2 Methodology . . . 44
2.9 Metabolic phenotyping . . . 44
2.9.1 Thermo-imaging . . . 44
2.9.2 Cold challenge and rectal temperature measurement . . . 45
2.9.3 Metabolic cage . . . 45
2.9.3.1 Local-motor activity . . . 45
2.9.3.2 Indirect calorimetry . . . 46
2.10 Single-cell RNA-sequencing (scRNA-Seq) analysis . . . 46
2.11 Statistics . . . 47

3 Anatomical Analysis of NPY$^+$ Sympathetic Neurons and Their Targets in Adipose Tissue 48

3.1 Introduction . . . 48
3.1.1 NPY$^+$ neurons in the sympathetic nervous system (SNS) . . . 48

3.1.2 NPY$^+$ axons in tissues . . . 50
3.1.3 NPY-receptors in tissues . . . 50
3.2 Methodology . . . 51
3.3 Results . . . 51
3.3.1 One-third sympathetic axons in adipose tissue are NPY$^+$ . . . 51
3.3.2 Non-neuron cells in adipose tissue do not express NPY . . . 53
3.3.3 NPY$^+$ axons preferentially innervate 4-6th orders of arterial branches . . . 55
3.3.4 Mural cells in adipose tissue highly express NPY1R . . . 56
3.3.5 NPY-receptors are not detectable in adipocytes or immune cells . . . 60
3.4 Discussion . . . 60

4 Functional Analysis of NPY-Mural Cell Interaction 63
4.1 Introduction . . . 63
4.1.1 The downstream pathway of NPY1R . . . 63
4.1.2 Functions of mural cells . . . 63
4.1.3 Regulation of mural cells . . . 64
4.2 Methodology . . . 64
4.2.1 *In vitro* experiments . . . 64
4.2.2 NPY1R lineage-tracing mouse model . . . 65
4.3 Results . . . 66
4.3.1 NPY promotes mural cell proliferation . . . 66
4.3.2 NPY1R$^+$ mural cells are the progenitors of thermogenic adipocytes . . . 66
4.3.3 NPY facilitates the differentiation to thermogenic adipocytes 69
4.3.4 NPY sustains the role of mural cells as progenitors of thermogenic adipocytes . . . 74

4.4 Discussion 78

5 Diet-induced Obesity and NPY^{+} axon-mural cell interaction 80

5.1 Introduction 80

5.1.1 Diet-induced Obesity (DIO) and sympathetic innervation . 80

5.1.2 Mural cell and vascular integrity 80

5.2 Methodology 82

5.3 Result 82

5.3.1 DIO depletes NPY^{+} innervation and decreases NPY concentration in adipose tissue 82

5.3.2 DIO results in loss of mural cell coverage and increased vascular leakiness in adipose tissue 83

5.3.3 DIO does not affect Npy levels, mural cell coverage or vascular leakiness in sympathetic ganglia 83

5.3.4 Discussion 87

6 Sympathetic-Neuron-Derived NPY and Immunometabolic Homeostasis 91

6.1 Introduction 91

6.1.1 TH and NPY collocalisation 91

6.1.2 Thermogenesis and adipose tissue inflammation 91

6.2 Result 92

6.2.1 Th^{Cre};$Npy^{flox/flox}$ mouse model removes NPY from SNS efficiently and specifically 92

6.2.2 Loss of SNS-derived NPY depletes mural cells and increases immune infiltration in adipose tissues 94

6.2.3 Loss of SNS-derived NPY whitens BAT, reduces its thermogenic ability, and lowers energy expenditure (EE) . . . 98

6.2.4 Loss of SNS-derived NPY leads to adult-onset obesity and makes mice more susceptible to obesity without changing food consumption 99
6.2.5 Loss of NPY from the hindbrain does not affect thermogenesis or body weight. 102
6.3 Discussion 106

7 Conclusion and Discussion **109**
7.1 Main findings of my research 109
7.2 Source of NPY in adipose tissues 110
7.3 Analysis of peripheral NPY in adipose tissue 110
7.4 Mural cell as a source of thermogenic adipocytes 112
7.5 NPY and other physiological processes 113
7.6 The protective functions of thermogenic adipocytes 113
7.7 Conclusion and future directions 114

Bibliography **116**

List of Figures

1.1 **Anatomical localisation of main scWATs and BATs in mice, human infants, and adults.** scWATs are localised at various regions such as the anterior scWAT and the inguinal WAT (iWAT). BATs in mice and infants are mainly localised at the interscapular and perirenal parts, while in adults, they are localised at the cervical-supraclavicular and paravertebral parts. 2

1.2 **The cellular components of adipose tissue.** Two types of adipocytes can be found in white adipose tissue: the white and beige adipocytes. Sympathetic axons are detected in detected adipose tissue. Immune cells including T cells, T_{reg}, NK cells, ILCs, neutrophils, B cells, and macrophages abundantly exist in adipose tissue. A special type of macrophages is associated with sympathetic axons and can degrade NE. Fibroblast and mural cells can be found around blood vessels. 3

1.3 **The progenitors of white, brown and beige adipocytes.** Brown adipocytes are derived from $Myf5^{+}$ progenitors, white adipocytes are derived from $Myf5^{-}$ progenitors, and beige adipocytes are derived from $Myh11^{+}$ progenitors. 5

1.4 **Sympathetic innervation and regulation of adipose tissue.** iBATs are innervated by the stellate ganglion (SG), thoracic ganglia T2-T5. iWATs are innervated by thoracic ganglia T12-T13, and lumbar ganglion L1. The brain-adipose axis regulates the homeostasis of adipose tissue: white adipose tissue releases Leptin; Leptin activates SNS and makes SNS release NE to trigger lipolysis and thermogenesis. 19

2.1 **The principle of oxygen consumption assay** 39

3.1 **40% neurons in sympathetic neurons express *Npy*.** (a) Schematic showing the tissues innervated by each sympathetic ganglia. (b) A scRNA-Seq dataset of sympathetic ganglia chain published by Linnarsson Lab to show the clustering of neurons. (c) Violin plot showing the expression of Npy.(d-e) Confocal image of cryo-sectioned (d) superior-cervical ganglion (SCG) and (e) stellate ganglia (SG) of ND-treated WT male 8-week-old mice stained with anti-TH (red) and anti-NPY (cyan). Scale bar=100μm. (f) The percentage of NPY$^+$ sympathetic neurons quantified based on images as in Extended Data Fig. 5d-e (n=5 sections from 3 mice). 49

3.2 **A third of sympathetic axons in iWAT and iBAT are NPY$^+$ and preferentially innervate the vasculature.** (a) Confocal image of an axonal bundle from the iWAT, stained with anti-TH (red) and anti-NPY (cyan). Scale bar=50μm.(b) Confocal image of a capillary within a cleared iWAT stained with anti-CD31 (red) and anti-NPY (cyan). Scale bar=100μm.(c) Confocal images of cleared iWAT stained with anti-TH (green), anti-NPY (white), and anti-CD31 (red). Scale bar=50μm. (d) Confocal images of cleared iWAT as in (c) stained with anti-TH (green), anti-NPY (white), and anti-CD31 (red). Scale bar=100μm. (e-f) The quantification of images as in (d) for TH/NPY overlap: TH$^+$NPY$^-$ (dark green), TH$^+$NPY$^+$ (light green), and TH$^-$NPY$^+$ (white). The percentage is shown via (e) histogram and (f) Venn diagram (n=5 views from 3 mice). (g) The quantification of images as in (d) shows the proportion of TH$^+$ and NPY$^+$ axons overlapping with CD31$^+$ endothelial cells. (h) Confocal Images of cleared iBAT from lean adult male mice stained with anti-TH (green), anti-NPY (white), and anti-CD31 (red). White arrows in the images indicate TH$^+$NPY$^-$ axons. Scale bar=100μm. 52

3.3 **Npy is not expressed in adipose tissues, and NPY receptors are not expressed in macrophages.** (a-b) Embedding plots showing different clusters of cells in the SVF of murine (a) iWAT1 and (b) iBAT2. (c-d) Violin plot showing the expression of Npy in the SVF of murine (c) iWAT and (d) iBAT. (e) Gating strategy of sorting adipose-associated macrophages (ATM) from Cx3cr1$^{GFP/+}$ reporter mice. ATMs were sorted as live/CD45.2^{+}/GFP^{+} cells. (f) The expression of *Adgre1* (F4/80), *Npy*, and *Npy1r* in adipose associated macrophages (ATM) (n=2). (g) Gating strategy for sorting mural cells from the SVF of the iWAT. Mural cells (green box) are sorted as live/CD31^{-}/CD45^{-}/PDGFRα^{-}/NG2^{+} cells; immune cells (blue box) are sorted as live, CD31^{-}/CD45^{+} cells. All values are expressed as mean ± SEM 54

3.4 **NPY does not exist in SAMs.** Immunofluorescent staining of NPY (Red) in lean and obese male Cx3cr1$^{GFP/+}$ reporter mice to show NPY (red) and macrophages (green) do not colocalise with each other. Scale bar=100 μm 55

3.5 **NPY$^+$ axons preferentially innervate the 5th order arteriole branches.** (a) Confocal images of cleared adipose tissue stained with anti-NPY (cyan) and anti-CD31 (red). The number indicates the branch orders. Scale bar=150μm. (b) Zoom-in of (a), scale bar=50μm. (c-d) (c) The diameters of vessels and (d) the density of NPY$^+$ axons at each branch level quantified based on images as in (a) (n=6 views from 2 mice); NPY$^+$ axon density on Branch #1 vs. #5, P<0.0001. (e) Light-sheet images of cleared adipose tissue stained with anti-NPY (red) and anti-EPHB4 (cyan). Scale bar=500μm. (f) Confocal images of cleared adipose tissue stained with anti-NPY (red) and anti-SOX17 (cyan). Scale bar=100μm. All values are expressed as mean $\pm$ SEM. Statistical comparisons were made using 2-tailed Student T-tests, ****p<0.0001. 57

3.6 **Npy1r is mainly expressed in mural cells which are a source of thermogenic adipocytes.** (a&c) Dot plot showing the expression of *Npy1r*, *Des*, *Myh11*, *Acta2* (αSMA), *Tagln*, *Cspg4* (NG2), *Pdgfrb*, *Pdgfra*, and *Pecam1* (CD31) in the SVF of (a) iWAT or (c) iBAT. (b&d) Embedding plots showing the expression of Npy1r, Des, Myh11, and Acta2 (αSMA) in the SVF of (b) iWAT and (d) iBAT. Mural cell clusters are highlighted with red rectangles or red dashed lines. (e) The expression of Npy1r (P=0.0002) and Des (P=0.0024) mural cells and immune cells (n=5&3). (f) Confocal image of the capillary dissected from the iWAT of WT mice stained with anti-NPY1R (cyan) and anti-CD31 (red), scale bar=10μm. (g) Confocal images of vessels dissected from Npy1r^{Cre}; Rosa26^{tdTomato} mice stained with anti-DES (green), scale bar=20μm. All values are expressed as mean $\pm$ SEM. Statistical comparisons were made using 2-tailed Student T-tests, **p<0.01, ***p<0.001. . 58

3.7 **NPY1R-tdTomato is colocalised with NG2 and αSMA in mural cells.** (a) Embedding plot showing the co-expression of mural markers *Acta2* (αSMA), *Myh11*, and *Tagln* (red) with *Npy1r* (green). Co-expression is in yellow. (b) Confocal images of vessels dissected from adipose tissue of Npy1r^{Cre}; Rosa26^{tdTomato} mice stained with anti-αSMA (green), scale bar=100μm. (c) Zoomed-in images of vessels as in Extended Data Fig. 2b, scale bar=20μm. 59

3.8 **The expression levels of *Npy2r* and *Npy5r* in adipose tissues are negligible.** (a) Dot plot showing the expression of *Npy1r*, *Npy2r*, *Adra1a*, *Adra1b*, *Adra1b*, *Adrb1*, *Adrb2*, and *Adrb3* in different cells in the SVF of mice iWAT. (b) Dot plot showing the expression of *Npy1r*, *Adrb1*, *Adrb2*, *Adrb3*, *Adra1a*, *Adra1b*, *Adra2a*, and *Adra2b* in different types of cells in mouse iBAT. The size of the dot represents the percentage of cells expressing a certain gene, and the darkness of the dot represents the expression level. Mural cell clusters are highlighted with red rectangles. 61

3.9 **NPY$^+$ axons innervate mural cells.** Images of the cleared adipose tissue of NPY-GFP reporter mice stained with anti-GFP (green), anti-DES (cyan), and anti-CD31(red). Scale bar=50μm. 62

4.1 **EdU Cell Proliferation Assay Principle.** Cells grown in the presence of 5-EdU incorporate the compound during DNA synthesis. Fluorophore-labeled azide reacts with the incorporated EdU to allow detection by microscopy. 65

4.2 **NPY promotes the proliferation of both iWAT and iBAT mural cells via ERK.** (a) Schematic of isolating mural cells from iWAT. (b) Confocal image showing iWAT mural cells treated with or without 1Î¼M NPY stained with DES (cyan) and DAPI. EdU (red) indicates proliferating cells. Scale bar=80μm. (c) The percentage of EdU$^+$ mural cells quantified based on images as in (b) (n=10). (d) Schematic of isolating mural cells from iBAT. (e) Confocal image showing iBAT mural cells treated with or without 1μM NPY stained with DES (cyan) and DAPI. EdU (red) indicates proliferating cells. Scale bar=80μm. (f) The percentage of EdU$^+$ mural cells quantified based on images as in (d) (n=3). (g) Confocal images of isolated mural cells treated with or without 1μM NPY and 2μM PD98059, an ERK inhibitor, stained with anti-DES (cyan) and DAPI (blue). EdU (red) was used to indicate proliferation. Scale bar=80μm. (h) The percentage of EdU$^+$ cells quantified based on images as in (g) (n=6). All values are expressed as mean $\pm$ SEM. Statistical comparisons were made using 2-tailed Student T-tests, *p<0.05, ***p<0.001. 67

4.3 **Previously identified progenitors of thermogenic adipocytes (Lin$^-$/CD81$^+$) in iWAT express *Npy1r* and mural cell markers.** (a) Schematic of isolating previously identified progenitors of thermogenic adipocytes (Lin$^-$/CD81$^+$) in iWAT. (b-c) The expression level of (b) *Npy1r*, and (c) mural cell markers *Des* and *Acta2* in CD81$^-$ vs. CD81$^+$ progenitors (n=4). (d) Dot plot showing the expression of *Npy1r, Des, Myh11, Acta2, Tagln, Pdgfrb, Cspg4, Pdgfra, Pecam1*, and *Cd81* in different cells in the SVF of mice iWAT. The size of the dot represents the percentage of cells expressing a certain gene, and the darkness of the dot represents the expression level. NPY1R$^+$ mural cell clusters are highlighted with red rectangles. All values are expressed as mean ± SEM. Statistical comparisons were made using 2-tailed Student T-tests, *p<0.05, **p<0.01, ***p<0.001. 68

4.4 **Mural cells isolated from both iWAT and iBAT can differentiate into thermogenic adipocytes.**(a) Schematic of isolating mural cells from adipose tissue. (b) The expression level of mural cell markers *Des, Pdgfrb*, and *Acta2* in isolated mural cells. The red dashed line indicates the expression level of the reference gene Hprt (n=4). (c&e) Schematic of isolating and differentiating mural cells from (c) iWAT and (e) iBAT. (d&f) The expression of thermogenic and adipogenic genes in adipocytes differentiated from the stromal-vascular fraction (SVF) and mural cells isolated from (d) iWAT (n=5&6) and (f) iBAT (n=5&5). All values are expressed as mean ± SEM. Statistical comparisons were made using 2-tailed Student T-tests, *p<0.05, **p<0.01, ***p<0.001. . . 70

4.5 **A subgroup of thermogenic adipocytes in iBAT can be lineage-traced to NPY1R^{+} mural cells.** (a) The gene construct of the lineage-tracing mouse model for NPY1R. (b) Confocal images of vessels dissected from the iBAT of ND-treated, RT-housed 12-week-old Npy1r^{Cre}; Rosa26^{tdTomato} mice stained with anti-UCP1 (cyan), scale bar=100μm. (i) Zoomed-in images of (b), scale bar=50μm. 71

4.6 **Only UCP1^{+} multi-locular adipocytes are lineage-traced to NPY1R** (a) Confocal images of paraffin-embedded slides of iBAT and iWAT of 12-week-old male Npy1r^{Cre}; Rosa26^{tdTomato} mice stained with UCP1 (Cyan), scale bar=50μm. (b) is zoomed-in (a), scale bar=10μm. 72

4.7 **NPY increases the proportion of αSMA^{+} mural cells in SVF and CD81^{+} progenitors.** (a) Schematic of isolating iWAT SVF and CD81^{+} cells for NPY treatment experiments and flow cytometry analysis. (b) Gating strategy for measuring the percentage of αSMA^{+} mural cells in cultured SVF and CD81^{+} cells by flow cytometry. (c-d) The percentage of αSMA^{+} mural cells in (c) SVF (n=6) and (d) CD81^{+} cells (n=8) after incubating with or without 1μM NPY. (e) Schematic showing NPY treatment increases the percentage of mural cells in cultured SVF or CD81^{+} cells, and mural cells are the progenitor of thermogenic adipocytes. All values are expressed as mean $\pm$ SEM. Statistical comparisons were made using 2-tailed Student T-tests, *p<0.05. 73

4.8 **NPY facilitates the neogenesis of thermogenic adipocytes from iWAT SVF and mural progenitors isolated from both iWAT and iBAT.** (a) Schematic of differentiating primary stromal vascular fraction (SVF) of iWATs to thermogenic adipocytes. (b) The expression *Ucp1*, *Cidea, Pgc1a, Serca2b, Pparg*, and *Plin1* (n=4&3&3 for *Plin1* and n=3&5&5 for other genes). (c) Schematic of differentiating beige adipocyte progenitors ($Lin^-/CD81^+$) isolated from iWAT. (d) The expression of thermogenic and adipogenic genes in adipocytes differentiated from iWAT beige adipocyte progenitors ($Lin^-/CD81^+$) with or without 1μM NPY (n=4). (e) Oxygen consumption in adipocytes differentiated from beige adipocyte progenitors ($Lin^-/CD81^+$) with or without 1μM NPY (n=5). (f) The expression of thermogenic and adipogenic genes in adipocytes differentiated from iBAT mural cells or SVF (n=4&5&5). All values are expressed as mean $\pm$ SEM. Statistical comparisons were made using 2-tailed Student T-tests or 2-way ANOVA, $^*p<0.05$, $^{**}p<0.01$, $^{***}p<0.001$, $^{****}p<0.0001$. 75

4.9 **NPY does not affect the proliferation or adipogenesis of 3T3-L1.** (a) The expression of *Npy1r*, *Npy2r*, and *Npy5r* in 3T3-L1 preadipocyte cell line (n=3). (b) The impact of NPY on the proliferation of 3T3-L1 preadipocytes revealed by the cell number after incubating with or without 1μM NPY for 24, 48, and 72 hours (n=3). (c-d) The expression of adipogenesis markers *Pparg* and *Plin1* in differentiated 3T3-L1 preadipocytes induced by induction medium (c) with or (d) without 1μg/mL insulin (n=9, 8, 8, 9&7 for *Pparg*, n=9, 9, 9, 9& 7 for *Plin1*). The concentration of NPY is indicated in the plot. All values are expressed as mean $\pm$ SEM, *p<0.05, **p<0.01, ***p<0.001, ****p<0.0001, Student T-tests. 76

4.10 **NPY sustains mural cell identity against PDGF-BB.** (a) Confocal images of primary mural cells stained with anti-DES (cyan) and anti-PDGFRα (red), cultured under different conditions. Scale bar=100μm. (b) The percentage of PDGFRα^{+} cells under different stimulating conditions (n=6). Concentrations of NPY and PDGF-BB were 1μM and 250ng/mL respectively. (c-e) The expression of (c) *Npy1r* (n=8), (d) mural cell markers *Pdgfrb* (n=8) and Rgs5 (n=5&8&8), and (e) secretory factors in maintaining vascular integrity including *Tgfb1* (n=8) and *Angpt1* (n=4&8&8) in primary mural cells cultured with or without 1μM NPY or 250ng/mL PDGF-BB. All values are expressed as mean $\pm$ SEM. Statistical comparisons were made using 2-tailed Student T-tests, *p<0.05, **p<0.01, ***p<0.001, ****p<0.0001. 77

4.11 **NPY sustains the thermogenic ability of mural cells against PDGF-BB.** (a) Schematic of differentiating isolated mural cells to adipocytes with or without 1μM NPY or 250ng/mL PDGF-BB. (b-c) Expression levels of (b) thermogenic and (c) adipogenic genes expressed by adipocytes differentiated from mural cells under different conditions. All values are expressed as mean $\pm$ SEM. Statistical comparisons were made using 2-tailed Student T-tests, *p<0.05, **p<0.01, ***p<0.001, ****p<0.0001. 78

5.1 **Mural cells are heterogeneous and have different functions.** . . 81

5.2 **High-fat diet-induced obesity (DIO) depletes NPY$^+$ innervation.** (a) Light-sheet images of cleared iWAT of normal diet (ND)-treated and high-fat diet (HFD)-treated 17-week-old male WT mice stained with anti-NPY (cyan) and anti-CD31 (red). Scale bar=500μm. (b) NPY$^+$ innervation calculated as the ratio of NPY to CD31 quantified based on images as in (a) (n=3 mice, P=0.0112). (c-d) The concentration of NPY in (c) iWAT (n=5&4&4 mice) and (d) blood plasma of ND and HFD-treated 17-week-old male WT mice, and ND-treated Ob/Ob 17-week-old male mice (n=6&7&2 mice). P=0.0002 for both comparisons. All values are expressed as mean $\pm$ SEM. Statistical comparisons were made using 2-tailed Student T-tests, *p<0.05, **p<0.01, ***p<0.001, ****p<0.0001. . . 84

5.3 **DIO depletes mural cells in iWAT.** (a) Light-sheet images of cleared iWAT of ND- and HFD-treated 17-week-old male WT stained with anti-DES (cyan) and anti-CD31 (red). Scale bar=500μm. (b) Mural cell coverage was calculated as the ratio of DES$^+$ cells to CD31$^+$ cells quantified based on images as in (a) (n=3 mice, P=0.0021). 85

5.4 **DIO increases vascular leakiness in iWAT.**(a) Light-sheet images of iWATs of ND- and HFD-treated 17-week-old male mice stained with anti-DES (cyan) and anti-PV1 (red). Scale bar=500μm. (b) PV-1 density was quantified based on images as in (a) (n=3&4 mice, P=0.0053). All values are expressed as mean ± SEM. Statistical comparisons were made using 2-tailed Student T-tests, *p<0.05, **p<0.01, ***p<0.001, ****p<0.0001. 86

5.5 **DIO does not affect ganglionic NPY or SCG mural cell coverage.** (a-b) The expression of Npy and Th in the (a) superior cervical ganglia (SCG, n=6&5) and (b) stellate ganglia (SG, n=4&3) of ND- and HFD-treated 17-week-old WT male mice. (c) The images of cleared SCG and of ND- and HFD-treated 17-week-old WT male mice stained with anti-DES (cyan) and anti-CD31 (red) antibodies. Scale bar=100μm. All values are expressed as mean ± SEM. Statistical comparisons were made using 2-tailed Student T-tests, *p<0.05, **p<0.01, ***p<0.001, ****p<0.0001. 88

5.6 DIO does not affect mural cell coverage in SG. (a) The images of cleared SG of ND- and HFD-treated 17-week-old WT male mice stained with anti-DES (cyan) and anti-CD31 (red) antibodies. Scale bar=100μm. (e) The quantification of mural cell coverage in SG (n=4). All values are expressed as mean ± SEM. Statistical comparisons were made using 2-tailed Student T-tests, *p<0.05, **p<0.01, ***p<0.001, ****p<0.0001. 89

5.7 **Sympthetic-neuron-derived NPY maintains thermogenesis and vascular integrity by sustaining mural cells.** 90

6.1 **Ablating NPY from sympathetic neurons using Th^{Cre};$Npy^{flox/flox}$ mice does not affect NPY levels in VTA, hypothalamus or plasma.** (a&c) Confocal image showing a slice of (a) ventral tegmental area (VTA, Scale bar=500μm) and (c) arcuate nucleus (Arc, Scale bar=200μm) of the hypothalamus of an NPY-GFP mouse stained with anti-TH (red), anti-GFP (green), and DAPI (blue). (b&d) Quantification of TH/NPY-GFP overlap in (b) VTA and (d) hypothalamus (n=3 mice). (e) The expression of *Npy, Th*, and *Cre* in the hypothalamus of 12-week-old Th^{Cre};$Npy^{flox/flox}$ and $Npy^{flox/flox}$ male mice (n=3). (f) NPY concentration in the blood plasma of 12-week-old Th^{Cre};$Npy^{flox/flox}$ and $Npy^{flox/flox}$ male mice (n=6&5). All values are expressed as mean ± SEM. 93

6.2 **Th^{Cre};$Npy^{flox/flox}$ mice have depleted NPY from the sympathetic nervous system and unchanged sympathetic innervation.** (a-b) The expression of *Npy* and *Th* in (a) SCG (n=3&4 mice) and (b) SG (n=5 mice) of 12-week-old Th^{Cre};$Npy^{flox/flox}$ and $Npy^{flox/flox}$ male mice.(c-d) Light-sheet image of cleared iBAT of 12-week-old Th^{Cre};$Npy^{flox/flox}$ and $Npy^{flox/flox}$ male mice stained with (c) anti-NPY (cyan), scale bar=500μm, or (d) anti-TH (green), scale bar=200μm. (e-f) The image of cleared iWAT of 12-week-old Th^{Cre};$Npy^{flox/flox}$ and $Npy^{flox/flox}$ male mice stained with (e) anti-NPY (cyan) or (f) anti-TH (green) and anti-CD31 (red). Scale bar=500μm. All values are expressed as mean ± SEM. Statistical comparisons were made using 2-tailed Student T-tests, *p<0.05, ***p<0.001. 95

6.3 **Loss of NPY from sympathetic neurons depletes mural cells and increases vascular leakiness in both iBAT and iWAT.** (a-b) Light-sheet image of cleared (a) iBAT of 15-week-old ND-treated mice (scale bar=200μm) and (b) iWAT of 30-week-old ND-treated mice (scale bar=500μm) stained with anti-PV1 (red) and anti-TAGLN (cyan). (c-d) The expression levels of (c) mural cell markers *Des* (n=8 mice), *Rgs5* (n=7 mice), and (d) pro-inflammatory genes *Tnf* (n=7 mice), and *Il6* (n=7 mice) in the iBATs of ND-treated 12-week-old male Th^{Cre};$Npy^{flox/flox}$ and $Npy^{flox/flox}$ mice. All values are expressed as mean $\pm$ SEM. Statistical comparisons were made using 2-tailed Student T-tests, $^{*}p<0.05$, $^{***}p<0.001$. 96

6.4 **Loss of sympathetic NPY causes mural cell loss and immune infiltration.** (a-b) The percentage of (a) PDGFRα^{-} /$NG2^{+}$ mural cells (n=4&2 mice) and (d) $CD45^{+}$ immune cells (n=2&3 mice) in iBATs and iWATs of 30-week-old, ND-treated mice measured by flow cytometry. (c) The gating strategy of flow cytometry to quantify the percentage of $CD45^{+}$ immune cells DES^{+} mural cells. (d) The representative flow cytometry analysis of the percentage of mural cells (DES^{+}) in the iBAT (top) and iWAT (bottom) of HFD-treated male Th^{Cre};$Npy^{flox/flox}$ and $Npy^{flox/flox}$ mice. (e) The percentage of DES+ mural cells in iBATs and iWATs of 17-week-old, HFD-treated mice was measured by flow cytometry (n=4 mice). All values are expressed as mean $\pm$ SEM. Statistical comparisons were made using 2-tailed Student T-tests, $^{**}p<0.01$. 97

6.5 **The loss of sympathetic NPY increases vascular leakiness revealed by Dextran injection.** (a) Intravital microscopy of epididymal WATs of 23-week-old male Th^{Cre};$Npy^{flox/flox}$ and $Npy^{flox/flox}$ mice 12 minutes after i.v. injection of 70kDa Dextran at the orbital plexus. (b) Dextran intensity in vessels over time was measured with a 2-photon microscope. The arrow indicates the time when Dextran was injected. (c) The fluorescence intensity ratio between tissue parenchyma and the vessel was calculated based on images as (a) (n=5&4 mice). (d) Dextran intensity in the vessels of eWAT right after i.v. injection (n=5&4 mice). (e) Blood flow was calculated using the average of the raw intensity of Dextran inside the artery over 100 seconds right after the stabilization of the Dextran signal following administration (n=5&4 mice). All values are expressed as mean ± SEM. Statistical comparisons were made using 2-tailed Student T-tests, $^{*}p<0.05$. 98

6.6 **Loss of sympathetic NPY whitens iBATs and decreases thermogenesis and EE.** (a) iBATs dissected from ND-treated male $Npy^{flox/flox}$ and Th^{Cre};$Npy^{flox/flox}$ mice. Dashed lines encircle the lobes of iBATs. (b) Expression of *Ucp1*, *Cidea* (P=0.0024), *Pgc1a* (P=0.0018), *Prdm16* (P=0.0048), and *Pparg* (P=0.0012) in the iBATs of ND-treated 12-week-old male Th^{Cre};$Npy^{flox/flox}$ and $Npy^{flox/flox}$ mice (n=6 mice for *Ucp1*; n=7 mice for other genes). (c) Daily energy expenditure of 7-week-old male Th^{Cre};$Npy^{flox/flox}$ and $Npy^{flox/flox}$ mice was measured using an indirect calorimetry system (n=9 mice). (d) The quantification of daily energy expenditure (EE) (n=9 mice). (e) The percentage of lean body weight (LBM) of 8-week-old male mice was measured by MiniSpec MRI (n=9). (f) The locomotor activity was measured using a Multitake cage (n=6 mice). (g) Schematic of food deprivation and thermo-imaging. (h-i) Changes in (h) iBAT temperature and (e) body weights of 12-week-old mice after a 14-hour fast (n=6 for Th^{Cre};$Npy^{flox/flox}$ mice and n=3 for Th^{Cre} and $Npy^{flox/flox}$ mice). All values are expressed as mean $\pm$ SEM. Statistical comparisons were made using 2-tailed Student T-tests, $^{*}p<0.05$, $^{**}p<0.01$, $^{***}p<0.001$. 100

6.7 **Loss of sympathetic NPY causes decreased cold tolerance.** (a) Schematic of cold-challenging mice and recording rectal temperature. (b) Rectal temperature of 20-week-old $Npy^{flox/flox}$ and Th^{Cre};$Npy^{flox/flox}$ mice under cold exposure recorded using a rectal probe every hour (n=3&4 mice). (c-d) The expression of thermogenic and adipogenic genes in (c) iBATs (n=3&4 mice) and (d) iWATs (n=3 mice) of cold-challenged $Npy^{flox/flox}$ and Th^{Cre};$Npy^{flox/flox}$ mice. All values are expressed as mean ± SEM. Statistical comparisons were made using 2-tailed Student T-tests, $^{*}p<0.05$, $^{**}p<0.01$. . . . 101

6.8 **Loss of Sympathetic NPY increases RER, causes adult-onset obesity, and makes mice susceptible to DIO.** (a) Respiratory exchange ratio (RER) of 8-week-old mice recorded using a metabolic cage. (b) The quantification of (a) (n=9 mice). (c-f) (c) Body weight, weights of (d) iBATs, (e) iWATs, and (f) vWATs of ND-treated male Th^{Cre};$Npy^{flox/flox}$ and $Npy^{flox/flox}$ mice (n=4). (g-h) (g) Weekly body weights (n=8) and (h) averaged daily food consumption (n=4&6 cages) of male HFD-treated Th^{Cre};$Npy^{flox/flox}$ and $Npy^{flox/flox}$ mice. (i) Weights of iBATs (n=5&6 mice), (m) iWATs (n=6&7 mice), and vWATs (n=6&7 mice) of HFD-treated 17-week-old male Th^{Cre};$Npy^{flox/flox}$ and $Npy^{flox/flox}$ mice. All values are expressed as mean ± SEM. Statistical comparisons were made using 2-tailed Student T-tests, $^{*}p<0.05$, $^{**}p<0.01$. 103

6.9 **Loss of sympathetic NPY results in bigger adipocyte size.** (a-b) Histological staining of iBATs of (a) ND- (top) and (b) HFD- (bottom) treated 17-week-old male Th^{Cre};$Npy^{flox/flox}$ and $Npy^{flox/flox}$ mice. Scale bar=50μm. (b) The average adipocyte size in the iBATs of ND- and HFD-treated male Th^{Cre};$Npy^{flox/flox}$ and $Npy^{flox/flox}$ mice (n=2 for ND-treated mice, n=4 for HFD-treated mice). All values are expressed as mean ± SEM. Statistical comparisons were made using 2-tailed Student T-tests, $^{*}p<0.05$. 104

6.10 **Metabolic phenotype of female Th^{Cre};$Npy^{flox/flox}$ mice is similar to that of males.** (a) The weekly body weights of female Th^{Cre};$Npy^{flox/flox}$ and WT mice treated with high-fat diet (HFD) (n=4). (b-c) The weights of (b) iWAT and vWATs, and (c) iBAT and hearts of HFD-treated 18-week-old female Th^{Cre};$Npy^{flox/flox}$ and $Npy^{flox/flox}$ mice (n=3&4). All values are expressed as mean ± SEM. Statistical comparisons were made using 2-tailed Student T-tests, $^{*}p<0.05$, $^{**}p<0.01$. 105

6.11 **Ablating NPY from the hindbrain does not affect body weight, BAT weight or thermogenesis.** (a) Schematic of knocking out NPY in the hindbrain by AAV injection. (b) Schematic of metabolic phenotyping of mice with NPY knocked out in the hindbrain (Hindbrain: $Npy^{flox/flox}$;AAV-CRE-GFP) and WT ($Npy^{flox/flox}$;AAV-GFP) mice. (c) Confocal images of the sliced hindbrain stained with anti-NPY (magenta). Scale bar=100μm. (d) iBAT weight of 14-week-old ND-treated male Hindbrain: $Npy^{flox/flox}$;AAV-CRE-GFP and WT mice (n=7). (e) iBAT temperature change after a 14-hour fast (n=7). (f) Weekly body weight of ND-treated male Hindbrain: $Npy^{flox/flox}$;AAV-CRE-GFP and WT mice (n=7). (g) The expression levels of thermogenic and adipogenic genes in the iBAT of RT-housed ND-treated male Hindbrain: $Npy^{flox/flox}$; AAV-CRE-GFP and WT mice (n=5). All values are expressed as mean $\pm$ SEM. 107

6.12 **NPY mutation correlates with BMI but not an unhealthy diet.** 108

List of Tables

1.1 Mural cell markers 15
1.2 G proteins and their effectors 23

2.1 The sequences of primers for RT-qPCR 42

List of Abbreviations

NPY . . . . . Neuropeptide Y

SNS . . . . . Sympathetic nervous system

HFD . . . . . High-fat diet

EE . . . . . Energy expenditure

WAT . . . . . White adipose tissue

scWAT . . . . . Subcutaneous white adipose tissue

vWAT . . . . . Viceral white adipose tissue

BAT . . . . . Brown adipose tissue

iBAT . . . . . Intrascapular brown adipose tissue

cAMP . . . . . Cyclic adenosine monophosphate

PKA . . . . . Protein kinase A

MAPK . . . . . Mitogen-activated kinase A

PPAR . . . . . Peroxisome proliferator-activated receptor

PGC1α . . . . . PPARγ co-activator-1α

TF . . . . . Transcription factor

NE . . . . . Norepinephrine

NPY . . . . . Neuropeptide Y

RVLM . . . . . Rostral ventrolateral

PVN . . . . . paraventricular nucleus of the hypothalamus

SCG ..... Superior cervical ganglia

MCG ..... Middle cervical ganglia

SG ..... Stellate ganglia

CG ..... Celiac ganglia

APC ..... Adipocyte progenitors

LDL ..... Low-density lipid

PNPLA2 ..... Patatin-like phospholipase domain containing-2

ATGL ..... Adipocyte triglyceride lipase

MGL ..... Monoacylglycerol lipase

TAG ..... Triacylglycerol

DAG ..... Diacylglycerol

ABHD5 ..... Alpha/beta hydrolase domain-containing protein-5

LC-CoA ..... Long-chain acyl-CoA

PDE3B ..... Phosphodiesterase 3B

ER ..... Endoplasmic reticulum

SERCA2b ..... Sacro/endoplasmic reticulum Ca^{2+}-ATPase2b

RYR2 ..... Ryanodine receptor-2

ATM ..... Adipose-tissue-associated macrophages

(TNFα ..... Tumour necrosis factor-alpha

TLR4 ..... Toll-like receptor-4

HIF1α ..... Hypoxia-inducible factor-1α

PVM ..... Perivascular macrophage

CLS ..... Crown-like structure

SAM ..... Sympathetic neuron-associated macrophage

TH ..... Tyrosine hydroxylase

HFD ..... High-fat diet

ITGAX ..... Integrin alpha-X

MHC-II ..... Major histocompatibility complex-II

DTR ..... Diphtheria toxin receptor

ILC ..... Innate lymphoid cell

NK ..... Natural killer

LTi ..... Lymphoid tissue inducer

T_H ..... Helper T cell

SVF ..... Stromal-vascular fraction

scRNA-Seq .... Single-cell RNA-sequencing

snRNA-Seq .... Single-nucleus RNA-sequencing

SMC ..... Smooth muscle cell

LPL ..... Lipoprotein lipase

FFA ..... Free fatty acid

SNS ..... Sympathetic nervous system

POMC ..... Pro-opiomelanocortin

NGF ..... Neuron growth factor

DIO . . . . . Diet-induced obesity

GPCR . . . . . G-protin-coupled receptors

PLC . . . . . Phospholipase C

ND . . . . . Normal chow diet

JAX . . . . . Jackson Lab

BSA . . . . . Bovine serum albumin

ECi . . . . . Ethyl cinnamate

RCF . . . . . Relative centrifugal force

SEM . . . . . Standard error of the mean

IF . . . . . Immunofluorecent

MACS . . . . . Magnetic-activated cell sorting

RT . . . . . Room temperature

EE . . . . . Energy expenditure

cKO . . . . . Conditional knockout

i.v. . . . . . Intravenous

1 | Introduction

1.1 Adipose tissue

Adipose tissue is a complex metabolic and endocrine organ that not only stores fat but also regulates immune response and body temperature (Kumari, Heeren, & Scheja, 2018). There are generally 2 types of adipose tissue: white adipose tissue (WAT) and brown adipose tissue (BAT). WAT can be found under the skin, namely subcutaneous white adipose tissue (scWAT), and in the abdomen, namely visceral adipose tissue (vWAT). BAT can be found around the interscapular region in infants and mice, while in adult humans, BATs are predominantly located at the cervical-supraclavicular and paravertebral regions (Figure 1.1) (Kumari et al., 2018; Ikeda, Maretich, & Kajimura, 2018).

Both WATs and BATs are important for energy homeostasis: WATs store lipids and can secrete Leptin as a signal of energy sufficiency while BATs dissipate energy, In such ways, adipose tissues store, sense and consume lipids to maintain the balance between energy in and out. Dysfunction in adipose tissue can lead to multiple diseases including obesity, type 2 diabetes (T2D), and atherosclerosis (Klein, Wadden, & Sugerman, 2002).

1.1.1 The component of adipose tissue

Besides adipocytes, many different cells can be found in adipose tissue. Based on up-to-date single-cell and single-nucleus RNA-sequencing studies, fibroblasts, vascular endothelial cells, and perivascular mural cells exist in adipose tissue, as well as immune cells including T cells, B cells, innate lymphoid cells (ILCs), macrophages, monocytes, neutrophils, and mast cells (Shamsi et al., 2021; Hen-

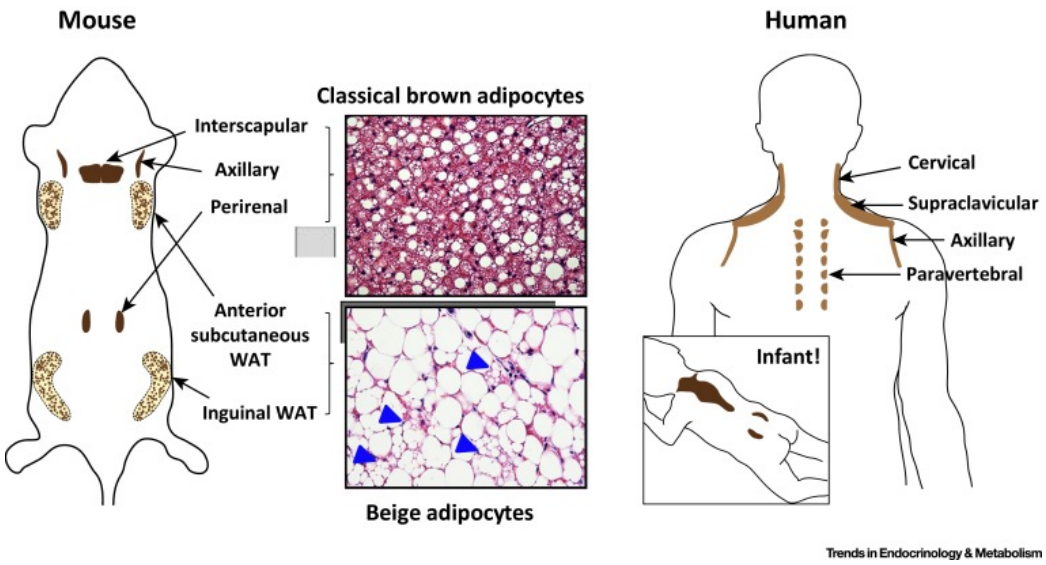


Figure 1.1: **Anatomical localisation of main scWATs and BATs in mice, human infants, and adults.** scWATs are localised at various regions such as the anterior scWAT and the inguinal WAT (iWAT). BATs in mice and infants are mainly localised at the interscapular and perirenal parts, while in adults, they are localised at the cervical-supraclavicular and paravertebral parts.

riques et al., 2020; W. Sun et al., 2020). Even though the function of these cells is not fully understood, previous studies have revealed that these cells actively regulate adipose tissue metabolism. Previous research indicates that fibroblasts can differentiate into adipocytes (Berry & Rodeheffer, 2013; Y.-H. Lee, Petkova, Mottillo, & Granneman, 2012), and immune cells, such as ILC2 and macrophages, can either directly affect lipolysis or by degrading NE (Cardoso et al., 2021; Pirzgalska et al., 2017). Besides these cells revealed by scRNA-Seq and snRNA-Seq, sympathetic-neuron axons and sensory-neuron neurites are detected in adipose tissue and both contribute to the homeostasis of adipose tissue (W. Zeng et al., 2015; Y. Wang et al., 2022). Although the cellular components of adipose tissue are well understood (Figure 1.2), it is still largely unclear how each type of these cells contributes to the homeostasis of adipose tissue, and how these cells interact with each other and affect adipose metabolism.

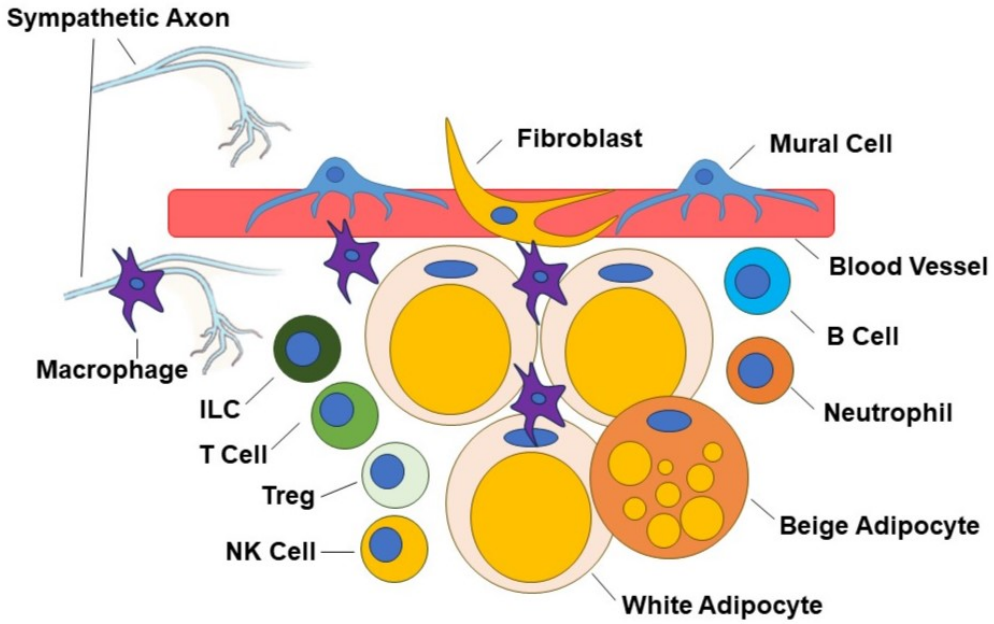


Figure 1.2: **The cellular components of adipose tissue.** Two types of adipocytes can be found in white adipose tissue: the white and beige adipocytes. Sympathetic axons are detected in detected adipose tissue. Immune cells including T cells, T_{reg}, NK cells, ILCs, neutrophils, B cells, and macrophages abundantly exist in adipose tissue. A special type of macrophages is associated with sympathetic axons and can degrade NE. Fibroblast and mural cells can be found around blood vessels.

1.1.2 Adipocytes

1.1.2.1 The progenitors of adipocytes

There are 3 types of adipocytes in our body: the white adipocytes, which are the main component of WATs, the brown adipocytes, which are the main component of BAT, and beige adipocytes, which are a kind of recently discovered thermogenic adipocytes (Ikeda et al., 2018). These 3 types of adipocytes have respective progenitors as shown in Figure 1.3 (P. Zhang et al., 2022): *Myf5*$^{-}$*Pdgfra*$^{+}$ mesenchymal stem cells give rise to white adipocytes; *Myf5*$^{+}$ cells, which also give rise to skeletal muscles, are the progenitor of brown adipocytes; mural cells marked by *Myh11* are progenitors of beige adipocytes. It has also been indicated that in neonates, PDGFRα^{+} adipogenic fibroblasts are progenitors for perivascular thermogenic adipocytes, while in adults, MYH11^{+} mural cells are progenitors of those thermogenic adipocytes (Angueira et al., 2021). This phenomenon indicates that different groups of progenitors contribute to the neogenesis of thermogenic adipocytes at different stages: some at the developmental stages, while others at adulthood in a context-dependent manner.

The progenitors of white adipocytes were identified by analysing lineage-tracing animal models such as Pdgfra^{Cre}; Rosa26^{mTmG} and Pdgfra^{Cre}; Rosa26^{tdTomato} (Berry & Rodeheffer, 2013; Y.-H. Lee et al., 2012); the progenitors of brown adipocytes were identified using Myf5^{Cre}; Rosa26^{YFP} (Seale et al., 2008); the progenitors of beige adipocytes were identified by analysing Myh11$^{Cre\text{-}GFP}$; Rosa26^{tdTomato} and Trpv1^{Cre}; Rosa26^{mTmG} (Long et al., 2014; Shamsi et al., 2021).

1.1.2.2 Adipogenesis and lipolysis

The homeostasis of adipose tissue is affected by two opposite driving forces: storing lipids in cells and consuming lipids in cells. The former is achieved by adipo-

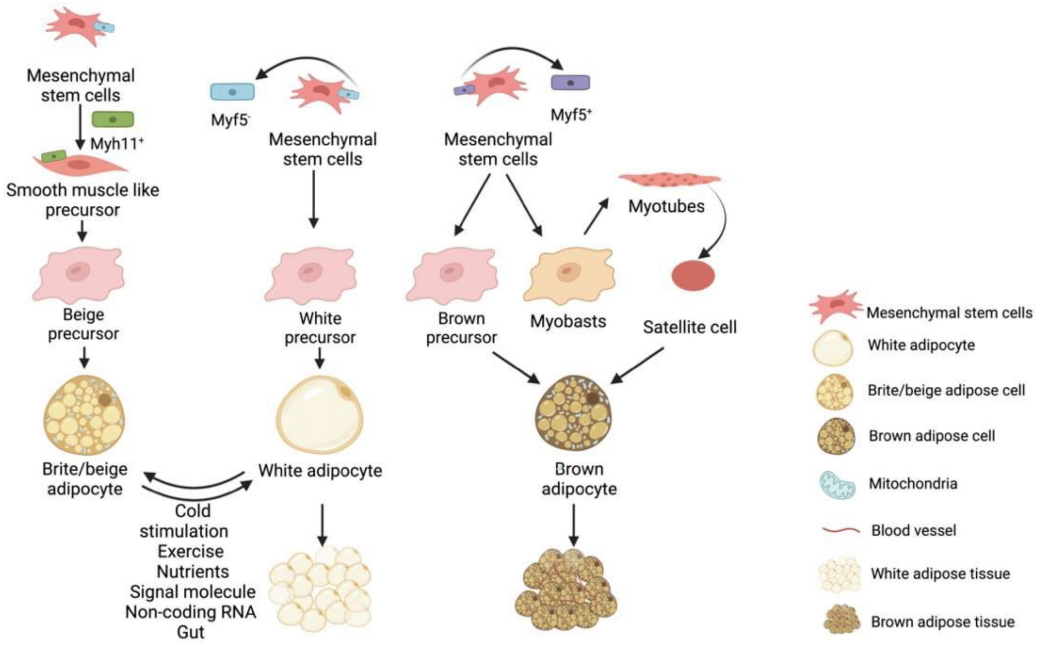


Figure 1.3: **The progenitors of white, brown and beige adipocytes.** Brown adipocytes are derived from Myf5$^+$ progenitors, white adipocytes are derived from Myf5$^-$ progenitors, and beige adipocytes are derived from Myh11$^+$ progenitors.

genesis or adipocyte hypertrophy, while the latter is achieved by lipolysis.

Adipogenesis is the differentiation of adipocyte progenitors (APCs) into adipocytes. Multiple receptors and transcription factors are involved in this process, and PPARγ and C/EBPα are the most important ones. PPARγ is the dominant factor for adipogenesis: knocking out PPARγ in the preadipocyte cell line 3T3-L1 completely abrogates its adipogenic ability (Rosen et al., 1999), and knocking down PPARγ in mice results in severe lipodystrophy (Koutnikova et al., 2003). Although many metabolites including polyunsaturated fatty acids, prostaglandins, and eicosanoids are known to bind to PPARγ, their affinity or abundance in adipocytes is low, and the physiological ligand for PPARγ is still unknown (Schupp & Lazar, 2010). After binding to its ligand, PPARγ then activates C/EBPα and functions with C/EBPα to transcribe genes such as lipoprotein lipase (Schoonjans et al., 1996),

fatty acid transport protein such as CD36 (Frohnert, Hui, & Bernlohr, 1999; Lefterova et al., 2008), and oxidized LDL receptor 1 (Chui, Guan, Lehrke, Lazar, et al., 2005). Unlike PPARγ, C/EBPα is dispensable for adipogenesis: C/EBPα cannot induce adipogenesis in cells without PPARγ, while PPARγ can induce adipogenesis in cells without C/EBPα (Rosen et al., 2002), which is probably due to the compensatory effect mediated by other members of C/EBP family, namely C/EBPβ and C/EBPδ. Many hormones such as insulin, thyroid hormones, glucocorticoids (Smas, Chen, Zhao, Latasa, & Sul, 1999), and estrogen (Dieudonne, Pecquery, Leneveu, & Giudicelli, 2000) can promote adipogenesis. In contrast, some nutritional factors such as polyunsaturated fatty acids (Madsen, Petersen, & Kristiansen, 2005), vitamins A and D (Bonet, Ribot, Felipe, & Palou, 2003; Cheng et al., 2010) can inhibit adipogenesis.

The primary pathway regulating lipolysis in adipocytes consists of 3 main enzymes: patatin-like phospholipase domain containing-2 (PNPLA2)/adipocyte triglyceride lipase (ATGL), hormone-sensitive lipase (HSL), and monoacylglycerol lipase (MGL). PNPLA2/ATGL was identified as the rate-limiting enzyme of triacylglycerol (TAG) hydrolysis that breaks down TAGs to generate diacylglycerol (DAG) (Haemmerle et al., 2006). PNPLA2/ATGL itself has low hydrolytic activity, but its activity is increased by 20-fold When binding with the co-lipase alpha/beta hydrolase domain-containing protein 5 (ABHD5) (Lass et al., 2006). ABHD5 is regulated allosterically by long-chain acyl-CoA (LC-CoA). When binding to LC-CoA, ABHD5 is associated with PLIN1, and when isolated from LC-CoA, ABHD5 is dissociated with PLIN1 and binds with PNPLA2/ATGL (Sanders et al., 2015). The dissociation of ABHD5 from PLIN1 is vital for the function of PLIN1 to recruit HSL (Sztalryd et al., 2003), which is the only DAG lipase (Holm et al., 1988), to lipid droplets, and this leads to the hydrolysis of DAG to MAG and the sequential hydrolysis of MAG to glycerol by MGL. Lipolysis can be induced

by nor-epinephrine (NE) via the cAMP-PKA pathway (Carpéné, Bousquet-mélou, Galitzky, Berlan, & Lafontan, 1998), which phosphorylates PLIN1 (Granneman et al., 2007), and negatively regulated by insulin via activating phosphodiesterase 3B (PDE3B) to decrease cAMP (Kitamura et al., 1999).

1.1.2.3 Beige adipocytes and thermogenesis

Beige adipocytes are generated in 2 different ways: neogenesis from beige adipocyte progenitors (marked by *Myh11* and *Trpv1*), and phenotypic conversion from white adipocytes to beige adipocytes (Q. A. Wang, Tao, Gupta, & Scherer, 2013). Both ways involve activating either UCP1-dependent or UCP1-independent thermogenic genes by adrenergic stimulation(Sakers, De Siqueira, Seale, & Villanueva, 2022). UCP1-dependent thermogenesis uses UCP1 to drive proton leak in the mitochondria and is activated by the following pathway: upon adrenergic stimulation, cyclic AMP (cAMP)-protein kinase A (PKA)-p38 pathway is activated, which then activates PPARγ co-activator-1α (PGC1α) (Cao et al., 2004). PGC1α co-activates multiple transcription factors (TFs) including PPARγ, PRDM16, and ERRα to increase *Ucp1* expression (Shapira & Seale, 2019). UCP1-independent thermogenesis uses different mechanisms including Ca^{2+} cycling and creatine cycling. Ca^{2+} cycling thermogenesis uses Ca^{2+} instead of protons to generate heat by leaking through the membrane of the endoplasmic reticulum (ER). Sacro/endoplasmic reticulum Ca^{2+}-ATPase2b (SERCA2b) transports Ca^{2+} into ER by ATP hydrolysis, and ryanodine receptor 2 (RYR2), which is a calcium channel, allows Ca^{2+} in the ER to leak to cytoplasm (Ikeda et al., 2017). The UCP1-independent mechanism is required for beige adipocyte thermogenesis, whereas it is dispensable for brown adipocytes where less ATP is synthesized since ATP is required for UCP1-independent thermogenesis (Ikeda et al., 2017). Nonshivering thermogenesis conducted by BATs and beige adipocytes is important for maintaining energy

balance since it amounts to nearly 15% of daily energy expenditure, and previous research has demonstrated that abrogated beige adipocyte neogenesis can lead to obesity (Oguri et al., 2020).

1.1.3 Immune cells and adipose metabolism

Immune cells exist in adipose tissue, and an increasing amount of research has indicated that adipose tissue-resident immune cells play an important role in regulating adipocyte metabolism. The most important kind of immune cells known to be increased in obese adipocytes are the macrophages, which normally make up 10% to 15% in lean adipose tissue and increase to 40% in obese adipose tissue (Weisberg et al., 2003; Xu et al., 2003). Other immune cells that exist in adipose tissue include $CD8^+$ T cells and Tregs. $CD8^+$ T cells can promote the differentiation of monocytes to pro-inflammatory adipose tissue-associated macrophages (ATMs) (Nishimura et al., 2009), while Tregs inhibit monocyte migration and direct them to anti-inflammatory macrophages (Romano et al., 2018).

Chronic inflammation caused by increased pro-inflammatory ATMs decreases insulin sensitivity (Feingold et al., 1989; Cook et al., 2000), and neutralising tumour necrosis factor-alpha (TNFα) secreted by ATMs mitigates insulin tolerance (Hotamisligil, Shargill, & Spiegelman, 1993). Although the exact mechanism initiating inflammation in adipose tissue is unclear, two factors are known to contribute to it: the binding of glucose or saturated-free fatty acid to Toll-Like receptor-4 (TLR4) and oxidative stress (Boeni-Schnetzler et al., 2009; Houstis, Rosen, & Lander, 2006). TLR4 can activate inflammasome NLRP3 and result in the consequent secretion of IL1β (Paik, Kim, Silwal, Sasakawa, & Jo, 2021), and adipocyte hypoxia can induce hypoxia-inducible factor-1α (HIF1α) to upregulate chemokines that attract monocytes to adipose tissue (Imtiyaz & Simon, 2010).

1.1.3.1 Myeloid cells

Myeloid cells, including macrophages, mast cells, and dendritic cells, are the most abundant tissue-residential immune cells in adipose tissue.

Tissue-residential macrophages originate in the yolk sac and are seeded in adipose tissue (Schulz et al., 2012). In lean adipose tissue, macrophages are marked as $CD206^{+}CD301^{+}CD11c^{-}$ and can secrete IL10 to inhibit IL1β signalling (Wu et al., 2011). These macrophages are maintained by IL4 secreted by eosinophils and help protect adipose tissue homeostasis by clearing dead adipocytes and debris via phagocytosis (Wu et al., 2011). In obese adipose tissue, pro-inflammatory macrophages are accumulated by chemokines such as CCL-2 and marked as $CD11c^{+}$. These pro-inflammatory are regarded as the source of pro-inflammatory cytokines such as TNFα and IL6, which can cause insulin resistance.

Recent sequencing datasets indicate that instead of the pro-anti-inflammatory macrophage dichotomy, ATMs have greater diversity and heterogeneity, and a few different kinds of macrophages with specified functions are identified. Perivascular macrophages (PVMs) are marked by LYVE1, a marker for lymphatic vessels (Sárvári et al., 2021). PVMs also express a scavenger receptor, TIM-4, which indicates their function of clearing apoptotic cells (Félix et al., 2021). They can also secrete PDGF-CC to control energy storage (Cox et al., 2021). Besides PVM, a group of $CD169^{+}CD11c^{+}$ ATMs are also found to be closely associated with the vasculature in eWAT, and they function to protect vascular integrity and hamper fibrosis (Q. Chen et al., 2021). In obesity, $CD11c^{+}$ ATMs form crown-like structures (CLS) around adipocytes (Lindhorst et al., 2021). These macrophages are shown to express genes associated with lysosome biogenesis (e.g. *Lamp2, Acp5, Ctsk, Npc1*) and lipid metabolism (e.g. *Lpl, Lipa, Fabp4, Fabp5, Pparg*) (Coats et al., 2017). TREM-2 is a *bona fide* marker of these macrophages, and ablat-

ing TREM-2 in bone marrow cells deteriorates the metabolic outcomes of obesity (Jaitin et al., 2019). Moreover, a unique group of macrophages associated with sympathetic nerves have recently been discovered, called sympathetic neuron-associated macrophages (SAMs). SAMs can uptake and degrade NE secreted by sympathetic nerves and inhibit thermogenesis or lipolysis (Pirzgalska et al., 2017). Although some studies indicate that macrophages can induce thermogenesis or lipolysis via norepinephrine, the mechanism by which macrophages affect thermogenesis remains controversial since no tyrosine hydroxylase (TH) is expressed in macrophages (Fischer et al., 2017).

Mast cells and dendritic cells are other myeloid cells discovered in adipose tissue. Similar to macrophages, they accumulate in adipose tissues when mice are treated with a high-fat diet (HFD). Mast cells are marked by tryptase and CD117 and capable of secreting a variety of pro-inflammatory cytokines including IFN-γ, IL6, and tryptase, which stimulate angiogenesis, promote adipocyte differentiation, and cause insulin resistance (Zhou et al., 2015). However, ablating mast cells using a mouse line in which diphtheria toxin is expressed under the control of Mcpt5-Cre does not affect obesity, which means even though mast cells can contribute to the development of chronic inflammation in adipose tissue, they are dispensable for obesity-related phenotype (Chmelař et al., 2016). Dendritic cells in adipose tissue are characterised by high expression of integrin alpha-X (*Itgax*, also known as CD11c) and major histocompatibility complex-II (MHC-II) and are distinguished from ATMs due to the lack of CD64 and MerTK on dendritic cells (Cho et al., 2016). Ablating dendritic cells using a mouse model in which diphtheria toxin receptor (DTR) is expressed under the control of CD11c promotor improves obesity-induced inflammation and insulin resistance, accompanied by reduced T cell activation and increased proportion of Treg (Cho et al., 2014).

1.1.3.2 Lymphocytes

Lymphocytes can be categorised into 3 types: innate lymphoid cells (ILC), T cells and B cells. ILCs do not express antigen-specific receptors expressed on B and T cells. The ILC family can be divided into 5 subsets: natural killer (NK) cells, ILC1, ILC2, ILC3, and lymphoid tissue inducer (LTi) cells (Vivier et al., 2018). NK cells and ILC1 can secrete IFN-γ to promote the differentiation of pro-inflammatory macrophages, resulting in adipose tissue inflammation and insulin resistance (B.-C. Lee et al., 2016; Sullivan et al., 2016). ILC2 are recruited and activated by IL33 sourced from PDGFRα^+PDNP$^+$ fibroblasts (Kolodin et al., 2015; Rana et al., 2019). They can increase the number of eosinophils and anti-inflammatory macrophages via IL4, IL5 and IL13, which improves insulin sensitivity (Molofsky et al., 2013). Recent studies indicate that ILC2 can regulate thermogenesis directly: IL13 secreted by ILC2 can bind to IL4R on PDGFRα^+ adipocyte progenitors and facilitate the biogenesis of beige cells in WAT (M.-W. Lee et al., 2015); ILC2 can also secrete methionine-enkephalin to upregulate *Ucp1* expression and facilitate the phenotypic conversion from white adipocytes to beige adipocytes (Brestoff et al., 2015).

T cells can be classified as CD4$^+$ and CD8$^+$ T cells. CD4$^+$ T cells, also known as helper T cells (T_H), can be further classified as T_H1, T_H2, T_H17, and Treg. In obese animals, the proportion of T_H1, T_H17, and CD8$^+$ T cells are increased in adipose tissue, while that of T_H2 is decreased (Rocha et al., 2008). T_H1 can secrete IFN-γ, which is known to promote inflammation (B.-C. Lee et al., 2016; Sullivan et al., 2016). Depleting T_H1 can improve insulin and glucose sensitivity (Stolarczyk et al., 2013). Like ILC2, T_H2 can help maintain an anti-inflammatory microenvironment in adipose tissue by secreting cytokines such as IL4 and IL5 (Molofsky et al., 2013; Wu et al., 2011). Treg is another type of CD4$^+$ cells having

anti-inflammatory function. They are marked by the expression of *Foxp3* and can secrete IL10 and TGFβ against inflammation (Cipolletta, Cohen, Spiegelman, Benoist, & Mathis, 2015).

1.1.3.3 Cytokines and thermogenesis

Previous publications indicate that anti-inflammatory cytokines including IL33, IL4, and IL13 are required for thermogenesis (Kolodin et al., 2015; M.-W. Lee et al., 2015; Haberman et al., 2024), but the mechanism mediating these effects remains unknown. Opposite to these anti-inflammatory cytokines, pro-inflammatory cytokines including IL1 and TNFα either suppress thermogenesis (Goto et al., 2016; Valladares, Roncero, Benito, & Porras, 2001) or the neogenesis of beige adipocytes (Estève et al., 2015), which can cause decreased energy expenditure (EE) and obesity.

1.1.4 Non-immune stromal-vascular fraction

The stromal-vascular fraction (SVF) of the adipose tissue is a heterogeneous cell system that mainly consists of vascular endothelial cells, fibroblasts, mural cells, and immune cells including myeloid cells and lymphocytes (Nunes et al., 2013; Koh et al., 2011). This section will focus on the non-immune compartment of SVF to discuss its impact on adipose tissue metabolism.

1.1.4.1 Fibroblasts

Fibroblasts are cells capable of producing extracellular matrix (ECM) which supports other tissue-resident cell types (Buechler & Turley, 2018). Fibroblasts are marked by the expression of *Pdgfra* in adipose tissue based on previously published single-cell RNA-sequencing (scRNA-seq) (Henriques et al., 2020). Consistent with other tissues including the lung, skeletal muscle, and intestine, adi-

pose fibroblasts can be generally classified into two clusters: the Pi16^{+}COL15A1^{-} cluster, which also highly express *Cd34* and *Ly6a*, and Pi16^{-}COL15A1^{+} cluster, expressing basement membrane proteins including *Col15a1*, *Hspg2*, and *Col4a1* (Buechler et al., 2021; Henriques et al., 2020).*Pparg, Cebpa*, and *Fabp4*, which are essential proteins for adipogenesis and lipid metabolism can be detected in Pi16^{-}COL15A1^{+} cluster, indicating they are the PDGFRα fibroblasts that can differentiate into adipocytes (Hepler et al., 2018). Although the functional analysis of Pi16^{+}COL15A1^{-} fibroblasts is absent, the high expression of fibrotic genes *Fn1*, *Tgfb2*, and *Loxl2*, and complement component gene *C3* implies that these fibroblasts can contribute to adipose tissue fibrosis and inflammation (Hepler et al., 2018; Henriques et al., 2020). Also, recent studies indicate that fibroblast-derived Pi16 can recruit macrophages and promote leukocyte infiltration into tissues (Garrity et al., 2023; Singhmar et al., 2020), which implies a pro-inflammatory function of Pi16^{+}COL15A1^{-} fibroblasts.

1.1.4.2 Mural cells

Mural cells surround vascular endothelial cells and can be subgrouped into smooth muscle cells (SMCs) associated with larger vessels and pericytes associated with capillaries (Armulik, Genové, & Betsholtz, 2011). A list of markers including PDGFRβ, NG2 (*Cspg4*), αSMA (*Acta2*), TAGLN, DES, MYH11, CD13 (*Anpep*), and RGS5 have been used to label mural cells (Armulik, Abramsson, & Betsholtz, 2005; Krueger & Bechmann, 2010; L. Zhu et al., 2006; Nehls, Denzer, & Drenckhahn, 1992; Sinha, Hoofnagle, Kingston, McCanna, & Owens, 2004). However, these markers cannot distinguish between SMCs and pericytes since they are dynamically expressed in both subtypes, and some of these markers also exist in other types of cells including fibroblasts, mesenchymal stem cells, endothelial and epithelial cells (Sheppard, 2006; L. Li, Miano, Cserjesi, & Olson,

1996) as indicated in table1.1. Therefore, identifying mural cells requires mural cell markers, well-preserved cell morphology, and counter-staining of endothelial cells.

Many signalling pathways regulate mural cells. The most important ones include PDGF-B/PDGFRβ and TGFβ pathways. PDGF-B is secreted by angiogenic endothelial cells whose target is PDGFRβ expressed on the surface of mural cells (Armulik et al., 2011). PDGF-B is required for early development as knockout of PDGF-B results in perinatal lethality due to vascular dysfunction (Levéen et al., 1994). Once secreted, PDGF-B needs to attach to the surface of the endothelium via its retention motif to achieve its function to recruit mural cells to the vessel walls (Lindblom et al., 2003). Different from its function in embryonic vascular developments, recent research also indicates that in postnatal animals, elevated levels of PDGF-B can induce mural cell-fibroblast transdifferentiation in both tumour and adipose tissue (Hosaka et al., 2016; Onogi et al., 2017), resulting in a reduced number of mural cell covering the vasculature and increased vascular leakiness. TGFβ is expressed in both endothelial cells and mural cells (Sato & Rifkin, 1989), and it can increase the production of ECM (Ronaldson, DeMarco, Sanchez-Covarrubias, Solinsky, & Davis, 2009) and the expression of tight junction proteins such as N-Cadherin to maintain vascular integrity and mural cell coverage (F. Li et al., 2011). Mural cells can also regulate vascular integrity via angiopoietin-1 (ANG-1), whose receptor, TIE-2, is expressed on the surface of endothelial cells (Davis et al., 1996; Sundberg, Kowanetz, Brown, Detmar, & Dvorak, 2002; Dumont, Gradwohl, Fong, Auerbach, & Breitman, 1993). Activating TIE-2 by ANG-1 maintains the integrity of vessels by upregulating cell-cell junction molecules and decreases inflammation (Ricard, Bailly, Guignabert, & Simons, 2021).

Mural cells can affect adipose tissue in two different ways: by regulating vascular

Table 1.1: Mural cell markers

Protein marker	**Gene Symbol**	**Cell types expressing the marker**	**Function**
PDGFRβ	Pdgfrb	Mural cells (pericytes and SMCs), Mesenchymal stem cells; Fibroblasts	Receptor tyrosine kinase important for mural cell recruitment during angiogenesis
NG2	Cspg4	Mural cells; Developing cartilage, bone, muscle; Skin stem cells; Neuronal progenitors; Oligodendrocyte progenitors	Integral membrane chondroitin sulfate proteoglycan required for mural cell recruitment
αSMA	Acta2	Mural cells; Myofibroblasts; Myoepithelium	Structural protein
TAGLN	Tagln	Mural cells; Myofibroblas; Endothelium	Actin-binding protein, capable of regulating contractile functions of mural cells
Desmin	Des	Mural cells; Cardiac and skeletal muscles.	Structural protein
MYH11	Myh11	Mural cells; Myofibroblasts	Contractile protein in SMCs
CD13	Anpep	Mural cells; Inflammed and tumour endothelium; myeloid cells	Type II membrane zinc-dependent metalloprotease
RGS5	Rgs5	Mural cells; Cardiomyocytes	Regulate heterotrimeric G proteins by activating GTPase activity

leakiness which affects immune infiltration and inflammation in adipose tissue (Onogi et al., 2017) and by differentiating into thermogenic adipocytes (Shamsi et al., 2021; Long et al., 2014). However, it is not feasible to distinguish which of them is a more predominant way to regulate adipose tissue since inflammation can reciprocally affect mural cell coverage, vascular integrity (H. Zeng et al., 2016) and thermogenesis (Goto et al., 2016; Valladares et al., 2001).

1.1.4.3 Vasculature and adipose tissue metabolism

The common units of all the vessels are $CD31^+$ endothelial cells, with mural cells and perivascular fibroblasts attaching to them. In the lean state, adipose tissues are heavily vascularized so that adequate oxygen supply can be provided. In the obese state, although acute hypoxia caused by the rapid expansion of adipose tissue can trigger the secretion of VEGF to promote angiogenesis to maintain oxygen supply (M.-W. Lee et al., 2015), the continuous tissue expansion will compromise the pro-angiogenic effect and result in vascular rarefaction (Sung et al., 2013), which can cause chronic hypoxia and adipose tissue inflammation. Vascular rarefaction also negatively affects thermogenesis (Shimizu et al., 2014). Therefore, counteracting vascular rarefaction by overexpressing VEGF in BATs and WATs mitigates insulin resistance and promotes beiging and thermogenesis (Elias et al., 2012). Besides VEGF, endothelial cells in the adipose tissue are regulated by multiple adipokines including adiponectin and leptin. Adiponectin binds to its receptors AdipoR1 and AdipoR2 expressed on endothelial cells to induce NO production promoting vasodilation (Vaiopoulos, Marinou, Christodoulides, & Koutsilieris, 2012). Adiponectin can also bind to T-cadherin and promote revascularisation (Parker-Duffen et al., 2013). Leptin can cause a rapid increase in vascular permeability, and hyperleptinaemia induces the secretion of pro-inflammatory cytokines and the expression of cell-cell junction proteins (Henning, 2021). En-

dothelial cells in adipose tissue participate in lipid metabolism: lipoprotein lipase (LPL) binds to the surface of endothelial cells via GPIHBP1 and hydrolyses lipids to release free fatty acids (FFA), which is then internalised by CD36 expressed on the surface of endothelial cells and undergoes transcytosis (Abumrad et al., 2021). The expression levels of GPIHBP1, fatty acid-binding proteins (FABPs), and CD36 can be upregulated by PPARγ in endothelial cells (Kanda et al., 2008), which can be activated by increased FFA (Gogg, Nerstedt, Boren, & Smith, 2019). Adipocyte-secreted ANGPT2 regulates lipid uptake by endothelial cells, and adipocyte-specific knockout of ANGPT2 decreases adipose tissue size while increasing lipid accumulation in the liver (Bae et al., 2020).

1.2 Sympathetic nervous system and its function in adipose metabolism

The sympathetic nervous system (SNS) is primarily recognised for its role in the "flight or fight" response, far beyond that, it is also indispensable for maintaining physiological homeostasis including adipose metabolism, cardiac input, and immune response (Scott-Solomon, Boehm, & Kuruvilla, 2021). SNS regulates peripheral tissues by establishing close contact between postganglionic axons and their postsynaptic target and releasing neurotransmitters including norepinephrine (NE) and neuropeptide Y (NPY).

1.2.1 The structure of sympathetic nervous system

SNS contains two kinds of neurons: preganglionic and postganglionic neurons. Preganglionic neurons are located in the intermediolateral column of the spinal cord and send out axons to connect the postganglionic neurons that lie in the

paravertebral ganglia chain in a generally ipsilateral fashion. Based on previous retrograde-tracing studies with pseudorabies virus, several regions in the brain project to preganglionic sympathetic ganglia: rostral ventrolateral medulla (RVLM), noradrenergic cell group A5, raphe nuclei, lateral hypothalamus, and paraventricular nucleus of the hypothalamus (PVN) (Jansen, Wessendorf, & Loewy, 1995; Nakamura et al., 2004; Cano et al., 2003). Different paravertebral sympathetic ganglia project to many different organs: eyes are innervated by the superior cervical ganglia (SCG); the heart is innervated by SCG, middle cervical ganglia (MCG), stellate ganglia (SG), the thoracic ganglia T2-T6; liver, kidney and digestive system including stomach and intestine are innervated by the celiac ganglia (CG) (Shields Jr, 1993).

1.2.2 Sympathetic regulation of adipose tissue

It is widely accepted that sympathetic axons innervate both BATs and WATs, and the neurotransmitter NE secreted by sympathetic axons is key to regulating lipolysis and thermogenesis. The paravertebral ganglia innervating adipose tissues were mapped in a retrograde-tracing study using pseudorabies virus and tissue clearing of the whole upper body of mice, which nicely demonstrates that iBATs are innervated by SG, T2-T5, and iWATs are innervated by T12-T13 and L1 (Figure 1.4) (Huesing et al., 2022). Sites in the hypothalamus including PVH and pro-opiomelanocortin (POMC) neurons are demonstrated to be upstream of the ganglia innervating WATs and BATs, and those hypothalamic neurons play important roles in regulating thermoactivity of adipose tissue (Oldfield et al., 2002; Cano et al., 2003; Foster, Song, & Bartness, 2010). Further studies concerning the lipolytic function of leptin established a brain-adipose axis as shown in Figure 1.4: white adipocytes release leptin to activate SNS by binding to $LEPR^{+}$ neurons in the hypothalamus, and sympathetic axons release NE in BATs and WATs to mo-

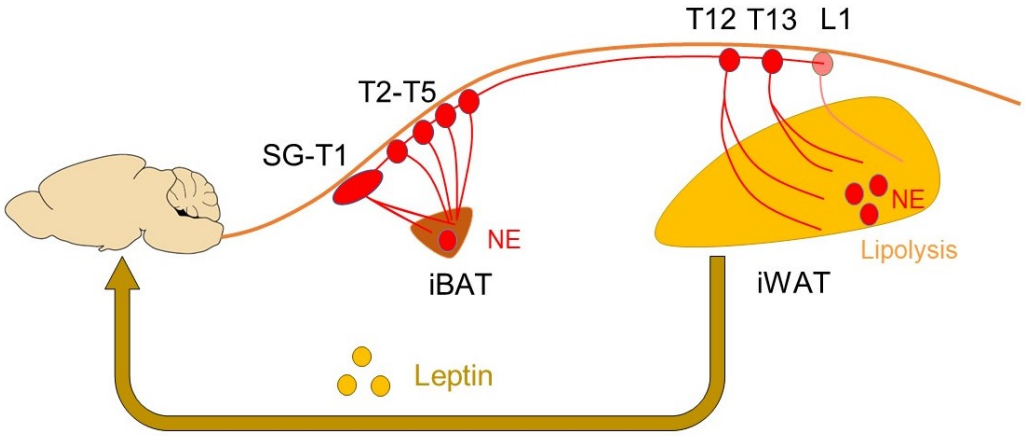


Figure 1.4: **Sympathetic innervation and regulation of adipose tissue.** iBATs are innervated by the stellate ganglion (SG), thoracic ganglia T2-T5. iWATs are innervated by thoracic ganglia T12-T13, and lumbar ganglion L1. The brain-adipose axis regulates the homeostasis of adipose tissue: white adipose tissue releases Leptin; Leptin activates SNS and makes SNS release NE to trigger lipolysis and thermogenesis.

bilise and consume stored lipids(W. Zeng et al., 2015). This brain-adipose is vital for maintaining adipose homeostasis as interfering with this axis by knocking out ADRβ3 (W. Zeng et al., 2015) or denervating adipose tissue (Cantu & Goodman, 1967) can increase fat mass and result in obesity.

The efferent end of this brain-adipose axis, namely sympathetic innervation in adipose tissue is dynamically regulated. Various growth factors including neuron growth factor (NGF) secreted by the stromal cells (Jiang, Ding, Cao, Wang, & Zeng, 2017) and S100b (X. Zeng et al., 2019) increase sympathetic innervation, and *Prdm16*, a protein regulating the differentiation of brown and beige adipocytes, is required for maintaining axon density in adipose tissue (Chi, Wu, et al., 2018; Chi et al., 2021). Sympathetic innervation is also affected by leptin that stimulates $BDNF^{+}$ neurons in the PVH: depleting leptin or leptin resistance caused by high-fat-diet-induced obesity (DIO) decreases sympathetic innervation

(P. Wang et al., 2020). Although it is well-accepted that sympathetic innervation is sufficient and indispensable in controlling adipose homeostasis, the major focus is only on one of the neurotransmitters secreted by sympathetic axons, the NE, while the function of other neurotransmitters, such as NPY, to regulate adipose tissue is still unclear.

1.3 Neuropeptide Y

Neuropeptide Y (NPY) is a 36-amino-acid neuropeptide that is mainly sourced from the arcuate nucleus (Arc) of the hypothalamus in the CNS, while in the periphery, it is expressed in SNS (LUNDBERG et al., 1982; Lundberg et al., 1990). Arc-derived NPY has been linked with appetite (Engström Ruud, Pereira, de Solis, Fenselau, & Brüning, 2020), but the function of SNS-derived NPY is unclear, especially in the adipose tissue.

1.3.1 Central Neuropeptide Y and feeding behaviour

NPY^+ neurons in Arc have been intensely studied concerning their function of regulating feeding behaviour. A large number of previous studies indicate that those NPY^+ neurons project to POMC neurons in the Arc and inhibit their functions to reduce feeding behaviour (Cowley et al., 2001; Cone, 2005; Balthasar et al., 2005). Also, NPY^+ neurons project to neurons that express NPY receptors in the PVH to induce appetite directly (Balthasar et al., 2005). More recent optogenetic studies indicate that NPY/Agrp neurons are sufficient to cause acute feeding behaviour (Aponte, Atasoy, & Sternson, 2011), and NPY is needed for the induction of acute feeding behaviour by activating NPY/Agrp neurons in Arc (Engström Ruud et al., 2020). Besides feeding behaviour, Arc-derived NPY is shown to downregulate *Th* expression in PVH thus affecting sympathetic inner-

vation in BAT (Shi et al., 2013). Despite these studies showing the connection between Arc-derived NPY and feeding behaviour, conventional knockout or over-expression of *Npy* does not affect long-term feeding behaviour or whole-body metabolism. Additionally, conventional knockout of NPY receptors does not greatly affect daily food intake but causes late-onset obesity (Marsh, Hollopeter, Kafer, & Palmiter, 1998; Pedrazzini et al., 1998; Naveilhan et al., 1999), which implies that NPY may control energy expenditure or adipose metabolism in the periphery.

1.3.2 Peripheral NPY in adipose tissue

Different from Arc-derived NPY, the function of peripheral NPY has not been well studied. NPY was shown to exist in SNS and co-released with NE, as revealed by immunofluorescent staining and *vas deferens* perfusion (LUNDBERG et al., 1982; Lundberg et al., 1990). Still, there has not been any quantitative evidence clarifying which compartment of the adipose tissue is innervated by NPY^{+} axons. Concerning the source of NPY in adipose tissue, some researchers claimed that besides sympathetic axons, adipose-tissue-associated macrophages (ATMs) are another source of NPY in the adipose tissue without providing convincing images showing immunofluorescent staining targeting NPY (Singer et al., 2013). Also, this conclusion is contradictory to published single-cell RNA-sequencing (scRNA-seq) datasets showing ATMs do not express *Npy* (Henriques et al., 2020).

There have been some *in vitro* studies using either the stromal vascular fraction (SVF) of adipose tissue or the pre-adipocyte cell line 3T3-L1 to determine the function of NPY in adipogenesis. Still, their conclusions are contradictory to each other: some studies showed that NPY promoted the proliferation and differentiation of preadipocytes (Kuo et al., 2007; Rosmaninho-Salgado et al., 2012), whereas others negated them (Yang, Guan, Arany, Hill, & Cao, 2008). More

contradictions were in the studies to determine the role of each NPY receptor in regulating adipogenesis: Some reported that only NPY1R agonists promoted the proliferation of preadipocytes (Yang et al., 2008), while others reported that only NPY2R and NPY5R agonists promoted the proliferation and differentiation of preadipocytes (Kuo et al., 2007; Rosmaninho-Salgado et al., 2012). Furthermore, the *in vivo* study showing that NPY2R on adipocytes mediates the expansion of WAT (Kuo et al., 2007) contradicts the previous publication characterising NPY2R-KO mice (Naveilhan et al., 1999), and it is negated by single-nucleus RNA-sequencing and scRNA-seq datasets showing that *Npy2r* is not expressed on either pre-adipocytes or adipocytes (Henriques et al., 2020; W. Sun et al., 2020). These contradictions indicate that efforts are needed to find the target of NPY and proper animal models need to be generated to study peripheral sympathetic neuron-derived NPY.

1.3.3 NPY receptors and their downstream pathways

NPY receptors are G-protein-coupled receptors (GPCR) which are integral membrane proteins containing one extracellular N terminus, 7 transmembrane domains and an intracellular C terminus (Rehman & Dimri, 2018). GPCRs are named due to their association with G proteins $G_{\alpha\beta\gamma}$ which connect GPCRs with other enzymes or ion channels or activate downstream pathways upon ligands binding to the extracellular N terminus of GPCRs. There are multiple subunits of $G\alpha$ with different functions as shown in Table 1.2: $G\alpha_s$ activates adenylate cyclase which generates cAMP; $G\alpha_{i/o}$ inhibits adenylate cyclase and activates cGMP phosphodiesterase to decrease cAMP and cGMP; $G\alpha_q$ activates phospholipase C (PLC) which generates IP_3. $G\beta\gamma$ can also activate various enzymes especially Pi3K and K^+ and Ca^{2+} channels (Syrovatkina, Alegre, Dey, & Huang, 2016). There are 4 NPY receptors discovered in humans, namely NPY1R, NPY2R, NPY4R and

Table 1.2: G proteins and their effectors

G proteins	**Well-defined G-protein effectors**
$G\alpha_s$, $G\alpha_{olf}$	Adenylate cyclase (+)
$G\alpha_o$, $G\alpha_{i1}$-$G\alpha_{i3}$, $G\alpha_{t1,2}$, $G\alpha_g$, $G\alpha_z$	Adenylate cyclase (-), cGMP phosphodiesterase (+)
$G\alpha_q$, $G\alpha_{11}$, $G\alpha_{14}$, $G\alpha_{15/16}$	Phospholipase C-β (+), p63RhoGEF
$G\alpha_{12}$, $G\alpha_{13}$	p115RhoGEF, LARG and PDZ-RhoGEF
$G\beta\gamma$ Complex	Adenylate cyclase (+), Phospholipase C-β (+), Phosphoinositide 3 Kinases (PI3K), G protein-coupled receptor kinases, K^+ and Ca^{2+} channels
(+) indicates activation; (-) indicates inhibition	

NPY5R, all of which are associated with $G\alpha_{i/o}$ which can inactivate adenylate cyclase and decrease the concentration of cAMP. Previous studies also indicated that NPY could activate Pi3K and induce the phosphorylation of the downstream mitogen-activated protein kinase (MAPK) such as ERK1/2 in various types of cells including adipose tissue SVF, smooth muscle cells, and cardiomyocytes (Hong et al., 2018; Pons et al., 2008; Yang et al., 2008; Pellieux et al., 2000). This effect might be mediated by $G\beta\gamma$ associated with $G\alpha_{i/o}$. Since the function of NPY is dependent on the type of cells expressing NPY receptors, it is important to determine the target of NPY in the adipose tissue.

1.4 Aim and Hypotheses

Previous studies have linked NPY with adipose metabolism: in mice, KO of NPY receptors result in late-onset obesity without changing daily food consumption (Naveilhan et al., 1999; Pedrazzini et al., 1998); in humans, NPY mutations have been linked to high body-mass index (BMI), but not an unhealthy diet pattern (*Common metabolic disease knowledge portal*, n.d.; Dornbos et al., 2022). However, it is still unclear to which extent adipose tissue is innervated by NPY^+ sympathetic axons; what types of cells are the target of NPY, and most importantly, what effect NPY has on its target and whole-body metabolism. Considering these unknowns, the aims of this research are listed as follows:

- to characterise the anatomy of NPY^+ sympathetic axons in the adipose tissue.
- to determine which type of cells are the target of NPY and the function of NPY on its target.
- to understand the role of sympathetic-neuron-derived NPY in the immunometabolic homeostasis of adipose tissue.

To accomplish these purposes, I applied the tissue-clearing technique to visualise the innervation of adipose tissue, conducted the scRNA-seq analysis to explore the potential target of periphery NPY, and used *in vitro* method to understand the effect of NPY on its target. To specifically study the function of sympathetic-neuron derived NPY, I generated a mouse model that selectively ablates NPY from TH^+ sympathetic neurons, while leaving the brain intact.

2 | Methodology

2.1 Animals

Many different animal models were used in this study for labelling NPY^+ axons, adipose tissue-resident macrophages, and $NPY1R^+$ cells, lineage-tracing thermogenic adipocytes, and generating conditional knockout model to determine the significance of NPY^+ axons in regulating adipose immunometabolism.

All the mice were group-housed in standard housing under a 12-12-hour light-dark cycle and given access to diet and water *ad libitum*. All experimental procedures were performed on living animals following the United Kingdom ANIMALS ACTS 1986 under the project license (PPL number: P80EDA9F7) and personal licenses granted by the United Kingdom Home Office. Ethical Approval was provided by the Ethical Review Panel at the University of Oxford.

2.1.1 Animal models for studying obesity

Two different obesity animal models are widely used: one is the Ob/Ob mouse model where leptin is deficient, and the other is the diet-induced obesity (DIO) model. The Ob/Ob mouse model develops obesity on a normal chow diet (ND) (Y. Zhang et al., 1994), while the DIO model requires HFD treatment for 6-12 weeks to develop obesity. Compared with the Ob/Ob mouse model which resembles congenital leptin deficiency, the DIO model is more relevant to the physiological condition where excessive energy intake results in increased lipid storage in adipose tissue depots. Ob/Ob mice (B6. Lep^{Ob}) used in this research were purchased from the Jackson Lab (JAX); DIO was achieved by treating mice with an HFD (Diet Research, D12492) when they were 7 weeks old, and lasted for 10

weeks. The body weight of each mouse and the food consumption in each cage were recorded weekly.

2.1.2 Reporting and lineage-tracing animal models

Reporting animal models were used for labelling macrophages, NPY^+ axons, and $NPY1R^+$ cells. The lineage-tracing model was used to determine if adipocytes can be lineage-traced to $NPY1R^+$ cells. $Cx3cr1^{GFP/+}$ mice (*Cx3cr1*^{tm1Litt}/LittJ; stock no. 008451), which were used for labelling macrophages, were purchased from JAX. Tissues of NPY-GFP mice (B6.FVB-Tg(Npy-hrGFP)1Lowl/J), which were used for labelling NPY^+ axons, are a gift from Tamas Horvath Lab at Brandy Memorial Laboratory, Yale University. Tissue of $Npy1r^{Cre}$; $Rosa26^{tdTomato}$ mice, which were used for labelling $NPY1R^+$ cells and their descendants, were from Professor Michael Roberts at the Department of Otolaryngology-Head and Neck Surgery, University of Michigan.

2.1.3 Sypathetic neuron-specific NPY-knockout model

To determine the significance of sympathetic neuron-derived NPY, a mouse model with NPY specifically removed from sympathetic neurons was generated by crossing Th^{Cre} mice with $NPY^{flox/flox}$ mice. Th^{Cre} mice (B6.Cg-*7630403G23Rik*$^{Tg(Th\text{-}cre)1Tmd}$/J; stock no. 008601) were purchased at the JAX, and $Npy^{flox/flox}$ mice were a donation from Ivo Kalajzic Lab at the Department of Reconstructive Science, the University of Connecticut(Wee et al., 2019) under MTA.

2.2 Animal dissection

Mice were culled using CO_2 exposure or fix-perfusion before dissection. To cull mice with CO_2 exposure, mice were first put in a chamber connected with

a CO_2 tank. Mice were then exposed to low-concentration CO_2 until they lost their righting reflex. Afterwards, CO_2 concentration was increased and the mice were exposed to high-concentration CO_2 for 3-4 minutes, and death of the mice was finally confirmed by cervical dislocation. To cull mice with the fix-perfusion method, mice were first intraperitoneally injected with 10μL/g Pentoject$^{@}$ (Animalcare, XVD133), e.g. 250μL for a 25g mouse, and their thoracic cavity was opened with scissors after they lost their pedal-withdrawal reflex. A small cut was made on their right atrium, and the mice were perfused with 10mL PBS and 10mL 4% paraformaldehyde (ThermoFisher, 043368.9M) through their left ventricle. Death of mice was confirmed via exsanguination.

2.2.1 Dissection of sympathetic ganglia

Two different sympathetic ganglia were used in this study: SCG and SG.

SCGs are adjacent to the second and third cervical vertebrae (C2 and C3) (Maningat & Munakomi, 2023). To dissect SCGs, the mouse head was cut and placed on a pad with the ventral side facing up and the caudal end oriented towards the operator and pinned at the mouth and trachea. The mouse head was then dissected under a dissecting microscope with two pairs of fine forceps. To find SCGs, muscles around the trachea were removed to make a pair of parallel muscles near the trachea visible, and SCGs were underneath that pair of muscles. Then, the muscles were removed to expose the side closer to the trachea, and the connective tissues with arteries attached to them were lifted with the forceps. The SCG, a piece of rice-shaped pale shiny tissue, was dissociated and cleaned in a petri dish.

SGs are adjacent to the bottom of the first and second ribs. To dissect SGs, the front of the ribcage was removed, and the heart and lungs were entirely removed from the thoracic cavity. The thoracic cavity was then flushed with PBS to remove

blood. Since the SGs are located bilaterally between the spine and the *longus colli* muscles, to expose SGs, fine forceps were used to separate *longus colli* muscles from the spine and the SGs, a long triangular pale tissue, were dissociated and cleaned in a petri dish.

2.2.2 Dissection of brown and white adipose tissues

iBATs were located bilaterally posterior to the scapulae, and to dissect iBATs, an incision was made along the midline of the dorsal of a culled mice, and skin was removed to expose iBATs. Both lobes of the iBATs were moved to a petri dish and cleaned under a dissecting microscope to remove the connective tissue and white adipose tissue attaching to iBATs.

iWATs are located bilaterally at the inguinal region. To dissect iWATs, an incision was made on the skin along the abdominal midline and cut to the left and right sides to separate the skin from the trunk. The skins were flipped to expose the underneath of the skin where iWATs are located, and then iWAT was picked up using forceps removed from the skin using scissors. Isolated iWATs were put in a petri dish to remove any skeletal muscles attaching to it. vWATs were located inside the abdominal cavity. To dissect vWATs, an incision was made on the *rectus abdominis* muscle along the midline of the abdomen, and the vWATs are located at the posterior part of the abdomen. vWATs were then picked with forceps and collected into a petri dish.

2.2.3 Dissection of sympathetic axons

Sympathetic axons were dissected under a dissection microscope with a pair of fine forceps. Adipose tissues were gently dissociated with forceps to expose thick neuron bundles inside the adipose tissue. Neuron bundles were carefully pulled

out from the adipose tissue and further cleaned in a petri dish.

2.3 Immunofluorescent Imaging (IF)

2.3.1 Tissue Fixation

Superior-cervical ganglia (SCG) and sympathetic axon bundles were dissected adipose tissues of mice perfused with 20mL PBS and fixed in 4% paraformaldehyde (ThermoFisher, 043368.9M) for at least 4 hours. Cells collected after *in vitro* experiments were washed once with PBS and fixed using 4% PFA for at least 4 hours. Whole brains or adipose tissues for IF staining were fixed in 4% PFA overnight and washed for 15 minutes in PBS 3 times.

2.3.2 Whole-mount IF

Axon bundles were stained by first incubating with primary antibodies dissolved in the permeabilising buffer (3% BSA, 2% goat serum, 0.1% triton x-100, and 0.1% sodium azide in PBS) overnight at 4°C, followed by incubation with secondary antibodies and DAPI dissolved in the permeabilising buffer for 1 hour with gentle agitation. As for IF in fixed cells, cells were first incubated with the permeabilising buffer for 1 hour at room temperature (RT), and then stained at 4°C overnight with primary antibodies diluted in the permeabilising buffer. Then, samples were washed and stained with DAPI and secondary antibodies for 1 hour at RT. Sympathetic fibres or fixed cells were then mounted on slides with Fluoromount-G mounting medium (ThermoFisher, 00-4958-02).

For whole-mount ganglia staining, PFA-fixed ganglia were dehydrated in 30%, 50%, 70%, and 90% once and twice in 100% ethanol, and the ganglia were kept shaking for 20 minutes at each concentration, and then ganglia were rehydrated

in 90%, 70%, 50%, and 30% ethanol. Afterwards, ganglia were digested with 1.5 U/mL dispase-1 (Roche- 04942078001), 0.5 mg/mL collagenase (Sigma, C2674), and 300μg/mL hyaluronidase (Sigma, H3884) diluted in PBS, shaking in 37°C water bath for 30 minutes. Ethanol-treated ganglia were blocked in blocking solution (3% BSA, 2% goat serum, 0.1% triton x-100, and 0.1% sodium azide in PBS) for 2 hours and then incubated with primary antibodies diluted in the permeabilising buffer for 3 days at 4°C. 3 days later, ganglia were incubated in secondary antibodies diluted in the permeabilising buffer for another 3 days at 4°C. Finally, ganglia were dehydrated in 30%, 50%, 70%, 90% ethanol and twice in 100% ethanol, and were cleared using ethyl cinnamate (ECi). Cleared ganglia were mounted in a coverslip-slide sandwich filled with ECi.

2.3.3 Cryosection and IF

For cryosection, samples were first embedded in OCT (VWR, 361603) and frozen at -20°C until cryosectioning. Samples were cut into 10μm-thick sections and mounted on charged SuperFrost Plus slides (VWR, 631-0108). Afterwards, the samples were stained using the same procedure as fixed cells.

2.3.4 Paraffin embedding and IF

For paraffin-embedding, fixed samples were processed in 70%, 80%, and 90% ethanol, and then in 100% ethanol, 100% xylene, and 60°C paraffin wax 3 times for each condition. The samples were embedded in paraffin wax, sectioned at 7μm, mounted on coverslips, and dried with 45-50°C oven overnight. Before staining, samples were deparaffinised in 100% xylene for 5 minutes twice and rehydrated twice in 100% ethanol, then once in 95%, 80% ethanol, and water for 10 minutes each. Antigen retrieval was done by adding 0.05% trypsin to each slide and incubating at 37°C for 20 minutes. After washing with running water,

the samples were stained using the same procedure as fixed cells.

2.3.5 Adipo-Clear

Whole fat pads were stained and cleared using a modified version of iDISCO as previously described(Renier et al., 2014; Chi, Crane, Wu, & Cohen, 2018). Briefly, white adipose tissues (WATs) were dissected from mice perfused with 20mL PBS and fixed with 4% paraformaldehyde overnight. Tissues were pre-treated with 20%, 40%, 60%, 80% and twice in 100% methanol for 30 minutes each at RT, and then bleached using 5% H_2O_2 diluted in 100% methanol for 24 hours at 4 shaking. Bleached samples were rehydrated using 80%, 60%, 40%, and 20% methanol for 30 minutes each and then in PTwH buffer (0.2% Tween-20, 10Î¼g/mL heparin, and 0.02% sodium azide in PBS) for 30 minutes. Afterwards, samples were incubated in permeabilising solution (20% DMSO, 0.2% Triton x-100, 0.3M glycine in PBS) at 37°C water bath overnight and blocked using blocking buffer (10% DMSO, 2% Triton x-100, 0.02% sodium azide and 5% goat serum in PBS).

For immunolabeling, samples were incubated in primary antibodies diluted in antibody dilution buffer (5% DMSO, 5% goat serum, 0.2% Tween-20 and 10 Î¼g/mL heparin in PBS) at 37°C shaking for 5 days, then washed with PTwH for 1 day, and then incubated with secondary antibodies and DAPI diluted using antibody dilution buffer at 37°C shaking for another 3 days.

Immunolabelled tissues were embedded in 1% agarose and dehydrated in 20%, 40%, 60%, 80%, and 100% methanol for 1 hour each, and then 100% overnight at room temperature. Samples were incubated in dichloromethane (DCM) (Sigma, 270997) until they sank, and then incubated in dibenzyl ether (DBE) (Sigma, 179272) until clear. Samples were stored in DBE at room temperature, and trans-

ferred into ECi before imaging.

2.3.6 Antibodies for IF staining

The following primary antibodies were used for immunofluorescent staining: rat anti-CD31 (BioLegend, 102501, MEC13.3,1:100 dilution), rat anti-PLVAP (BioLegend, 120503, MECA32, 1:100 dilution), rabbit anti-DES (Abcam, AB15200, 1:500 dilution), rabbit anti-NPY (Cell Signalling, D7Y5A, 1:500 dilution), rabbit anti-NPY (Abcam, AB30914, 1:500 dilution), chicken anti-TH (Aves Labs, TYH73787982, 1:500 dilution), rabbit anti-TH (Sigma, Ab152, 1:500 dilution), mouse anti-NPY1R (Santa Cruz, sc-393192, 1:200 dilution), rat anti-PDGFRα (BioLegend, 135902, APA5, 1:200 dilution), rabbit anti-TAGLN (Abcam, AB14106, 1:250 dilution), Cy3 anti-αSMA (Sigma, C6198, 1A4, 1:250 dilution), goat anti-SOX17 (R&D, AF1924, 1:250), goat anti-EPHB4 (R&D, AF3034, 1:250), rabbit anti-UCP1 (Abcam, Ab10983, 1:500).

2.4 Microscopy

2.4.1 Confocal microscopy

Images were acquired using a Zeiss LSM880 confocal microscope with Zen-black software (V2.1). The samples were imaged using a 10$\times$/0.45NA objective, with a 1.04μm, 1.04μm, 3.64μm xyz voxel size, a 20$\times$/0.8NA objective, with a 0.52μm, 0.52μm, 1.00μm xyz voxel size, or a 63$\times$/1.4NA oil-immersion objective, with a 0.13μm, 0.13μm, 1.00μm xyz voxel size. Solid-state 405nm, 561nm, 633nm, and Argon 488 lasers were used for DAPI, AF488, AF546, and AF647 fluorophores respectively.

2.4.2 Light-sheet microscopy

Images of cleared tissues were required using a Miltenyi Biotec Ultramicroscope II light-sheet microscope. The step size was 8Î¼m; the thickness of the light sheet was 3.98μm; the horizontal dynamic focusing was set to 8 steps; and the exposure time was set at 180ms. The samples were illuminated using a bi-directional light sheet and scanned under a 2x/0.5 NA objective, with a 4.03μm, 4.03μm, 8μm xyz voxel size. A 488nm laser with a 525/50 filter, a 561nm laser with a 620/60 filter, and a 638nm laser with a 680/30 filter were used for AF488, AF546, and AF647 respectively.

2.4.3 Dextran-70kDA injection and intravital microscopy

Animals were anaesthetized with ketamine (100mg/kg) and xylazine (10mg/kg) and a small incision was made to expose the epididymal adipose tissue (eWAT) for microscope analysis. Intravital images with space resolution (1024$\times$1024 pixels) from eWAT were obtained by Optical microscope CARS (Coherent Anti-stokes Raman Scattering), TPEF (Two-photon excitation fluorescence) and Bright-field microscope, simultaneously, using confocal LSM 780-NLO Zeiss in the inverted microscope Axio Observer Z.1 (Carl Zeiss AG, Alemanha). All the procedures were performed at the National Institute of Science and Technology on Photonics Applied to Cell Biology (INFABIC) at the State University of Campinas.

The adipocyte images from CARS were acquired using two lines of lasers in a wavelength of λpump=803 nm and λStokes=1040 nm, and fluorescence images were acquired by TPEF using exogenous fluorescence dye Tetramethylrhodamine isothiocyanate dextran (Sigma, T1162) in wavelength of excitation of λStokes=1040nm. After the identification of a blood vessel and acquisition of an initial image, the video was started and after 10 frames, 50μl (30mg/kg) of

Dextran 70KDa (Sigma, T1162) was injected in the orbital plexus of the mice. The video continued recording for approximately 12 minutes to capture vessel fluorescence and leakage.

Fluorescence intensity over time was analysed for the whole duration of the video. A static image was analysed after dextran administration using FIJI. To evaluate tissue leakage, an ROI was selected inside the vessel and another ROI was selected in the tissue (outside the vessel). Fluorescence intensity was measured in both areas. The intensity ratio between the tissue and inside the vessel was calculated. Blood flow was calculated using the average of the raw intensity of Dextran inside the artery over 100 seconds right after the stabilization of the Dextran signal following administration.

2.4.4 Image analysis

The overlapping between TH, NPY and CD31 was calculated using JACoP(Bolte & Cordelières, 2006), a plugin in FIJI(Schindelin et al., 2012). To make this calculation, 472.33μm, 472.33μm, 30μm xyz regions were randomly picked and maximally projected to z using the Fiji script. The labelled areas were automatically segmented using a threshold set by default, and the overlapping percentages were calculated automatically by JACoP.

The innervation of NPY$^+$ axons was quantified using the "Surface" tool in Imaris V9.2. The labelled area of NPY$^+$ axons and CD31$^+$ vessels in whole cleared iWATs were automatically segmented, and the innervation of NPY in vasculature was calculated as $\frac{Volume_{NPY+}}{Volume_{CD31+}}$. The coverage of DES$^+$ mural cells in iWAT was calculated similarly as $\frac{Volume_{DES+}}{Volume_{CD31+}}$. Confocal images showing NPY$^+$ innervation were quantified using FIJI with an automatic unbiased method. $Area_{NPY+}$ and $Area_{CD31+}$ were segmented using the Otsu thresholding method and measured

using the "measure" program.

The percentage of PDGFRα^+ and DES$^+$ cells were counted manually based on the PDGFRα and DES signals. The percentage of TH$^+$ and NPY$^+$ neurons in the hypothalamus and VTA was also counted manually. To calculate the ganglionic mural cell coverage, 531μm, 531μm, 30μm xyz views were randomly picked and maximally projected to z using Fiji script. The labelled areas were segmented using the threshold set by default, and the coverage was calculated as $\frac{Area_{NPY+}}{Area_{CD31+}}$.

The size of adipocytes in WAT and iBAT was quantified as previously described(Parlee, Lentz, Mori, & MacDougald, 2014) using FIJI. Briefly, WAT and iBAT were processed to paraffin-embedded sections (3μm sections), stained with H&E and scanned into digital images using a NanoZoomer-SQ Digital slide scanner -Hamamatsu. Images were randomly picked and the plugin "Analyse Particles" was used to count the number and measure the size of adipocytes and droplets in iBAT. For each iBAT, 11000 lipid droplets were measured.

2.5 Primary cell culture

2.5.1 Isolation of the adipose stromal-vascular faction (SVF)

Dissected adipose tissues were minced and digested in the enzyme mixture (for each sample, 500μL Collagenase II (4mg/mL, C6885), 500μL Hyaluronidase (5.3mg/mL=40000U/mL, H3884), and 5μL Dnase I (BioLabs, M0303L)) in a 37°C-water bath shaking for 45 minutes, and samples were pipetted every 10 minutes. Digestion was stopped by adding FACS buffer (PBS containing 2% FBS), and single-cell suspension was collected by filtering the digested sample using EASYStrainer cell sieves with 70Î¼m mesh (Greiner, 542070).

2.5.2 Purification of mural cells from the adipose SVF

Mural cells were isolated and cultured following a modified version of the protocol previously published(Tang et al., 2022). Briefly, the mice were euthanised by i.p. injection with 10μL/g pentobarbital and perfused with 15mL PBS to remove blood. The stromal vascular fraction (SVF) of the iBATs was isolated using the method described above. Then, the cells were seeded in 10cm dishes with 10mL DMEM with 10% FBS for 2 days for the cells to attach to the bottom. Afterwards, 5mL of the medium was replaced with mural cell-specific medium (DMEM with 2% FBS supplied with 1% mural cell-growth supplement (Science Cell, 1252)). 5mL of the medium in the dishes was refreshed every 2 days until the cells grew confluent. To get pure mural cells, cells were labelled with an APC anti-CD104b antibody (BioLegend, 136007), and mural cells were sorted using MojoSort^{TM} magnetic sorting protocol with MojoSort^{TM} buffer (BioLegend, 480017) and anti-APC nanobeads (BioLegend, 480071).

2.5.3 *In vitro* differentiation of adipocytes

2.5.3.1 White adipocytes

To differentiate 3T3-L1 cells into white adipocytes, cells were seeded in 12-well plates at a density of 1×10^5 cells/mL. The medium was refreshed until the cells were confluent. 2 days after the cells were confluent, induction medium (10% FBS, 500μM 3-Isobutyl-methylxanthine and 1μM dexamethasone in DMEM) with or without 1μg/mL insulin were added into each well. 3 days later, the induction medium was replaced with the maintenance medium (DMEM with 10% FBS and with or without 1μg/mL insulin). Afterwards, the medium was refreshed with the maintenance medium every 2 days. The total differentiation time for each well was 8 days. NPY treatments in the experimental groups started when the induction

medium was added and lasted through the whole differentiation process.

2.5.3.2 Beige-like adipocytes

SVF and mural cells were differentiated into thermogenic adipocytes as previously published(Oguri et al., 2020). SVF and mural cells were isolated and seeded in 12-well plates at 1×10^5 cells/mL. When cells reach 95% confluency, beige cell induction medium (DMEM with 10% FBS, 125μM Indomethacin, 5μM Dexamethasone, 500μM 3-Isobutyl-methylxanthine, and 0.5μM Rosiglitazone) was added to each well. 2 days later, the induction medium was replaced with maintenance medium (DMEM with 10% FBS, 5μg/mL Insulin, and 1nM Triiodothyronine). Afterwards, the maintenance medium was refreshed every 2 days. The total differentiation time for each well was 8 days. NPY treatments in the experimental groups started when the induction medium was added and lasted through the differentiation process. Oxygen consumption was measured using a Seahorse XF Analyzer.

2.5.4 Proliferation assay with EdU

Cell proliferation assay was done with Click-iT EdU Cell Proliferation Kit for imaging (Thermo Fisher, C10340). Mural cells were seeded at 0.5×10^5 cells/ml in 12-well plates on coverslips and cultured overnight before the experiments. Afterwards, cells were labelled with EdU and cultured with or without 1μM NPY or 2μM PD98059 (Cell Signalling 9900S) for 6 hours in medium for mural cells (low-glucose DMEM with 2%FBS). Cells were then fixed with 4% PFA and permeabilising buffer for 30 minutes respectively, and EdU was labelled with AF647 using the Click-iT Plus reaction cocktail. After IF staining with anti-DES, cells were imaged using a Zeiss LSM880 confocal microscope with Zen-black software (V2.1), with a 20×/0.8NA objective, a 0.52μm, 0.52μm, 1.00μm xyz voxel size.

An area of 3072×3072 pixels was imaged for each biological replicate.

The percentage of EdU^+ cells was counted with an unbiased automatic method using "detect particles" in FIJI. The threshold was set automatically using the Otsu thresholding method.

2.5.5 Oxygen consumption assay

The oxygen consumption of differentiated adipocytes was measured using a Seahorse XF Analyzer. The basal oxygen consumption rate was recorded when no drugs were added to the cells; the oxygen consumption caused by proton leak was recorded after oligomycin, an ATP synthase inhibitor was added; the maximal respiratory rate was recorded when FCCP, an uncoupler was added; non-mitochondrial respiration was measured when antimycin A and rotenone were added to disrupt the whole electron transport chain of oxidative phosphorylation. The principle of oxygen consumption assay is shown below in Figure 2.1 (Rose et al., 2014).

2.6 Quantitative real-time qPCR

2.6.1 Isolation of mRNA

To isolate mRNA from cultured cells, 1mL Trizol reagent (Thermofisher, 15596026) was added to each well, and the culturing dish or well plate was gently shaken to facilitate cell lysis. After keeping at RT for 5 minutes, liquid in each well was mixed by pipetting, and lysate was collected into EP tubes. 200μL chloroform was added to each tube, and tubes were vortexed for 15 seconds and kept at RT for 5 minutes before centrifuging at 4°C, 12,000 relative centrifugal force (RCF) for 15 minutes. Afterwards, the transparent layer was collected, mixed with 500μL

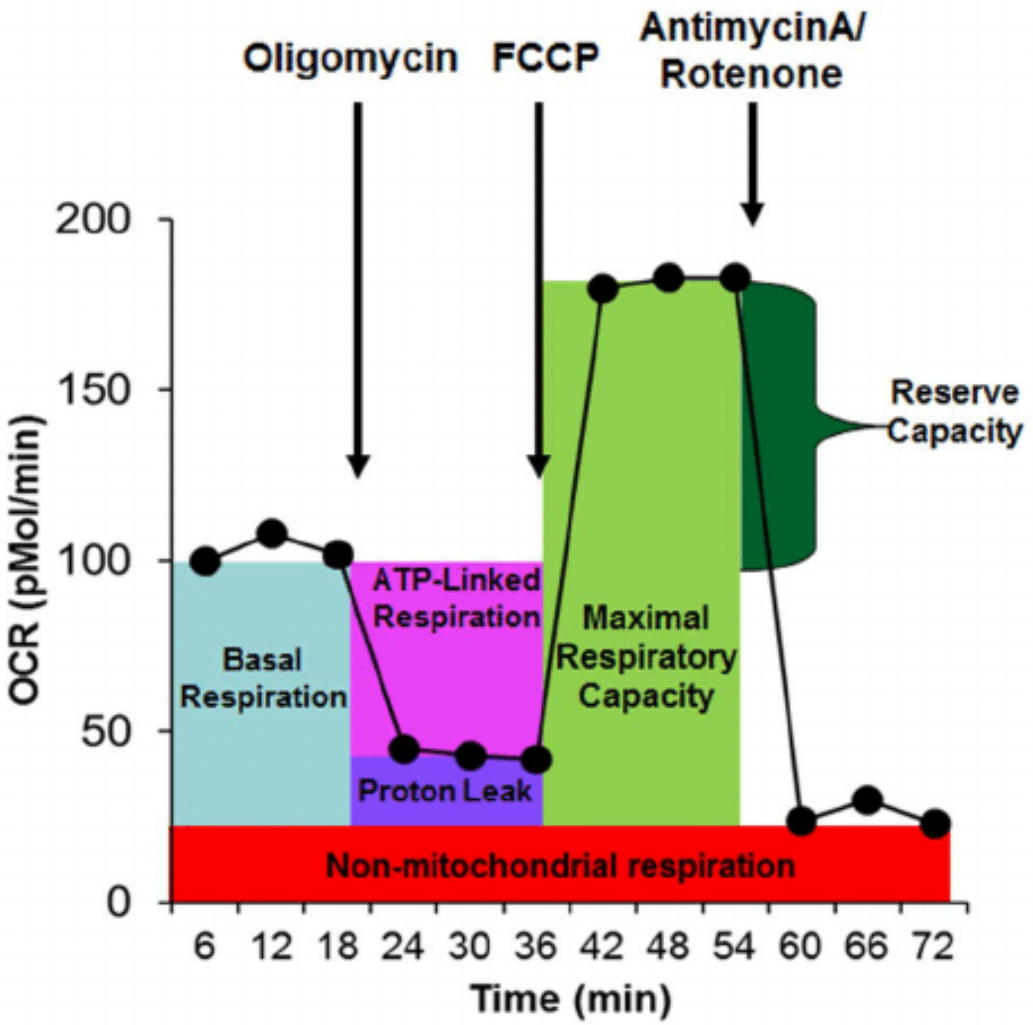


Figure 2.1: **The principle of oxygen consumption assay**

isopropanol, and incubated at -20°C for 15 minutes. Then, the tubes were centrifuged at 4°C, 12,000 relative centrifugal force (RCF), and the supernatant was removed. Finally, the pellets were washed with 75% ethanol, and dissolved with about 20μL nuclease-free water.

To isolate mRNA from whole tissues, tissues were put into homogenising tubes (Precellys, MK28-R-2mL) and homogenised using a Precellys 24 Touch Homogenizer for 30 seconds twice. The tubes were kept at RT for 5 minutes for complete lysis and then centrifuged at 4°C, 12,000 RCF for 10 minutes, and the lysate was collected in EP tubes. When collecting lysate from lipid-rich tissues such as brains and adipose tissue, the lipid layer was first removed, and the clear part was collected into EP tubes. The following steps were the same as those of isolating mRNA from cells.

After resuspending isolated mRNA with water, mRNA concentration and purity were measured using a NanoDrop ND-1000 UV Vis Spectrophotometer.

2.6.2 First-strand synthesis of cDNA

To synthesise cDNA, 1000ng mRNA was added into 20μL tubes and topped up with nuclease-free water to 10μL. A mixture of 1μL dNTP, 0.1μL random primers, and 0.9μL water was added to each tube, and tubes were incubated at 65°C for 5 minutes. Then, a mixture of 4μL 5X First-strand buffer, 2μL DTT, and 1μL RNAsae-OUT (Invitrogen, 10777019) was added to each tube. After 2-minute incubation at RT, a mixture of 0.25μL Superscript II Reverse Transcriptase (Invitrogen, 18064022) and 0.75μL water was added into each tube. After mixing well, the tubes were put in a PCR thermal cycler with the following steps set up:25°C for 10 minutes; 42°C for 50 minutes; 70°C for 15 minutes.

2.6.3 qPCR and the list of primers

qPCR was done using Power SYBR Green PCR Master Mix (LifeTech 4368706). Data were recorded using a StepOneTM qPCR system and analysed using StepOne Software v2.3. Primers used in this research are shown in Table2.1.

2.6.4 Data analysis

qPCR data were analysed using either ΔCt method, where the relative expression levels were calculated as $2^{-(Ct_{targetgene}-Ct_{referencegene})}$, or $\Delta\Delta$Ct method where the relative expression levels were calculated as $2^{\Delta Ct_{Experimental}-\Delta Ct_{NegativeControl}}$.

2.7 Flow cytometry and cell sorting

2.7.1 Single-cell suspension

To get single-cell suspensions from adipose tissues, Dissected adipose tissues were minced and digested in the enzyme mixture (for each sample, 500Î¼L Collagenase II (4mg/mL, C6885), 500μL Hyaluronidase (5.3mg/mL=40000U/mL, H3884), and 5μL Dnase I (BioLabs, M0303L)) in a 37°C-water bath shaking for 45 minutes, and samples were pipetted every 10 minutes. Digestion was stopped by adding FACS buffer (PBS containing 2% FBS), and single-cell suspension was collected by filtering the digested sample using EASYStrainer cell sieves with 70μm mesh (Greiner, 542070).

2.7.2 Staining

To prepare the samples for sorting or flow cytometry, cells were first treated with red-blood-cell lysis buffer (BioLegend, 420301) to remove red-blood cells, and

Table 2.1: The sequences of primers for RT-qPCR

Gapdh	Forward	5'-AACTTTGGCATTGTGGAAGG-3'
	Reverse	5'-ACACATTGGGGGTAGGAACA-3'
Hprt	Forward	5'-CAGTCCCAGCGTCGTGATTA-3'
	Reverse	5'-TGGCCTCCCATCTCCTTCAT-3'
Plin1	Forward	5'-TAGAGTTCCTCCTGCCACCA-3'
	Reverse	5'-GTGCTGACCCTCCTCACAAG-3'
Pparg	Forward	5'-TCAAGGGTGCCAGTTTCG-3'
	Reverse	5'-GGAGGCCAGCATCGTGT-3'
Des	Forward	5'-TCCAGTCCTACACCTGCGAGAT-3'
	Reverse	5'-CGCAATGTTGTCCTGATAGCCA-3'
Npy	Forward	5'-CCCCAGAACAAGGCTTGAAG-3'
	Reverse	5'-TTGGAAAAGTCGGGAGAACAA-3'
Npy1r	Forward	5'-CTGATGGACCACTGGGTCTT-3'
	Reverse	5'-GAAGAAGCCACTGCAAGGAC-3'
Npy2r	Forward	5'-ATCATCTTGCTAGGGGTAGTTGG-3'
	Reverse	5'-CGGACCCATTTTCCACTCTCC-3'
Npy5r	Forward	5'-GTGAACTTTCTCATAGGCAACCT-3'
	Reverse	5'-GCATGATATGGCACATGGCTTT-3'
Pdgfrb	Forward	5'-AGGACAACCGTACCTTGGGTGACT-3'
	Reverse	5'-CAGTTCTGACACGTACCGGGTCTC-3'
Rgs5	Forward	5'-CAAAATGGCGGAGAAGGCAA-3'
	Reverse	5'-CCAAGTCAAAGCTGCGAGGA-3'
Tgfb1	Forward	5'-TGATACGCCTGAGTGGCTGTCT-3'
	Reverse	5'-CACAAGAGCAGTGAGCGCTGAA-3'
Cidea	Forward	5'-TGCTCTTCTGTATCGCCCAGT-3'
	Reverse	5'-GCCGTGTTAAGGAATCTGCTG-3'
Pgc1a	Forward	5'-CCCTGCCATTGTTAAGAC-3'
	Reverse	5'-TGCTGCTGTTCCTGTTTTC-3'
Ucp1	Forward	5'-ACTGCCACACCTCCAGTCATT-3'
	Reverse	5'-CTTTGCCTCACTCAGGATTGG-3'
Prdm16	Forward	5'- CAGCACGGTGAAGCCATT-3'
	Reverse	5'-GCGTGCATCCGCTTGTG-3'
Serca2b	Forward	5'-ACCTTTGCCGCTCATTTTCCAG-3'
	Reverse	5'-AGGCTGCACACACTCTTTACC-3'
Angpt1	Forward	5'-TGCAGCAACCAGCGCCGAAA-3'
	Reverse	5'-CACGGCAGTTCCCGTCGTGT-3'
Tnf	Forward	5'- ATGAGCACAGAAAGCATGA-3'
	Reverse	5'- TACAGGCTTGTCACTCGAA-3'

treated with Fc block (ThermoFisher, 14-9161-73) before staining with antibodies. Before immunolabelling for intracellular markers, cells were fixed and permeabilised using the eBioscience Intracellular Fixation and Permeabilization Buffer Set (ThermoFisher, 88-8824-00). Cell sorting was done using a BD FACSAria III sorter, and flow cytometry data were acquired using a BD FACSAria III sorter or a BD LSRFortessa X20 cytometer with a BD FACSDiva v6.0 software. Cytometry data were analysed using FlowJo v10.8.1.

2.7.3 Antibodies for flow cytometry or cell sorting

The following antibodies were used for FACS and flow cytometry: AF700 anti-CD45 (BioLegend, 103128), BUV395 anti-CD45 (BD Horizon, 564279), Pacific Blue anti-CD31 (BioLegend, 102421), APC anti-PDGFRα (BioLegend 135907), AF488 anti-NG2 (Sigma, MAB5384A4), and AF488 anti-DES (Abcam, AB185033, Y66). All antibodies for FACS and flow cytometry were diluted at 1:500. LIVE/DEAD^{TM} Fixable Near-IR Dead Cell Stain Kit (1:1000, ThermoFisher, L10119) was used for live/dead staining.

2.8 Enzyme-linked immunosorbent assay (ELISA)

2.8.1 Sample preparation

2.8.1.1 Blood plasma

To do terminal blood collection, the mice were euthanised by i.p. injection with 10μL/g pentobarbital, and then blood was collected from the left ventricle using 25G needles and syringes coated with 100 mM EDTA. The blood was then put into tubes with 5μL 100mM EDTA and centrifuged at 1000$\times$ rgf at 4°C for 15 minutes to separate blood plasma from blood cells, and then the supernatant was moved to

new tubes with DPP-IV inhibitor (final concentration 50μM) and Aprotinin (final concentration 500 KIU/mL).

2.8.1.2 Protein extraction from adipose tissue

Proteins were extracted from iWATs as previously described in a published paper. Briefly, dissected iWATs were put in homogenising tubes filled with 300μL/50mg RIPA lysis buffer (Sigma, 20188) containing 50μM DPP-IV inhibitor (Sigma, DPP4-010) and 500KIU/mL Aprotinin (Sigma, A6103-1MG) and homogenised using Precellys 24 homogeniser. The lipid in the tissue homogenise was removed by centrifuging the tissue homogenise at 20000x rcf at 4°C for 15 minutes, and the clear part was kept. The process was repeated 3 times to remove lipids completely.

2.8.2 Methodology

The concentration of NPY in the iWAT and blood plasma of mice was determined using an NPY ELISA kit (Merck, EZRMNPY-27K). ELISA data were recorded using a FLUOstar Omega microplate reader with Omega v6.20 software.

2.9 Metabolic phenotyping

2.9.1 Thermo-imaging

Animals with 12-14 weeks were used for thermoimaging. Data in Figure 5E were recorded using Optris thermo-cameras (Optris PI 160 with standard 61 lens, Optris GmbH, Berlin, Germany), and Data in Supplementary Figure 16F were recorded using an FOTRIC 225s infrared camera and analysed using FOTRIC software. Animals were single-housed and put under the thermo-cameras, and their backs were shaved to expose skin above iBATs. Animals were acclimatised for 4 days

in individual cages with *ad libitum* access to food and water at room temperature under a 12/12 light-dark cycle before a 14-hour fast. Mice have *ad libitum* access to water during fasting.

iBAT temperature was recorded every second for 6 days by storing the temperature of the warmest pixel in view using the software provided by the camera's manufacturer (Optris PIX Connect, Optris GmbH). The iBAT temperature at 0 and 14 hours was an average of temperatures during a one-hour period.

2.9.2 Cold challenge and rectal temperature measurement

Animals with 20 weeks were single-housed in a thermoneutral environment (31°C, 50% humidity) under a 12/12 light-dark cycle for a week, with ad libitum access to food and water. Afterwards, the mice were cold-challenged at 4°C, and their rectal temperatures were measured every hour. Animals were sacrificed immediately after 8-hour cold exposure, and their iBATs were harvested for RT-qPCR analysis.

Mice's rectal temperatures were measured using a rectal probe. To conduct measurements, mice were gently put on a frame which they could grab, and the rectal probe was covered with Vaseline and inserted into the anus of the mice. The temperature was then recorded after the number was stabilized.

2.9.3 Metabolic cage

2.9.3.1 Local-motor activity

Animals with 8-9 weeks were analyzed for spontaneous locomotor activity (Panlab; Harvard Apparatus; LE001 PH Multitake Cage). Animals were maintained in individual cages, following a 12h light/dark cycle, with water and food sup-

plied *ad libitum*, and controlled room temperature (21-23°C) and humidity. Data was collected for 72 hours, after a one-day acclimatation period. The activity was recorded by COMPULSE v1.0 Software (PanLab). Animals with 7-9 weeks were analyzed for body composition using Minispec LF50 (Brucker).

2.9.3.2 Indirect calorimetry

Animals with 6 weeks were analyzed for Oxygen Consumption (V_{O2}), Carbon Dioxide Production (V_{CO2}), Energy Expenditure (EE) and Respiratory Exchange Rate (RER) using an indirect calorimetry system (Panlab; Harvard Apparatus; LE405 Gas Analyzer and Air Supply & Switching). Animals were maintained in individual cages, following a 12h light/dark cycle, with water and food supplied *ad libitum*, and controlled room temperature (21-23°C) and humidity. Metabolic data was collected for five days, after a two-day acclimatation period. Animal's body weight (g) and food (g) were measured before entering, and after exiting the cage. Results were normalized by weight, and graphs and statistical analysis were obtained using the CalR Web-based Analysis Tool for Indirect Calorimetry Experiments.

2.10 Single-cell RNA-sequencing (scRNA-Seq) analysis

Public scRNA-Seq datasets were downloaded from GEO and were analysed using the following method. Cells with <200 unique detected genes or >5% mitochondrial counts were discarded. After filtering, the gene x cell matrix was normalised using "NormalizeData()" in Seurat v4.2.0(Hao et al., 2021) in the R (v4.2.2) environment. Then, the data were scaled using "ScaleData()", and we performed linear dimensional reduction by PCA and calculated UCMP coordinates for all

cells using Seurat v4.2.0. The cells were clustered using "FindNeighbour()", with dimensions set to 15 and "FindClusters()", with resolution set to 0.5. Each cluster was identified based on differentially expressed genes and known markers in published literature(Muhl et al., 2020; Carr et al., 2019; Shamsi et al., 2021; Henriques et al., 2020; Kalucka et al., 2020; Emont et al., 2022).

2.11 Statistics

GraphPad Prism v.9.5.0 was used for statistical analysis. Mean and standard error of the mean (SEM) were used to represent a sample. Chi-square test and paired two-tailed Student T-test were used to compare two samples; ANOVA was used to compare multiple data points.

All experiments were replicated at least twice with the same conclusion and all *in vivo* experiments were replicated in at least 2 independent cohorts. The exact numbers of replicated experiments are stated in each figure legend. Samples and animals were randomly allocated to experimental groups and proceeded in experiments, and data were collected and analysed blind, and ad hoc registered to groups or genotypes.

3 | Anatomical Analysis of NPY$^+$ Sympathetic Neurons and Their Targets in Adipose Tissue

3.1 Introduction

3.1.1 NPY$^+$ neurons in the sympathetic nervous system (SNS)

NPY exists in the SNS. Previous research using IF staining demonstrated NPY$^+$ immunoreactivity in the sympathetic ganglia (LUNDBERG et al., 1982), and further *ex vivo* research indicates that NPY is co-released with NE in isolated rat *vas deferens* (Torres, Bitran, & Huidobro-Toro, 1992). However, NPY and TH, a marker for the SNS, are not 100% co-localised, a paper published in 1986 indicates that there are some NPY$^-$TH$^+$ neurons in the rat SG; although the iBATs are intensely innervated by TH$^+$ axons, NPY$^+$ axons sparsely appear in in the parenchyma (Cannon et al., 1986). A recently published scRNA-Seq dataset of the SNS also indicates that not all the sympathetic neurons express *Npy*: only 2 out of 5 clusters of neurons in the sympathetic ganglia are NPY$^+$ (Furlan et al., 2016), as shown in Figure 3.1a-c. To confirm this scRNA-Seq dataset, I immunolabelled for TH and NPY in SCG and SG, and by quantifying the images as shown in Figure 3.1d-e, I found that about 40% of sympathetic neurons are NPY$^+$ (Figure 3.1f). These data indicate that NPY is not just a redundant marker for sympathetic neurons in the periphery in that it marks a certain subgroup of sympathetic neurons.

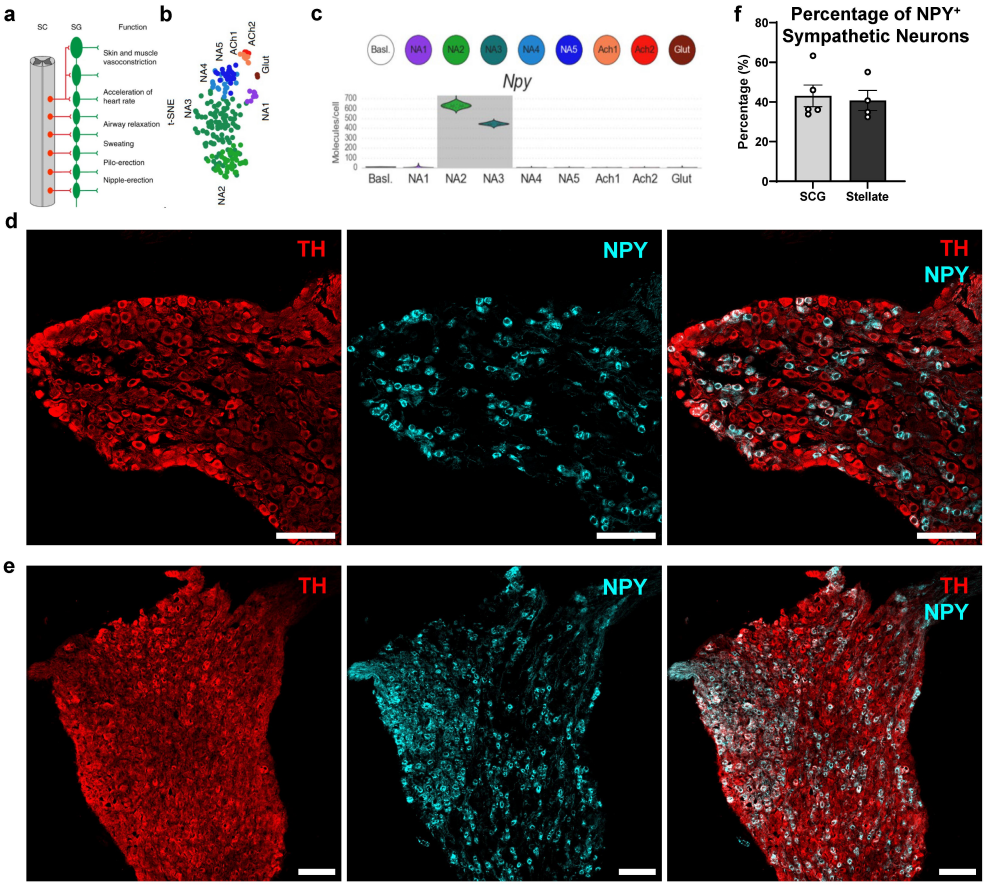


Figure 3.1: **40% neurons in sympathetic neurons express *Npy*.** (a) Schematic showing the tissues innervated by each sympathetic ganglia. (b) A scRNA-Seq dataset of sympathetic ganglia chain published by Linnarsson Lab to show the clustering of neurons. (c) Violin plot showing the expression of Npy.(d-e) Confocal image of cryo-sectioned (d) superior-cervical ganglion (SCG) and (e) stellate ganglia (SG) of ND-treated WT male 8-week-old mice stained with anti-TH (red) and anti-NPY (cyan). Scale bar=100μm. (f) The percentage of NPY$^+$ sympathetic neurons quantified based on images as in Extended Data Fig. 5d-e (n=5 sections from 3 mice).

3.1.2 NPY$^+$ axons in tissues

Since NPY exists in the SNS, NPY can be detected in sympathetic axons. Previous research using NPY anti-serum detects NPY$^+$-immunoreactivity (IR) in axons around vessel-like structures in iBATs and hearts (Cannon et al., 1986; Masliukov et al., 2016). However, it is still not clear to which extent NPY$^+$ axons innervate the vasculature of the adipose tissue and what percentage of sympathetic axons are NPY$^+$.

3.1.3 NPY-receptors in tissues

NPY receptors include NPY1R, NPY2R, NPY4R, and NPY5R. In the periphery, NPY1R is detectable in the adipose tissue (Castan et al., 1993), heart (Ejaz, LoGerfo, Khabbaz, & Pradhan, 2011), intestine (Jackerott & Larsson, 1997), and blood vessels (Grundemar et al., 1992). NPY2R is mainly detectable in presynaptic neurons and can modulate neurotransmitter release (Wahlestedt, Yanaihara, & Håkanson, 1986). NPY5R is expressed in the gastrointestinal tract and has a high affinity for PYY, a gastrointestinal hormone belonging to the NPY family (Lundell et al., 1995). Although the existence of NPY receptors in tissues can be detected, due to the lack of good antibodies targeting NPY1R, it remains unclear which types of cells express *Npy1r* and the distribution of those types of cells in tissues. The impact of these NPY receptors on adipose tissue has been studied using conventional global knockout mice. Contradictory to the traditional idea that NPY receptors can affect body weight by controlling appetite, the loss of NPY receptors leads to late-onset obesity without increases in food intake (Naveilhan et al., 1999; Pedrazzini et al., 1998; Nguyen et al., 2012). Taken together, these results point to a role of NPY in body weight homeostasis independently of regulating appetite.

3.2 Methodology

In this chapter, I aim to analyse the anatomy of NPY$^+$ axons in the adipose tissue, specifically the percentage of NPY$^+$ axons in sympathetic axons and the compartment innervated by NPY$^+$ axons. To achieve this goal, I used the adipoclearing technique and light-sheet microscopy to visualise the inside of iBATs and iWATs. Also, I aimed to determine the type of cells able to respond to NPY and to achieve this, I reanalysed public scRNA-Seq datasets of iBATs and iWATs and used NPY1R-reporter mice to characterize NPY1R$^+$ cells in the adipose tissue.

3.3 Results

3.3.1 One-third sympathetic axons in adipose tissue are NPY$^+$

The public single-cell RNA-sequencing (scRNA-Seq) dataset of sympathetic ganglia (Furlan et al., 2016) reveals that only two out of five clusters of sympathetic neurons express elevated levels of NPY (Figure 3.1a-c). This proportion of NPY$^+$ sympathetic neurons, approximately 40%, was confirmed by immunofluorescent (IF) co-staining of NPY and the sympathetic neuron marker tyrosine hydroxylase (TH) in superior cervical ganglia (SCG) and stellate ganglia (SG) (Figure 3.1d-f). A similar TH/NPY overlap was also observed in sympathetic axon bundles dissected from the inguinal adipose tissue (iWAT) (Figure 3.2a). In iWAT, NPY$^+$ axons are associated with the vasculature and form a plexus around the vessels (Figure 3.2b).

To determine the distribution of TH$^+$ and NPY$^+$ axons throughout the adipose tissue, I performed tissue clearing of the iWAT (Chi, Crane, et al., 2018) and immunolabelled for TH, NPY and CD31, the latter of which marks the vascular

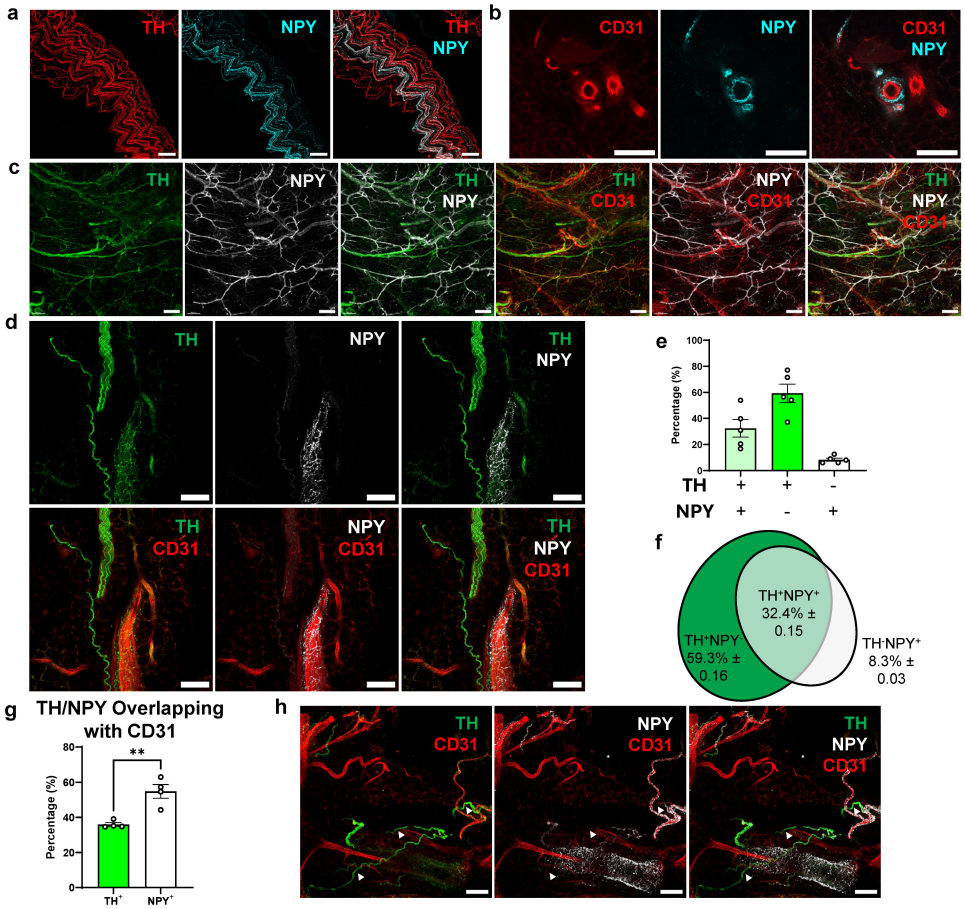


Figure 3.2: **A third of sympathetic axons in iWAT and iBAT are NPY$^+$ and preferentially innervate the vasculature.** (a) Confocal image of an axonal bundle from the iWAT, stained with anti-TH (red) and anti-NPY (cyan). Scale bar=50μm.(b) Confocal image of a capillary within a cleared iWAT stained with anti-CD31 (red) and anti-NPY (cyan). Scale bar=100μm.(c) Confocal images of cleared iWAT stained with anti-TH (green), anti-NPY (white), and anti-CD31 (red). Scale bar=50μm. (d) Confocal images of cleared iWAT as in (c) stained with anti-TH (green), anti-NPY (white), and anti-CD31 (red). Scale bar=100μm. (e-f) The quantification of images as in (d) for TH/NPY overlap: TH$^+$NPY$^-$ (dark green), TH$^+$NPY$^+$ (light green), and TH$^-$NPY$^+$ (white). The percentage is shown via (e) histogram and (f) Venn diagram (n=5 views from 3 mice). (g) The quantification of images as in (d) shows the proportion of TH$^+$ and NPY$^+$ axons overlapping with CD31$^+$ endothelial cells. (h) Confocal Images of cleared iBAT from lean adult male mice stained with anti-TH (green), anti-NPY (white), and anti-CD31 (red). White arrows in the images indicate TH$^+$NPY$^-$ axons. Scale bar=100μm.

endothelium. I confirmed that NPY^+ axons are a subgroup of sympathetic axons (Figure 3.2a-c). Quantifying the images, I found that TH^+NPY^+ axons make up 32.4% of all labelled axons, while 59.3% are TH^+NPY^- (Figure 3.2e-f). The images also indicate that NPY^+ axons preferentially innervate $CD31^+$ endothelium, and this was confirmed by quantifying images (Figure 3.2g). Consistent with iWAT, in intrascapular BAT (iBAT), NPY^+ axons mainly innervate the vasculature (Figure 3.2h).

3.3.2 Non-neuron cells in adipose tissue do not express NPY

In the confocal images showing NPY^+ axons in adipose tissues, the NPY stains are exclusively axonal, which negates the previous conclusion that NPY can be secreted in various non-neuron cells including white adipocytes (Yang et al., 2008), fibroblasts (Killough, Lundy, & Irwin, 2010), and macrophages (Singer et al., 2013), which may be caused by the unspecificity of antibodies or PCR primers (Kumari et al., 2018). Recently published scRNA-Seq datasets of the stromal-vascular fraction (SVF) of murine iWAT and iBAT (Shamsi et al., 2021; Henriques et al., 2020) also favour that NPY is not detected in any type of cells in the SVF including macrophages (Figure 3.3a-d), which means that NPY is only sourced from neurons or plasma in the adipose tissue. Consistently, using qPCR, I did not detect Npy expression in sorted ATMs from $Cx3cr1^{GFP/+}$ reporter mice, despite the positivity of the *Adgre1* (F4/80) control (Figure 3.3e-f).

Besides ATMs, another group of macrophages exists in the adipose tissue, the sympathetic neuron-associated macrophages (SAMs) (Pirzgalska et al., 2017). These macrophages are in close contact with sympathetic neurons and sympathetic axons and differ from ATMs in that they express NET and higher MAOA. To confirm that NPY does not exist in SAMs, I isolated sympathetic axon bundles from the adipose tissue of lean and obese $Cx3Cr1^{GFP/+}$ reporter mice and

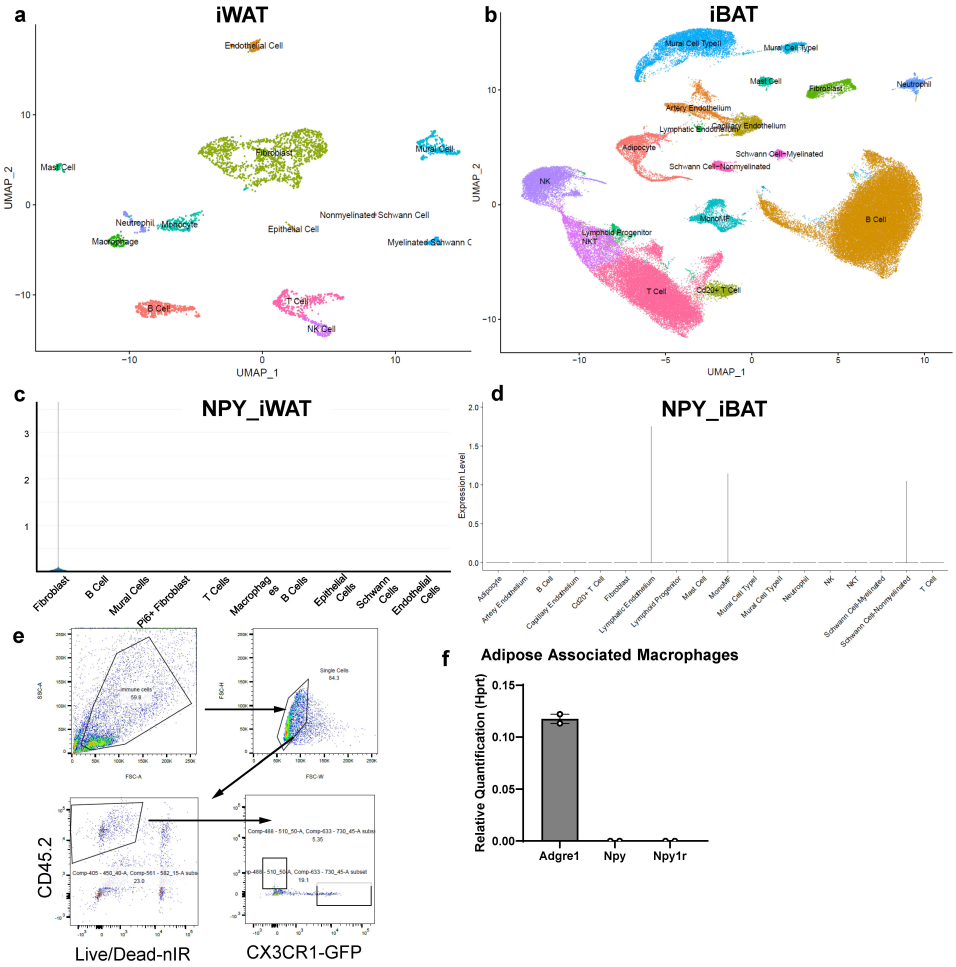


Figure 3.3: **Npy is not expressed in adipose tissues, and NPY receptors are not expressed in macrophages.** (a-b) Embedding plots showing different clusters of cells in the SVF of murine (a) iWAT1 and (b) iBAT2. (c-d) Violin plot showing the expression of Npy in the SVF of murine (c) iWAT and (d) iBAT. (e) Gating strategy of sorting adipose-associated macrophages (ATM) from Cx3cr1$^{GFP/+}$ reporter mice. ATMs were sorted as live/CD45.2^{+}/GFP^{+} cells. (f) The expression of *Adgre1* (F4/80), *Npy*, and *Npy1r* in adipose associated macrophages (ATM) (n=2). (g) Gating strategy for sorting mural cells from the SVF of the iWAT. Mural cells (green box) are sorted as live/CD31^{-}/CD45^{-}/PDGFRα^{-}/NG2^{+} cells; immune cells (blue box) are sorted as live, CD31^{-}/CD45^{+} cells. All values are expressed as mean $\pm$ SEM

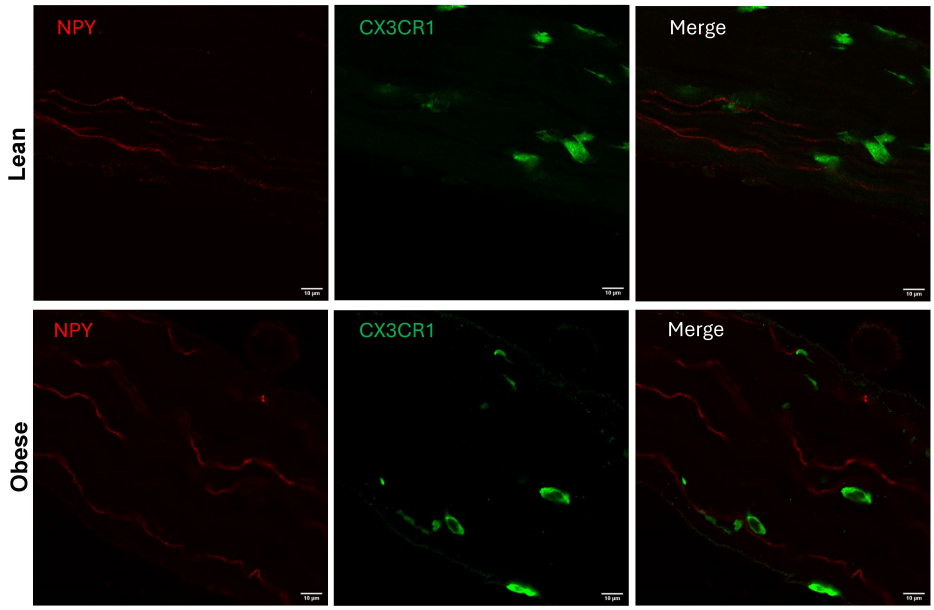


Figure 3.4: **NPY does not exist in SAMs.** Immunofluorescent staining of NPY (Red) in lean and obese male Cx3cr1$^{GFP/+}$ reporter mice to show NPY (red) and macrophages (green) do not colocalise with each other. Scale bar=100 μm

confirmed that NPY does not exist in SAMs (Figure 3.4).

3.3.3 NPY^{+} axons preferentially innervate 4-6th orders of arterial branches

The images of cleared adipose tissues demonstrate that NPY^{+} axons preferentially innervate the vasculature of adipose tissue. To further determine which vessel branches are innervated by NPY^{+} axons, I quantified light-sheet images as in Figure 3.5a and found that the density of NPY^{+} axons is the highest in 5th-order branches (Figure 3.5c-d), while NPY^{+} axons do not innervate the 8th-order branches (Figure 3.5b-d).

Blood vessels can be classified as arteries, veins and capillaries based on their structures and functions. To identify whether arteries or veins are innervated by

NPY$^+$ axons in adipose tissue, we co-stained iWAT for NPY and EPHB4, a vein marker (H. U. Wang, Chen, & Anderson, 1998), or SOX17, an artery marker (Kim et al., 2023). The images show that NPY$^+$ axons do not innervate EPHB4$^+$ vessels, while they innervate SOX17$^+$ vessels (Figure 3.5e-f). Based on these observations, I conclude that NPY$^+$ sympathetic axons in adipose tissue preferentially innervate arterioles but not veins or venules.

3.3.4 Mural cells in adipose tissue highly express NPY1R

Since NPY$^+$ axons innervate the vasculature, it is likely that endothelial cells and perivascular cells including mural cells, fibroblasts and macrophages can potentially be the target of NPY. By reanalysing the scRNA-Seq dataset of iWAT (Henriques et al., 2020) and iBAT (Shamsi et al., 2021), I found that *Npy1r* is highly expressed in mural cells that are marked by *Des*, *Myh11*, *Acta2* (αSMA), *Tagln*, *Cspg4* (NG2), and *Pdgfrb*, and NPY1R is a *bona fide* marker for mural cells within iWAT and iBAT (Figure 3.6a-d; Figure 3.3a-b). To validate the scRNA-Seq datasets by qPCR, we sorted mural cells (live/CD31$^-$/CD45$^-$/PDGFRα^-/NG2$^+$ cells) and immune cells (live, CD31$^-$/CD45$^+$ cells) from the SVF of iWAT and iBAT (Figure 3.3g) and performed qPCR. We independently confirmed that *Npy1r* and *Des* are highly expressed in mural cells but not in immune cells (Figure 3.6e).

To confirm the existence of NPY1R in mural cells at the protein level, I dissected fine blood vessels from the adipose tissue and stained them with anti-CD31 and anti-NPY1R. I detected an NPY1R$^+$ cell wrapping the vessel (Figure 3.6f), whose morphology matches that of mural cells of fine capillaries, which are conventionally named pericytes (Attwell, Mishra, Hall, OFarrell, & Dalkara, 2016).

The analysis of the scRNA-Seq dataset also indicates the localisation of ^{Npy1r} with mural cell markers including *Acta2* (αSMA), *Myh11*, and *Tagln* (Figure

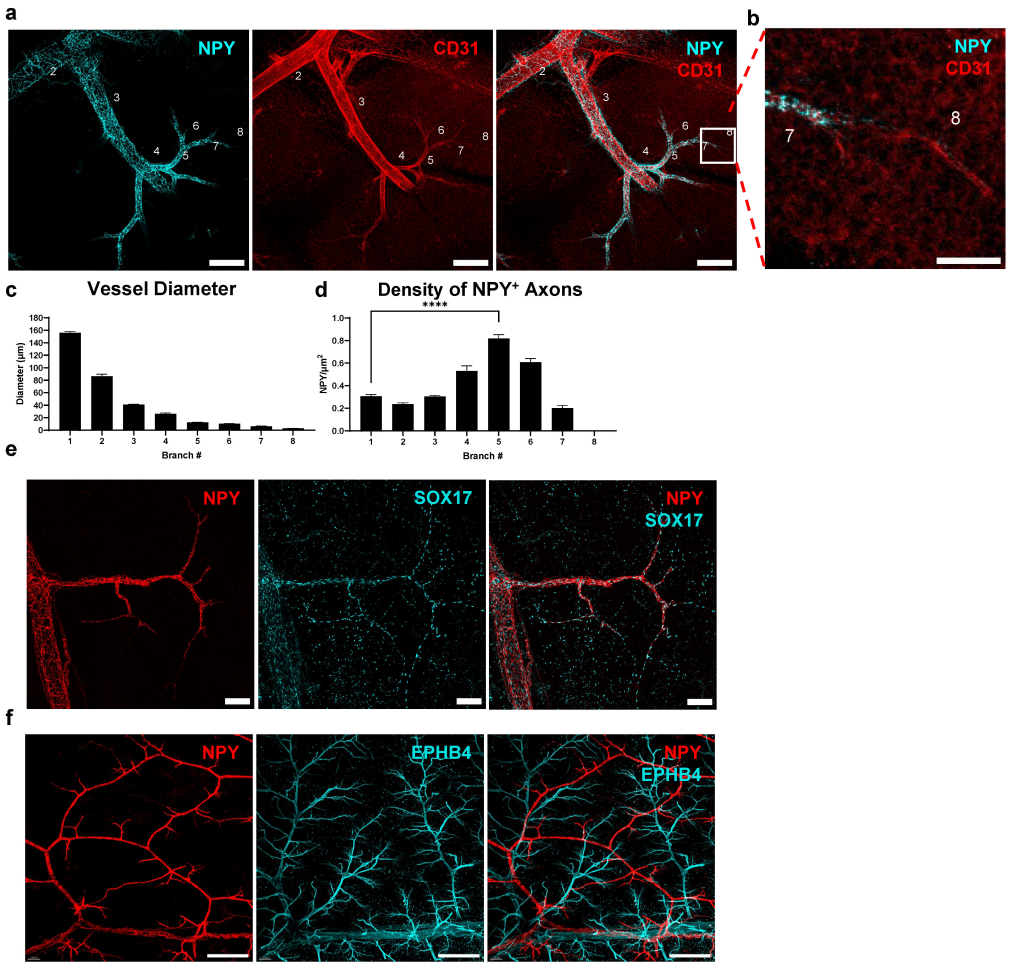


Figure 3.5: **NPY$^+$ axons preferentially innervate the 5th order arteriole branches.** (a) Confocal images of cleared adipose tissue stained with anti-NPY (cyan) and anti-CD31 (red). The number indicates the branch orders. Scale bar=150μm. (b) Zoom-in of (a), scale bar=50μm. (c-d) (c) The diameters of vessels and (d) the density of NPY$^+$ axons at each branch level quantified based on images as in (a) (n=6 views from 2 mice); NPY$^+$ axon density on Branch #1 vs. #5, P<0.0001. (e) Light-sheet images of cleared adipose tissue stained with anti-NPY (red) and anti-EPHB4 (cyan). Scale bar=500μm. (f) Confocal images of cleared adipose tissue stained with anti-NPY (red) and anti-SOX17 (cyan). Scale bar=100μm. All values are expressed as mean $\pm$ SEM. Statistical comparisons were made using 2-tailed Student T-tests, ****p<0.0001.

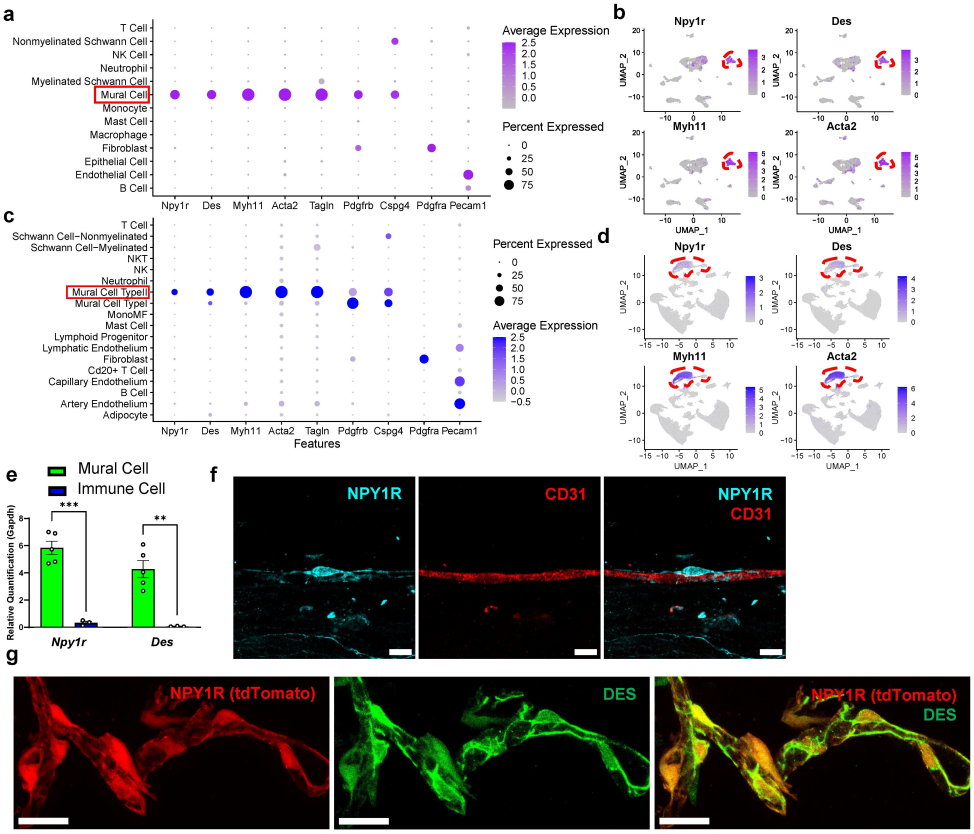


Figure 3.6: **Npy1r is mainly expressed in mural cells which are a source of thermogenic adipocytes.** (a&c) Dot plot showing the expression of *Npy1r*, *Des*, *Myh11*, *Acta2* (αSMA), *Tagln*, *Cspg4* (NG2), *Pdgfrb*, *Pdgfra*, and *Pecam1* (CD31) in the SVF of (a) iWAT or (c) iBAT. (b&d) Embedding plots showing the expression of Npy1r, Des, Myh11, and Acta2 (αSMA) in the SVF of (b) iWAT and (d) iBAT. Mural cell clusters are highlighted with red rectangles or red dashed lines. (e) The expression of Npy1r (P=0.0002) and Des (P=0.0024) mural cells and immune cells (n=5&3). (f) Confocal image of the capillary dissected from the iWAT of WT mice stained with anti-NPY1R (cyan) and anti-CD31 (red), scale bar=10μm. (g) Confocal images of vessels dissected from Npy1r^{Cre}; Rosa26^{tdTomato} mice stained with anti-DES (green), scale bar=20μm. All values are expressed as mean $\pm$ SEM. Statistical comparisons were made using 2-tailed Student T-tests, **p<0.01, ***p<0.001.

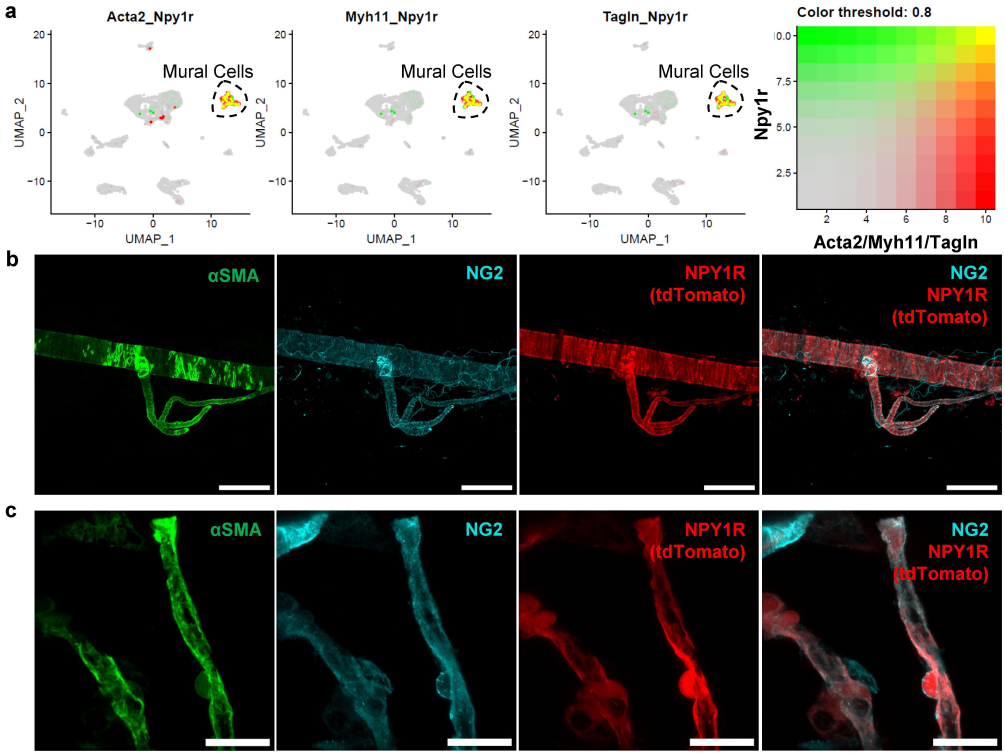


Figure 3.7: **NPY1R-tdTomato is colocalised with NG2 and αSMA in mural cells.** (a) Embedding plot showing the co-expression of mural markers *Acta2* (αSMA), *Myh11*, and *Tagln* (red) with *Npy1r* (green). Co-expression is in yellow. (b) Confocal images of vessels dissected from adipose tissue of Npy1r^{Cre}; Rosa26^{tdTomato} mice stained with anti-αSMA (green), scale bar=100μm. (c) Zoomed-in images of vessels as in Extended Data Fig. 2b, scale bar=20μm.

3.7a), which is confirmed by immunolabelling vessel-containing samples dissected from adipose tissues of Npy1r^{Cre}; Rosa26^{tdTomato} mice for multiple mural cell markers including DES (Figure 3.6g), αSMA, and NG2 (Figure 3.7b-c). These images indicate that DES^{+}, αSMA^{+}, or NG2^{+} mural cells are all labelled with NPY1R-tdTomato (Figure 3.6g, Figure 3.7b-c). Based on the observations above, we demonstrate that mural cells are the target of NPY^{+} axons and that they are NPY1R^{+}.

3.3.5 NPY-receptors are not detectable in adipocytes or immune cells

It is worth noticing that earlier reports of *Npy2r* and *Npy5r* expression by immune cells, preadipocytes and adipocytes (Rosmaninho-Salgado et al., 2012; Yang et al., 2008; Kuo et al., 2007) are negated by our analysis of the two scRNA-Seq datasets of both iBAT and iWAT, where *Npy5r* is undetectable, and *Npy2r* expression is only detectable in iWAT but negligible (Figure 3.8a-b). Also, some previous reports of *Npy1r* expression by adipocytes or macrophages (Yan et al., 2021) are negated by a single-nucleus atlas of mouse white adipose tissue and a scRNA-Seq dataset of iBAT (Shamsi et al., 2021; Emont et al., 2022) as well as our qPCR result of sorted ATMs (Figure 3.3f). Therefore, other than mural cells, no immune cells or adipocytes are likely to be the postsynaptic targets of NPY^+ axons in adipose tissue. It is also worth noticing that the adrenergic receptors (ADRs), the receptors able to bind to epinephrine and NE are not highly expressed in mural cells (Figure 3.8a-b), which implies that NPY is the main sympathetic-neuron-derived neurotransmitter that regulates the biology of mural cells.

3.4 Discussion

Previous research indicates that sympathetic axons innervate the adipose tissues, and NPY exists in the SNS. However, there was no direct evidence to show the extent to which sympathetic axons innervating the adipose tissues are NPY^+, and which of the vascular branches are innervated by NPY^+ axons. By using the state-of-the-art adipo-clearing techniques, I visualised in detail the anatomy of NPY^+ axons and demonstrated that they are a third of the labelled axons and preferen-

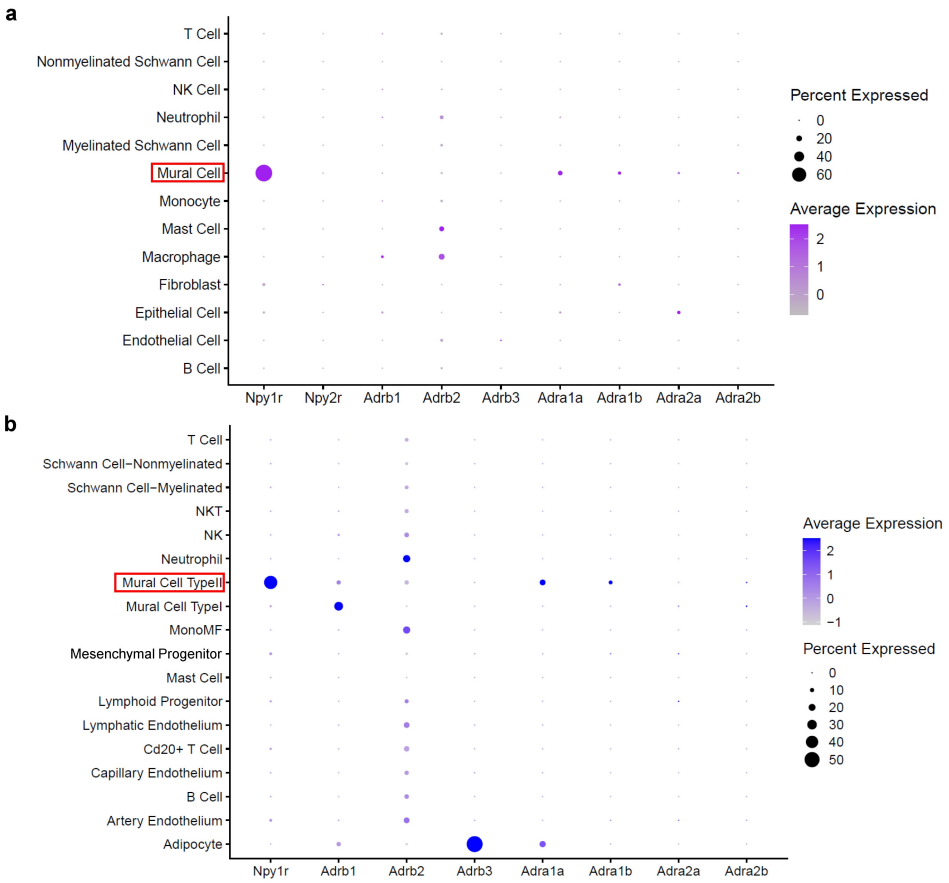


Figure 3.8: **The expression levels of *Npy2r* and *Npy5r* in adipose tissues are negligible.** (a) Dot plot showing the expression of *Npy1r*, *Npy2r*, *Adra1a*, *Adra1b*, *Adra1b*, *Adrb1*, *Adrb2*, and *Adrb3* in different cells in the SVF of mice iWAT. (b) Dot plot showing the expression of *Npy1r*, *Adrb1*, *Adrb2*, *Adrb3*, *Adra1a*, *Adra1b*, *Adra2a*, and *Adra2b* in different types of cells in mouse iBAT. The size of the dot represents the percentage of cells expressing a certain gene, and the darkness of the dot represents the expression level. Mural cell clusters are highlighted with red rectangles.

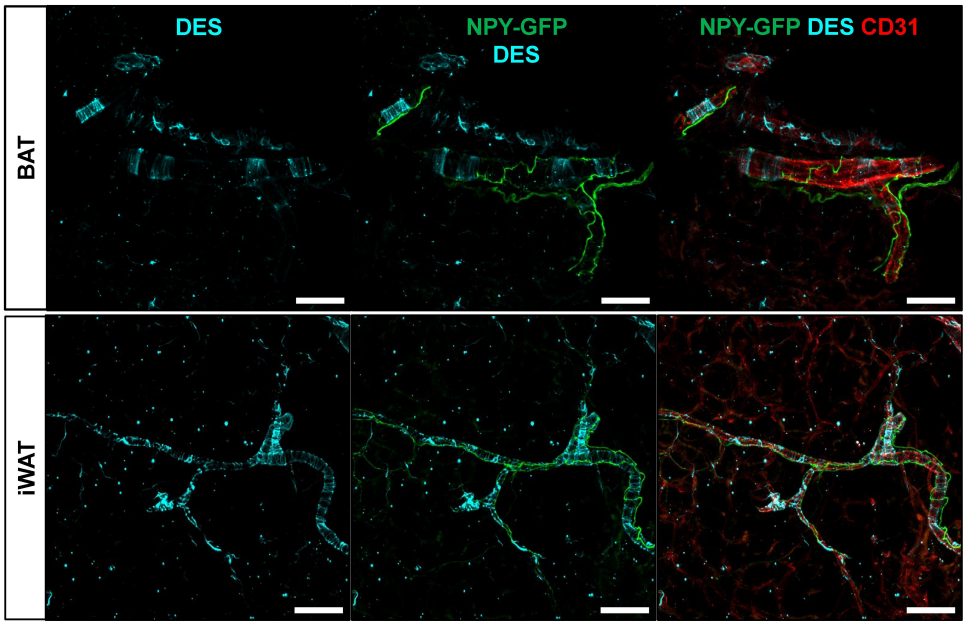


Figure 3.9: **NPY$^+$ axons innervate mural cells.** Images of the cleared adipose tissue of NPY-GFP reporter mice stained with anti-GFP (green), anti-DES (cyan), and anti-CD31(red). Scale bar=50μm.

tially innervate the 5th- to 7th-order arterial branches. It was also confirmed that the SNS is the main source of NPY in adipose tissue.

There have been debates about which types of cells express NPY receptors due to the lack of convincing data and specific antibodies for NPY receptors. In this chapter, by reanalysing recently published scRNA-Seq datasets and dining IF staining, I demonstrate that *Npy1r* is the only highly expressed NPY receptor in the SVF of adipose tissues, and it is mainly expressed by mural cells, a kind of cells closely associated with the vasculature. Immune cells including macrophages do not express a detectable level of *Npy1r*. The data above establish an NPY-mural connection in both iBAT and iWAT as demonstrated in Figure 3.9.

4 | Functional Analysis of NPY-Mural Cell Interaction

4.1 Introduction

4.1.1 The downstream pathway of NPY1R

NPY1R is a GPCR associated with G$\alpha_{i/o}$, which can inactivate cAMP (Park et al., 2022). Previous reports indicate that NPY can activate Pi3K and induce the phosphorylation of the downstream ERK1/2 in cells including adipose tissue SVF, smooth muscle cells, and cardiomyocytes (Hong et al., 2018; Pons et al., 2008; Yang et al., 2008; Pellieux et al., 2000).

4.1.2 Functions of mural cells

Mural cells consist of smooth muscle cells and pericytes and are marked by various markers including PDGFRβ, NG2, αSMA, TAGLN, DES, MYH11 etc (Table 1.1). However, no single markers can differentiate SMCs from pericytes because these markers are dynamically expressed in both subgroups, and the conventional classification of SMCs and pericytes was based on their morphology but not transcriptomes (Attwell et al., 2016; Armulik et al., 2011). Mural cells regulate the vasculature: loss of mural cells increases vascular leakiness and immune infiltration in adipose tissue (Onogi et al., 2017). Recent studies reveal another function of mural cells, which is to differentiate into thermogenic adipocytes and maintain energy homeostasis (Shamsi et al., 2021; Long et al., 2014). It is worth noticing that the neogenesis of thermogenic adipocytes not only happens in WATs but also in iBAT, as revealed by a study using TRPV1-reporter mice that demonstrates that

a subgroup of thermogenic adipocytes in iBATs can be lineage traced to TRPV1$^+$ SMCs. These data imply that the NPY1R$^+$ mural cells I identified in the previous chapter (Chapter 3) might be a source of thermogenic adipocytes and NPY may be able to affect thermogenesis via these cells.

4.1.3 Regulation of mural cells

Mural cells are conventionally known to be regulated by the PDGF-B/PDGFRβ pathway (Armulik et al., 2011). PDGF-B is required for recruiting mural cells (Levéen et al., 1994), but elevated levels can decrease mural cells both *in vitro* and *in vivo* by upregulating fibroblast markers and promoting fibroblast proliferation (Hosaka et al., 2016; Onogi et al., 2017). Also, Pi3K has been reported to be essential for maintaining the mural cell number and the mural cell coverage in the retina by promoting mural cell proliferation.(Figueiredo et al., 2020). These data altogether indicate the role of NPY1R in regulating cell proliferation, but it is unknown whether NPY can promote the proliferation of adipose mural cells and how they can affect the metabolism of adipose tissues.

4.2 Methodology

4.2.1 *In vitro* experiments

To understand the impact of NPY on mural cells, I planned to isolate mural cells and treat them with NPY *in vitro*. The isolation of mural cells from adipose tissues was based on a published protocol (Tang et al., 2022), which is first treating SVF with the conditioned medium for selecting mural cells and then conducting magnetic-activated cell sorting (MACS) targeting PDGFRβ. Sorted mural cells were used for proliferation assay to test the impact of NPY on mural cell

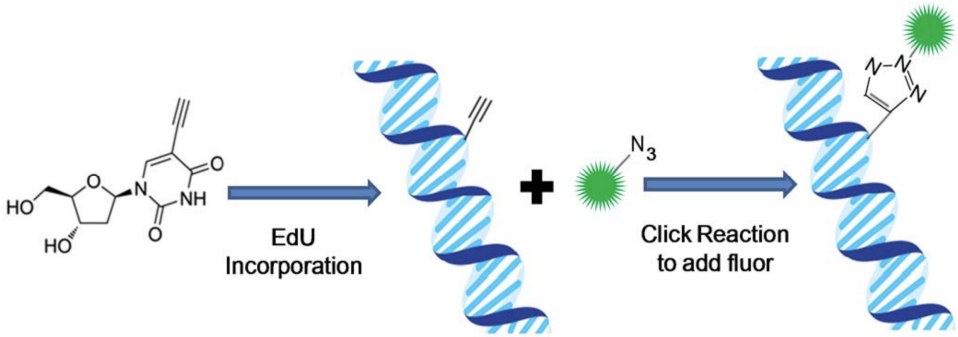


Figure 4.1: **EdU Cell Proliferation Assay Principle.** Cells grown in the presence of 5-EdU incorporate the compound during DNA synthesis. Fluorophore-labeled azide reacts with the incorporated EdU to allow detection by microscopy.

proliferation and differentiation assay to test how NPY affects the neogenesis of thermogenic adipocytes from mural cells. Mural cell proliferation was indicated using 5-Ethynyl-deoxyuridine (EdU), a thymidine analogue that is incorporated into DNA during DNA synthesis and can be detected after interacting with fluorophore-labelled azide (Figure 4.1) (Guan, van der Heijden, Bortvin, & Greenberg, 2011). The ability of mural cells to differentiate into thermogenic adipocytes was tested by measuring thermogenic genes.

4.2.2 NPY1R lineage-tracing mouse model

To test whether NPY1R^{+} mural cells can be a source of thermogenic adipocytes, I planned to use a lineage-tracing mouse line that labels all the cells expressing *Npy1r* and cells derived from them, where a Rosa26^{tdTomato} construct is expressed in cells expressing *Cre* under the control of a NPY1R promotor (Npy1r^{Cre}).

4.3 Results

4.3.1 NPY promotes mural cell proliferation

NPY1R is a kind of G protein-coupled receptor (GPCR) that can activate MAPK pathways after binding to NPY, with the MAPK downstream of NPY1R being ERK (Shimada et al., 2012). Since the MAPK pathway is a canonical regulator of cell proliferation (W. Zhang & Liu, 2002), we questioned if NPY could promote the proliferation of mural cells. By isolating mural cells from adipose tissues and adding NPY, I observed that NPY promoted the proliferation of both iWAT and iBAT mural cells (Figure 4.2a-f). To confirm if NPY acts through ERK, the ERK inhibitor PD98059 was used to inhibit ERK when NPY was added. The result shows that PD98059 blocked the mitogenic effect of NPY (Figure 4.2g-h), indicating that NPY promotes mural cell proliferation via ERK.

4.3.2 NPY1R^{+} mural cells are the progenitors of thermogenic adipocytes

Mural cells can give rise to thermogenic adipocytes (Shamsi et al., 2021; Long et al., 2014; Oguri et al., 2020), and previously identified progenitors of beige cells (Lin^{-}/CD81^{+}) express *Npy1r* and mural cell markers (Oguri et al., 2020) (Figure 4.3a-c), which is further proven via our analysis of iWAT scRNA-Seq data (Figure 4.3d).

To further confirm that mural cells from both iWAT and iBAT are progenitors of thermogenic adipocytes, I isolated and differentiated mural cells to adipocytes (Tang et al., 2022) (Figure 4.4a-b) and found that they are more potent in differentiating into thermogenic adipocytes than SVF as indicated by higher levels of

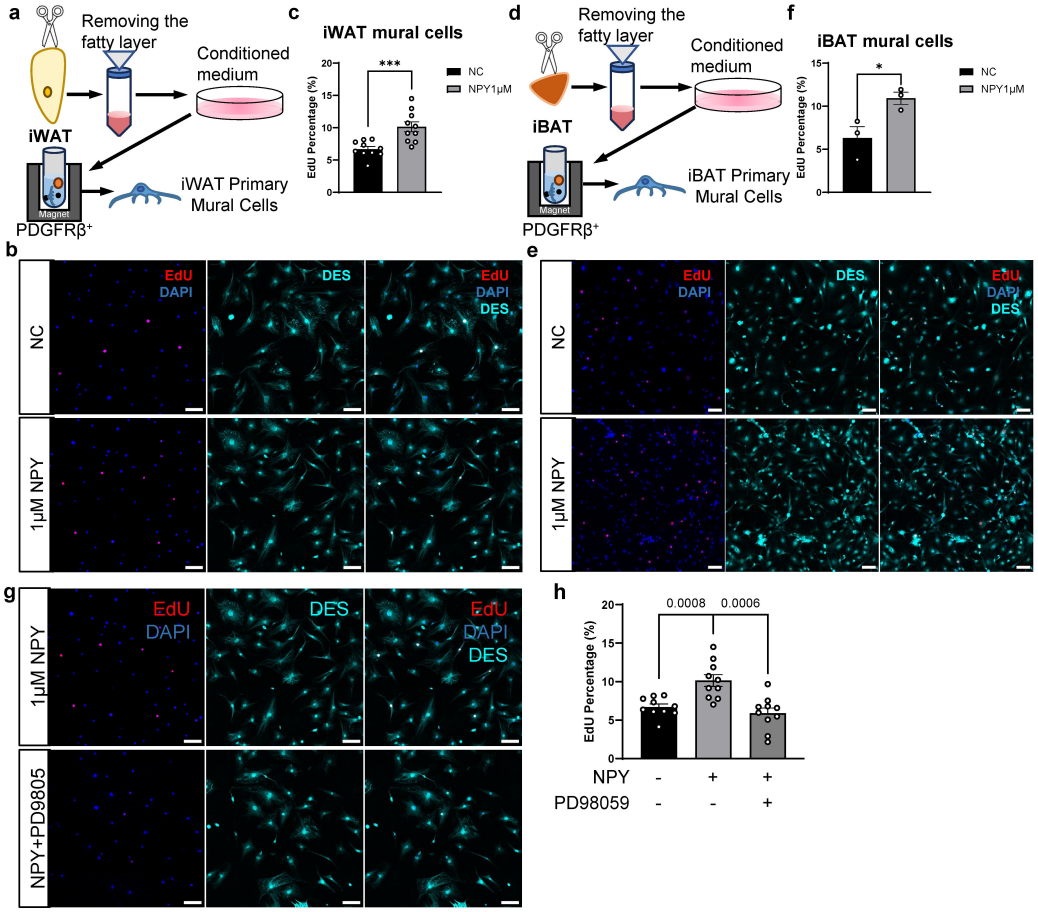


Figure 4.2: **NPY promotes the proliferation of both iWAT and iBAT mural cells via ERK.** (a) Schematic of isolating mural cells from iWAT. (b) Confocal image showing iWAT mural cells treated with or without 1Î¼M NPY stained with DES (cyan) and DAPI. EdU (red) indicates proliferating cells. Scale bar=80μm. (c) The percentage of EdU$^+$ mural cells quantified based on images as in (b) (n=10). (d) Schematic of isolating mural cells from iBAT. (e) Confocal image showing iBAT mural cells treated with or without 1μM NPY stained with DES (cyan) and DAPI. EdU (red) indicates proliferating cells. Scale bar=80μm. (f) The percentage of EdU$^+$ mural cells quantified based on images as in (d) (n=3). (g) Confocal images of isolated mural cells treated with or without 1μM NPY and 2μM PD98059, an ERK inhibitor, stained with anti-DES (cyan) and DAPI (blue). EdU (red) was used to indicate proliferation. Scale bar=80μm. (h) The percentage of EdU$^+$ cells quantified based on images as in (g) (n=6). All values are expressed as mean $\pm$ SEM. Statistical comparisons were made using 2-tailed Student T-tests, $^*p<0.05$, $^{***}p<0.001$.

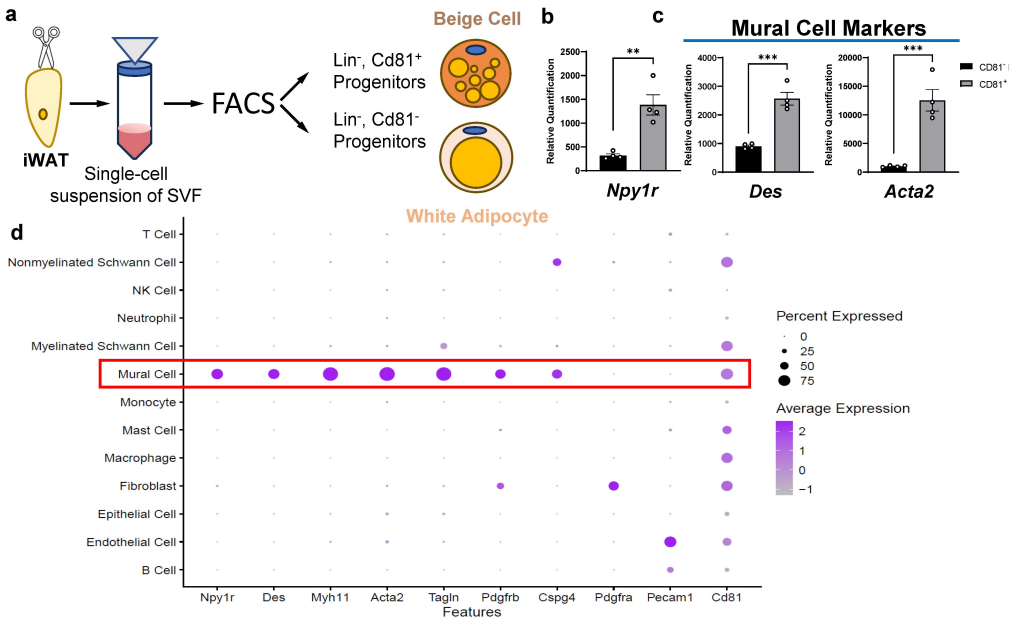


Figure 4.3: **Previously identified progenitors of thermogenic adipocytes (Lin$^-$/CD81$^+$) in iWAT express *Npy1r* and mural cell markers.** (a) Schematic of isolating previously identified progenitors of thermogenic adipocytes (Lin$^-$/CD81$^+$) in iWAT. (b-c) The expression level of (b) *Npy1r*, and (c) mural cell markers *Des* and *Acta2* in CD81$^-$ vs. CD81$^+$ progenitors (n=4). (d) Dot plot showing the expression of *Npy1r, Des, Myh11, Acta2, Tagln, Pdgfrb, Cspg4, Pdgfra, Pecam1*, and *Cd81* in different cells in the SVF of mice iWAT. The size of the dot represents the percentage of cells expressing a certain gene, and the darkness of the dot represents the expression level. NPY1R$^+$ mural cell clusters are highlighted with red rectangles. All values are expressed as mean ± SEM. Statistical comparisons were made using 2-tailed Student T-tests, *p<0.05, **p<0.01, ***p<0.001.

thermogenic genes expressed by adipocytes differentiated from mural cells (Figure 4.4c-f).

To demonstrate that NPY1R^{+} mural cells are progenitors of thermogenic adipocytes under physiological conditions, we immunolabelled iBAT of Npy1r^{Cre}; Rosa26^{tdTomato} room-temperature (RT) -housed mice for UCP1 (Figure 4.5a). Using this lineage-tracing approach, we observed that both mural cells and a subgroup of UCP1^{+} adipocytes were co-labelled with NPY1R-tdTomato (Figure 4.5b-c). Since adipocytes do not express *Npy1r* (Figure 3.6a-d), we reasoned that these NPY1R^{-}tdTomato^{+}UCP1^{+} thermogenic adipocytes (about 10%-20%) are lineage-traced to NPY1R^{+} mural cells.

It is worth noticing that NPY1R-tdTomato only labels multi-locular UCP1^{+} adipocytes in iBAT and iWAT, but not UCP1^{-} unilocular white adipocytes (Figure 4.6), which indicates that NPY1R is specifically expressed in the progenitor of thermogenic adipocytes. Based on the observations above, we conclude that NPY1R^{+} mural cells are progenitors of thermogenic adipocytes.

4.3.3 NPY facilitates the differentiation to thermogenic adipocytes

Since NPY promotes the proliferation of mural cells, I then tested if NPY can increase the proportion of mural cells in cultured SVF or CD81^{+} progenitors. By isolating SVF and CD81^{+} progenitors from iWATs and treating them with NPY (Figure 4.7a), I found that NPY increased the proportion of αSMA^{+} mural cells in cultured SVF and CD81^{+} progenitor cells (Figure 4.7b-d).

Since mural cells are proven to be the progenitors of thermogenic adipocytes (Figure 4.5, Figure 4.6), we reasoned that NPY could facilitate the neogenesis of thermogenic adipocytes (Figure 4.7e). To directly prove this, I differentiated iWAT SVF and progenitors of thermogenic adipocytes isolated from iWAT

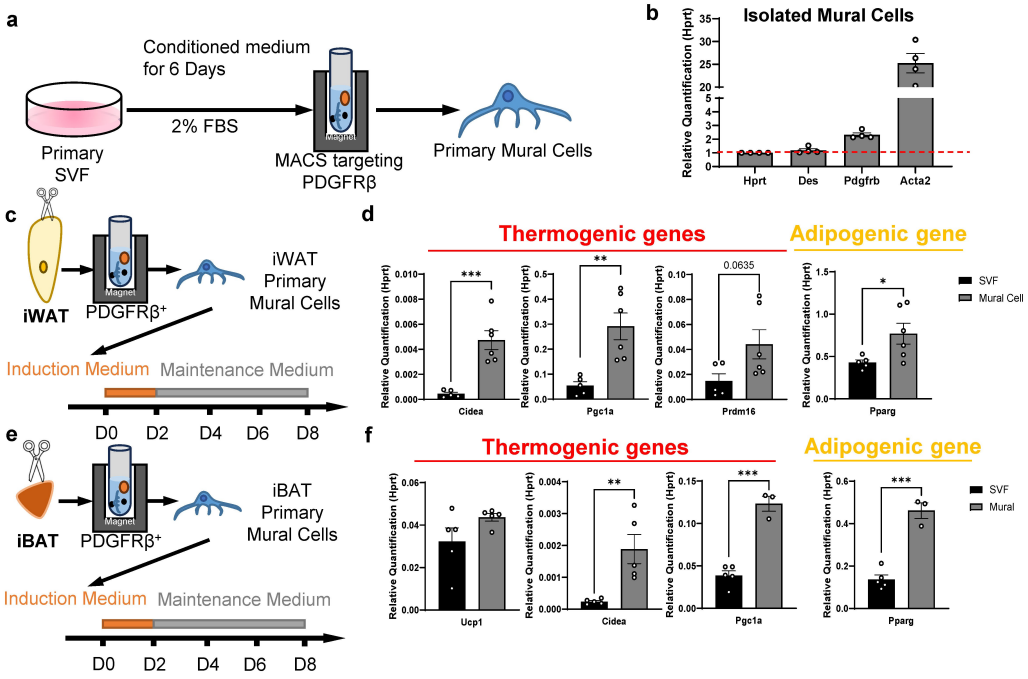


Figure 4.4: **Mural cells isolated from both iWAT and iBAT can differentiate into thermogenic adipocytes.**(a) Schematic of isolating mural cells from adipose tissue. (b) The expression level of mural cell markers *Des, Pdgfrb*, and *Acta2* in isolated mural cells. The red dashed line indicates the expression level of the reference gene Hprt (n=4). (c&e) Schematic of isolating and differentiating mural cells from (c) iWAT and (e) iBAT. (d&f) The expression of thermogenic and adipogenic genes in adipocytes differentiated from the stromal-vascular fraction (SVF) and mural cells isolated from (d) iWAT (n=5&6) and (f) iBAT (n=5&5). All values are expressed as mean ± SEM. Statistical comparisons were made using 2-tailed Student T-tests, $^{*}p<0.05$, $^{**}p<0.01$, $^{***}p<0.001$.

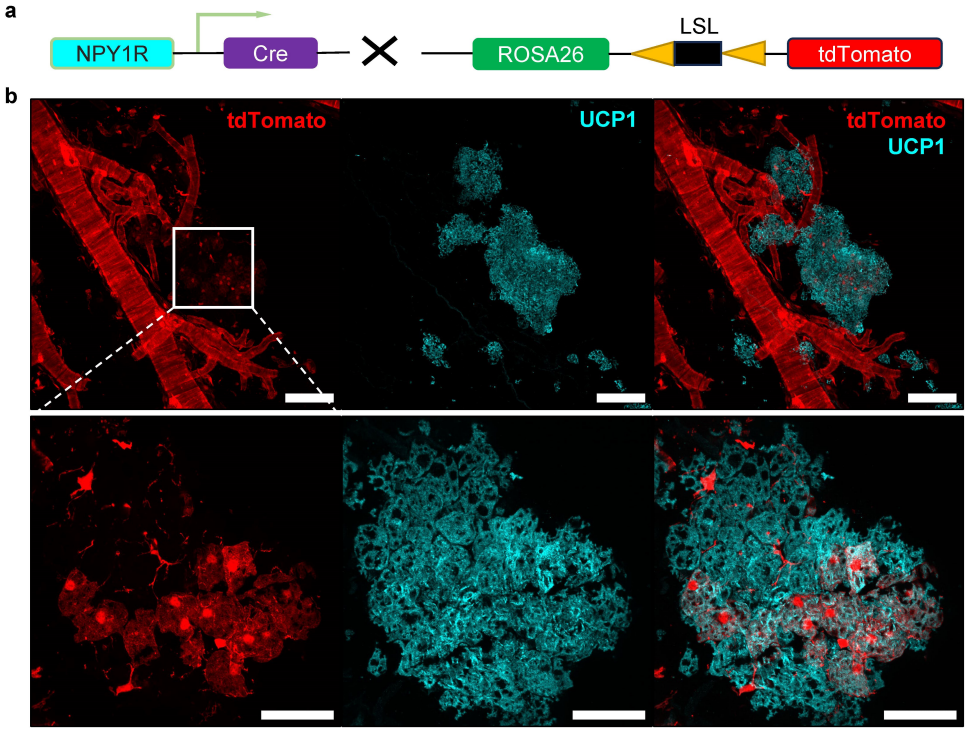


Figure 4.5: **A subgroup of thermogenic adipocytes in iBAT can be lineage-traced to NPY1R^{+} mural cells.** (a) The gene construct of the lineage-tracing mouse model for NPY1R. (b) Confocal images of vessels dissected from the iBAT of ND-treated, RT-housed 12-week-old Npy1r^{Cre}; Rosa26^{tdTomato} mice stained with anti-UCP1 (cyan), scale bar=100μm. (i) Zoomed-in images of (b), scale bar=50μm.

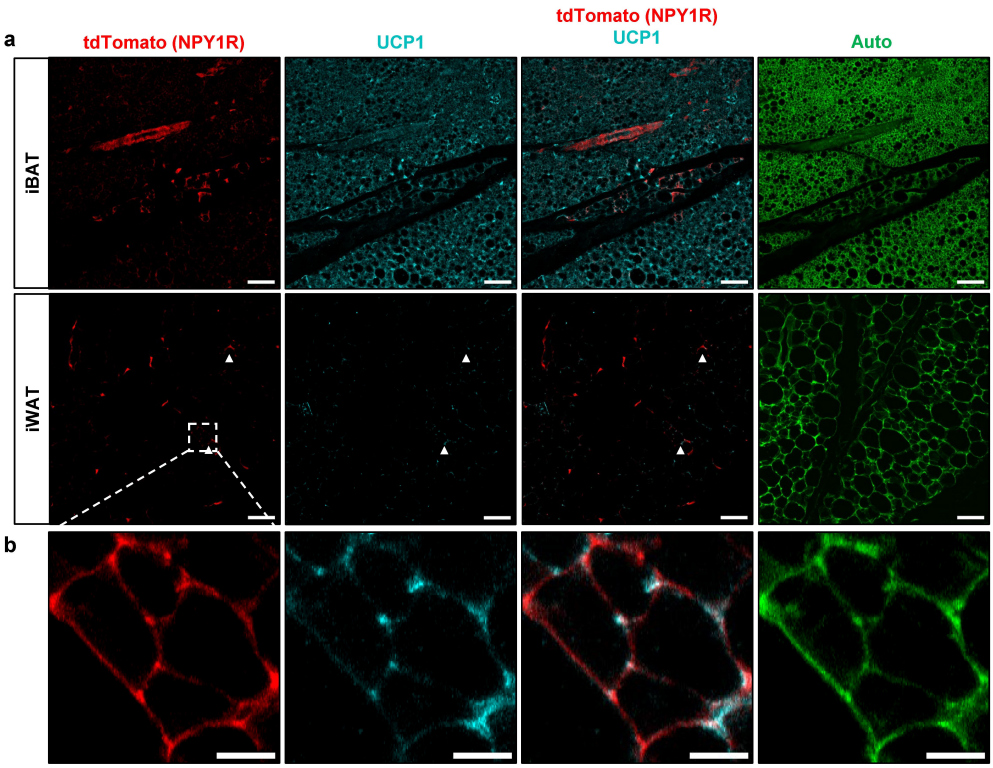


Figure 4.6: **Only UCP1^{+} multi-locular adipocytes are lineage-traced to NPY1R** (a) Confocal images of paraffin-embedded slides of iBAT and iWAT of 12-week-old male Npy1r^{Cre}; Rosa26^{tdTomato} mice stained with UCP1 (Cyan), scale bar=50μm. (b) is zoomed-in (a), scale bar=10μm.

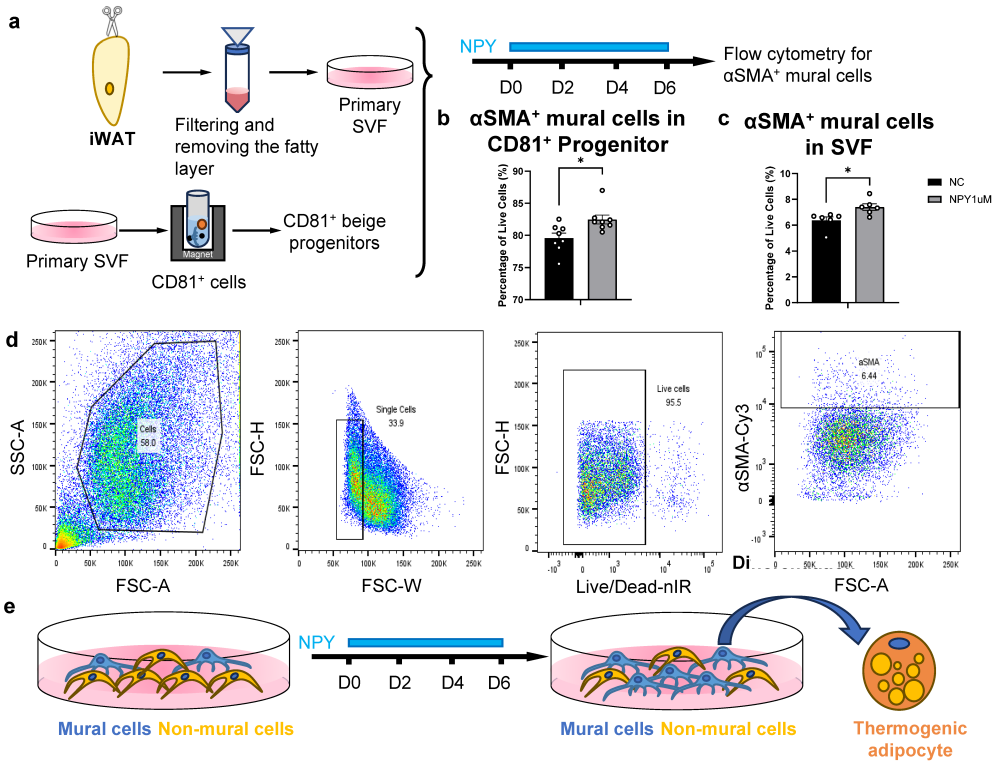


Figure 4.7: **NPY increases the proportion of αSMA$^+$ mural cells in SVF and CD81$^+$ progenitors.** (a) Schematic of isolating iWAT SVF and CD81$^+$ cells for NPY treatment experiments and flow cytometry analysis. (b) Gating strategy for measuring the percentage of αSMA$^+$ mural cells in cultured SVF and CD81$^+$ cells by flow cytometry. (c-d) The percentage of αSMA$^+$ mural cells in (c) SVF (n=6) and (d) CD81$^+$ cells (n=8) after incubating with or without 1μM NPY. (e) Schematic showing NPY treatment increases the percentage of mural cells in cultured SVF or CD81$^+$ cells, and mural cells are the progenitor of thermogenic adipocytes. All values are expressed as mean $\pm$ SEM. Statistical comparisons were made using 2-tailed Student T-tests, $^*p<0.05$.

and iBAT and found that NPY facilitated their differentiation into thermogenic adipocytes by upregulating thermogenic genes without affecting adipogenic genes (Figure 4.8a-d&f). Additionally, NPY increased the maximal respiratory capacity of adipocytes differentiated from iWAT beige adipocyte progenitors (Figure 4.8e).

We further demonstrated that NPY does not affect adipogenesis using NPY1R$^+$ 3T3-L1 pre-adipocytes (Figure 4.9), confirming that NPY specifically promotes the differentiation of thermogenic adipocytes.

4.3.4 NPY sustains the role of mural cells as progenitors of thermogenic adipocytes

PDGF-B can regulate mural cells in that it is required for recruiting them(Armulik et al., 2005). Still, elevated levels can decrease mural cells both *in vitro* and *in vivo* by upregulating fibroblast markers and promoting fibroblast proliferation (Hosaka et al., 2016; Onogi et al., 2017). I then questioned whether NPY could sustain mural cells when challenged with PDGF-B, which is physiologically relevant since diet-induced obesity (DIO) increases PDGF-B in adipose tissue (Onogi et al., 2017). By treating isolated mural cells with PDGF-BB (dimerised PDGF-B), we found that PDGF-BB decreased the proportion of mural cells and increased the number of spindle-shaped PDGFRα^+ fibroblasts, an effect that is counteracted by NPY (Figure 4.10a-b). Using qPCR, we demonstrated that PDGF-BB down-regulated the expression of *Npy1r* and mural cell markers, while NPY restored the expression of *Npy1r* and mural cell markers including *Pdgfrb* and *Rgs5* (Figure 4.10c-d). It is worth noticing that NPY can also restore genes associated with vascular integrity (Figure 4.10e), which indicates that NPY might be important for preventing vascular leakiness and immune infiltration associated with chronic adipose tissue inflammation.

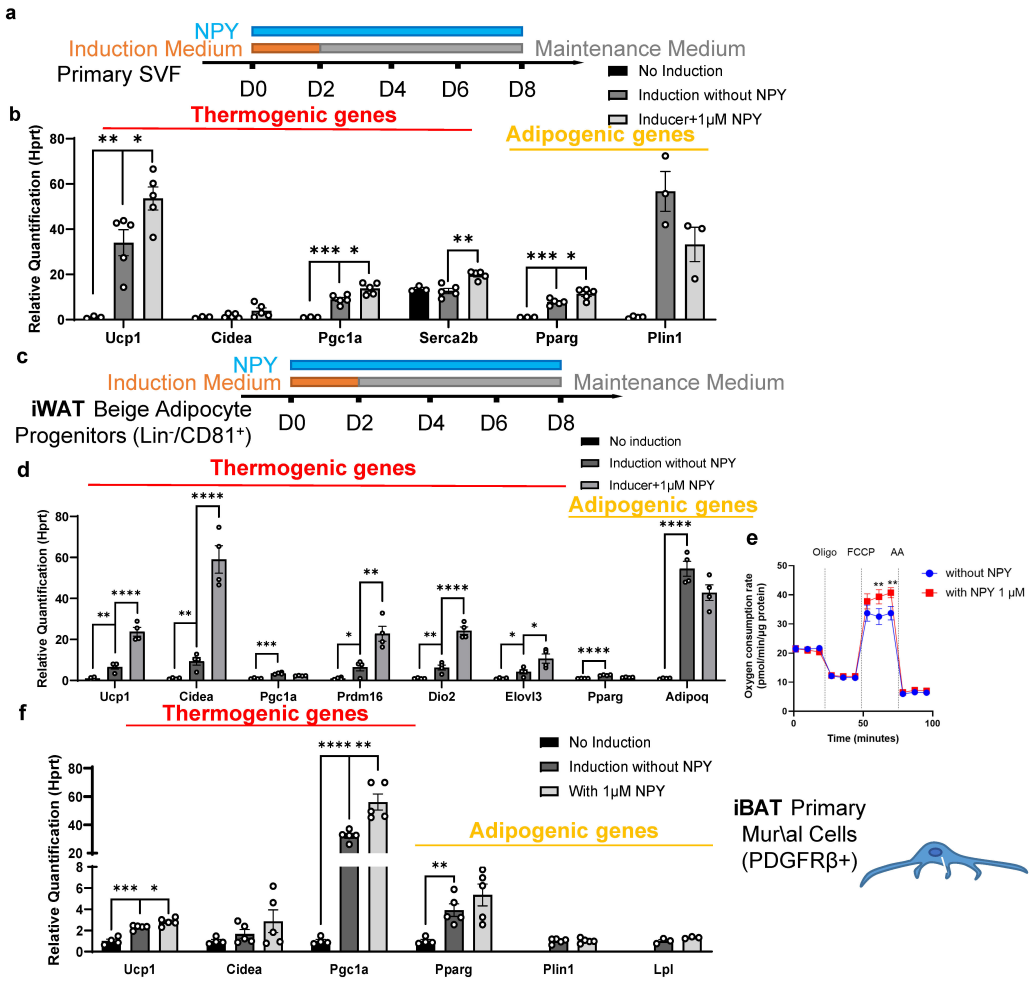


Figure 4.8: **NPY facilitates the neogenesis of thermogenic adipocytes from iWAT SVF and mural progenitors isolated from both iWAT and iBAT.** (a) Schematic of differentiating primary stromal vascular fraction (SVF) of iWATs to thermogenic adipocytes. (b) The expression *Ucp1*, *Cidea, Pgc1a, Serca2b, Pparg*, and *Plin1* (n=4&3&3 for *Plin1* and n=3&5&5 for other genes). (c) Schematic of differentiating beige adipocyte progenitors ($Lin^-/CD81^+$) isolated from iWAT. (d) The expression of thermogenic and adipogenic genes in adipocytes differentiated from iWAT beige adipocyte progenitors ($Lin^-/CD81^+$) with or without 1μM NPY (n=4). (e) Oxygen consumption in adipocytes differentiated from beige adipocyte progenitors ($Lin^-/CD81^+$) with or without 1μM NPY (n=5). (f) The expression of thermogenic and adipogenic genes in adipocytes differentiated from iBAT mural cells or SVF (n=4&5&5). All values are expressed as mean $\pm$ SEM. Statistical comparisons were made using 2-tailed Student T-tests or 2-way ANOVA, $^*p<0.05$, $^{**}p<0.01$, $^{***}p<0.001$, $^{****}p<0.0001$.

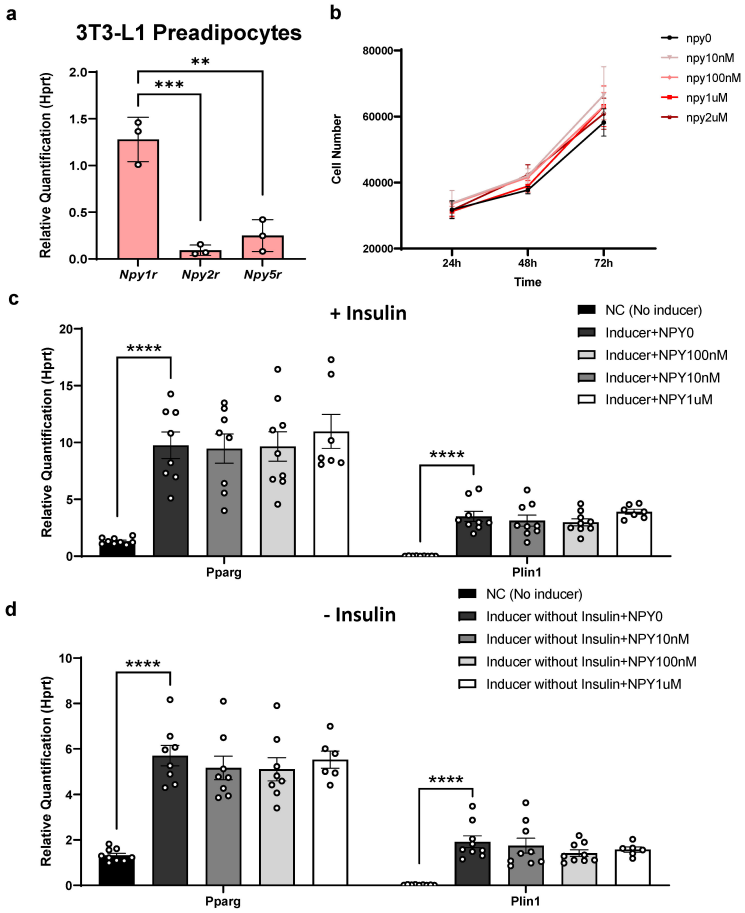


Figure 4.9: **NPY does not affect the proliferation or adipogenesis of 3T3-L1.** (a) The expression of *Npy1r*, *Npy2r*, and *Npy5r* in 3T3-L1 preadipocyte cell line (n=3). (b) The impact of NPY on the proliferation of 3T3-L1 preadipocytes revealed by the cell number after incubating with or without 1μM NPY for 24, 48, and 72 hours (n=3). (c-d) The expression of adipogenesis markers *Pparg* and *Plin1* in differentiated 3T3-L1 preadipocytes induced by induction medium (c) with or (d) without 1μg/mL insulin (n=9, 8, 8, 9&7 for *Pparg*, n=9, 9, 9, 9& 7 for *Plin1*). The concentration of NPY is indicated in the plot. All values are expressed as mean $\pm$ SEM, *p<0.05, **p<0.01, ***p<0.001, ****p<0.0001, Student T-tests.

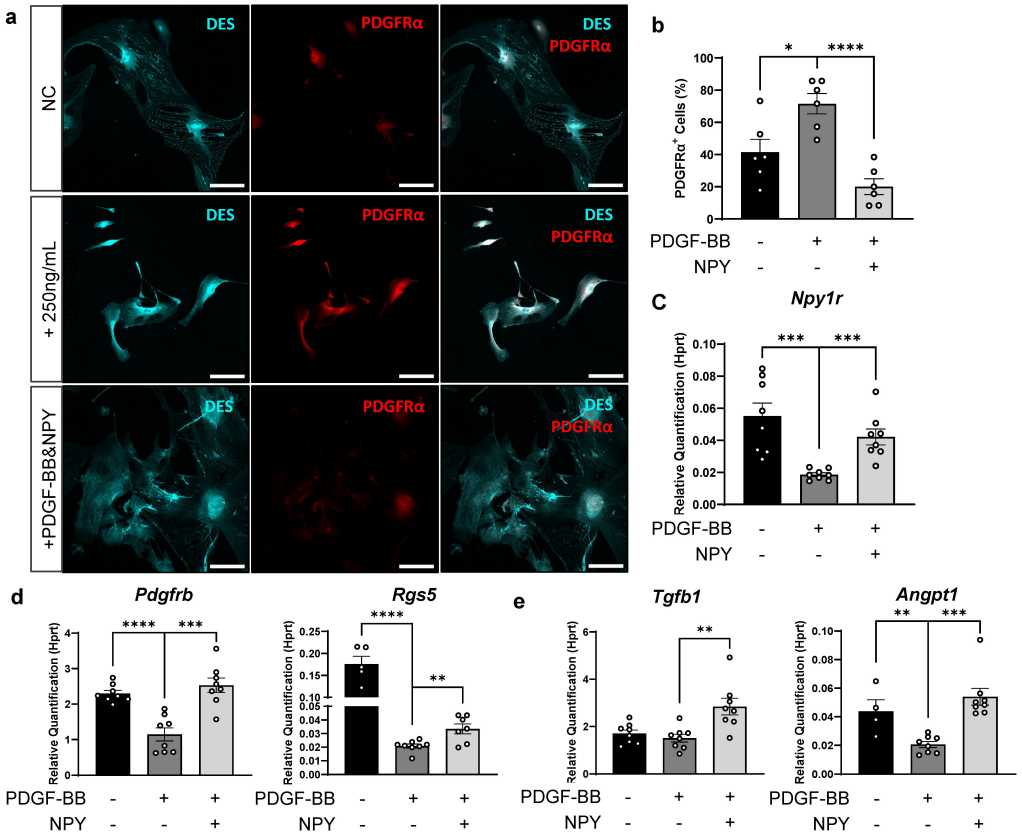


Figure 4.10: **NPY sustains mural cell identity against PDGF-BB.** (a) Confocal images of primary mural cells stained with anti-DES (cyan) and anti-PDGFRα (red), cultured under different conditions. Scale bar=100μm. (b) The percentage of PDGFRα^+ cells under different stimulating conditions (n=6). Concentrations of NPY and PDGF-BB were 1μM and 250ng/mL respectively. (c-e) The expression of (c) *Npy1r* (n=8), (d) mural cell markers *Pdgfrb* (n=8) and Rgs5 (n=5&8&8), and (e) secretory factors in maintaining vascular integrity including *Tgfb1* (n=8) and *Angpt1* (n=4&8&8) in primary mural cells cultured with or without 1μM NPY or 250ng/mL PDGF-BB. All values are expressed as mean $\pm$ SEM. Statistical comparisons were made using 2-tailed Student T-tests, *p<0.05, **p<0.01, ***p<0.001, ****p<0.0001.

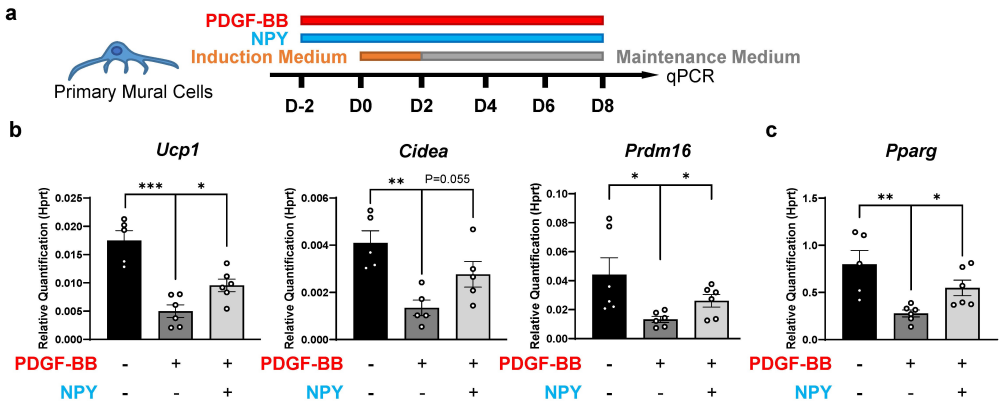


Figure 4.11: **NPY sustains the thermogenic ability of mural cells against PDGF-BB.** (a) Schematic of differentiating isolated mural cells to adipocytes with or without 1μM NPY or 250ng/mL PDGF-BB. (b-c) Expression levels of (b) thermogenic and (c) adipogenic genes expressed by adipocytes differentiated from mural cells under different conditions. All values are expressed as mean $\pm$ SEM. Statistical comparisons were made using 2-tailed Student T-tests, *p<0.05, **p<0.01, ***p<0.001, ****p<0.0001.

Since mural cells are identified as the progenitor of thermogenic adipocytes, we examined whether NPY can preserve their beiging ability against PDGF-BB. We observed that PDGF-BB treatment downregulated thermogenic and adipogenic genes, while NPY restored their expression (Figure 4.11a-c). Based on the observations above, we demonstrate *in vitro* that NPY can sustain mural cells as the progenitors of thermogenic adipocytes.

4.4 Discussion

Previous reports demonstrate that NPY could promote the proliferation of and adipogenesis of pre-adipocytes (Rosmaninho-Salgado et al., 2012; Kuo et al., 2007), which are negated by others (Yang et al., 2008). More contradictions were in the research to determine the role of each NPY receptor in regulating adipogenesis. Some reported that only NPY1R agonists promoted the proliferation of

preadipocytes (Yang et al., 2008), while others reported that only NPY2R and NPY5R agonists promoted the proliferation and differentiation of preadipocytes (Kuo et al., 2007; Rosmaninho-Salgado et al., 2012). These findings are not repeated in our *in vitro* experiment of treating 3T3-L1 preadipocytes with NPY (Figure 4.9). Previous *in vivo* studies demonstrating that conventional knockout of NPY receptors makes mice develop adult-onset obesity also disfavour the role of NPY to promote obesity (Naveilhan et al., 1999; Pedrazzini et al., 1998; Nguyen et al., 2012).

To find out the impact of NPY on its target, mural cells, which are the only type of cells highly expressing *Npy1r*, I isolated mural cells and used *in vitro* co-culturing method to find that NPY promotes the proliferation of mural cells. Since NPY1R$^+$ mural cells are a source of thermogenic adipocytes, the impact of NPY on mural cells also facilitates the neogenesis of thermogenic adipocytes from SVF and CD81$^+$ progenitors. In addition, I found that NPY contracts PDGF-BB and sustains mural cell identity and their ability to differentiate into thermogenic adipocytes. Taken together, the $^{\text{in vitro}}$ data imply that NPY may play a role in regulating thermogenesis and adipose tissue inflammation via mural cells.

In the experiments analysing the functions of thermogenic adipocytes, I only looked at oxygen consumption and the transcriptional abundance of thermogenic genes . This might omit the impact of NPY on mitochondria abundance, activation of lipolytic enzymes, or the sizes of lipid droplets. Still, it is sufficient to demonstrate that NPY affects the biogenesis of thermogenic adipocytes and their thermogenic capacity.

5 | Diet-induced Obesity and NPY$^+$ axon-mural cell interaction

5.1 Introduction

5.1.1 Diet-induced Obesity (DIO) and sympathetic innervation

It has been established that SNS is important for maintaining adipose tissue homeostasis via establishing a negative feedback loop involving the adipose tissue and the brain: WAT secretes leptin, which binds to its receptors in the Arc of the hypothalamus and activates the SNS downstream, and sympathetic axons innervating adipose tissues use NE to trigger lipolysis or thermogenesis (W. Zeng et al., 2015) (Figure 1.4). A recent study reveals that DIO-induced leptin resistance decreases sympathetic innervation reciprocally, mediated by the BDNF in the PVH of the hypothalamus (P. Wang et al., 2020). Also, epidemiological studies indicate that peripheral neuropathy is associated with obesity and type 2 diabetes, which confirms that obesity can affect neuronal innervation in humans (Callaghan et al., 2020). Still, it is unknown whether NPY$^+$ sympathetic innervation is also decreased.

5.1.2 Mural cell and vascular integrity

Mural cells are associated with the vasculature and regulate the biology of vascular endothelial cells. Previous reports indicate that mural cells can control vessel diameters since they are contractile cells (Attwell et al., 2016), and they can regulate angiogenesis and vascular leakiness via the ANGPT1/TIE2 and PDGF-B/PDGFRβ signalling pathways (Lindahl, Johansson, Leveen, & Betsholtz, 1997;

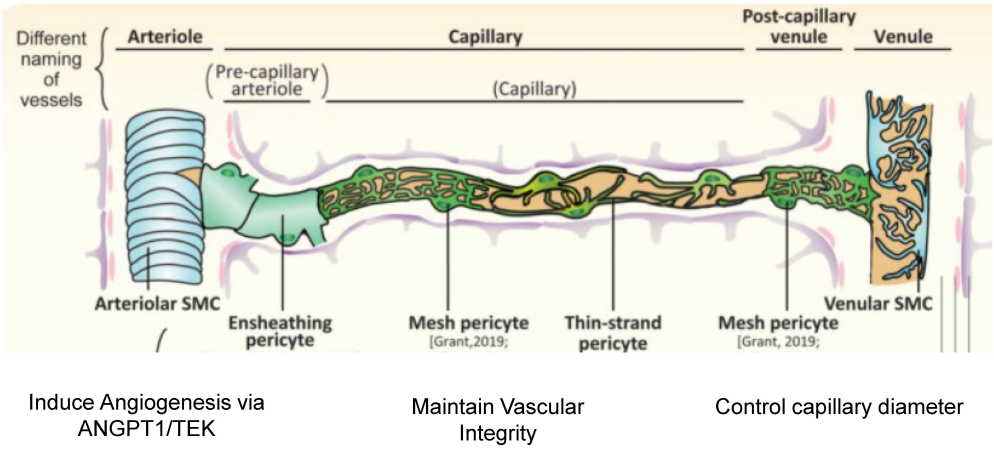


Figure 5.1: **Mural cells are heterogeneous and have different functions.**

Folkman & D'Amore, 1996; Uemura, Maki, Ihara, Lee, & Trojanowski, 2020) (Figure 5.1).

Based on previous reports, obesity and hyperglycaemia are associated with a lower mural cell coverage that can result in increased vascular leakiness in the retina, which is mediated by the morphological changes and remodelling of mural cells (Folkman, 2002; Glentis, Gurchenkov, & Vignjevic, 2014). More recent studies indicate that these morphological changes and remodelling might be mediated by PDGF-B, which in high concentration can promote mural cell-fibroblast transition and result in vascular leakiness and immune infiltration (Onogi et al., 2017; Hosaka et al., 2016). In Chapter 4, I demonstrated that NPY can sustain the identity of mural cells against PDGF-BB, so I hypothesize that DIO-associated sympathetic neuropathy in adipose tissue can deplete mural cells and increase vascular leakiness.

5.2 Methodology

To find out the effect of DIO on NPY$^+$ innervation, mice were treated with HFD for 10 weeks, and the innervation was evaluated by light-sheet microscopy of cleared adipose tissues immunolabelled for NPY and CD31. Similarly, adipose tissues immunolabeled for DES and CD31 or PV1, a marker for vascular leakiness (Hallmann, Mayer, Berg, Broermann, & Butcher, 1995; Carloni et al., 2021) were imaged, and mural cell coverage and vascular leakiness were calculated.

To assess whether mural cell coverage and vascular leakiness are only associated with NPY$^+$ innervation and are not changed when NPY levels are unchanged, I immunolabeled sympathetic ganglia, where NPY expression is not altered by obesity, for DES and CD31 or PV1, and calculated mural cell coverage and vascular leakiness.

5.3 Result

5.3.1 DIO depletes NPY$^+$ innervation and decreases NPY concentration in adipose tissue

To test whether NPY$^+$ sympathetic axons are affected by the obesity-induced sympathetic neuropathy in the adipose tissue (P. Wang et al., 2020), I immunolabelled the cleared iWAT of normal diet (ND)- and high-fat diet (HFD)-treated mice for NPY and CD31. The light-sheet images show a decreased density of NPY$^+$ axons and a decreased percentage of vessels innervated by NPY$^+$ axons in the iWAT of HFD-treated mice compared with ND-treated lean mice (Figure 5.2a-b). Consistently, NPY concentration also diminished in the iWAT of HFD-induced and leptin-deficient obese mice (Ob/Ob) (Figure 5.2c). It was further confirmed that

the decrease in NPY concentration was not due to the changes in the NPY concentration in the blood plasma since the plasma NPY concentration was not affected by obesity (Figure 5.2d).

5.3.2 DIO results in loss of mural cell coverage and increased vascular leakiness in adipose tissue

I then investigated if mural cells, the postsynaptic targets of NPY^+ innervation in iWAT, were also affected by obesity. By immunolabelling cleared iWATs for DES and CD31, I found that there were fewer mural cells covering the vasculature of the iWAT of DIO mice compared with age-matched lean mice (Figure 5.3).

Given that mural cells are essential for vascular integrity (Onogi et al., 2017), we observed increased vascular leakiness in the iWAT of DIO mice, as revealed by PV-1 staining (Hallmann et al., 1995; Carloni et al., 2021; Spadoni et al., 2015) (Figure 5.4). This result is consistent with previous reports indicating increased immune infiltration in the adipose tissues of obese individuals (Guzik, Skiba, Touyz, & Harrison, 2017).

5.3.3 DIO does not affect Npy levels, mural cell coverage or vascular leakiness in sympathetic ganglia

It has been established that NPY^+ innervation and NPY concentration were decreased in the iWAT of DIO mice. This decrease was not due to any changes in *Npy* expression in the ganglionic neuronal soma since *Npy* expressions in both SCG and SG were unaltered (Figure 5.5). These results indicate that obesity-induced sympathetic neuropathy reduces the NPY^+ innervation in the adipose tissue, which decreases the local concentration of NPY in the iWAT. DIO depletes mural cells in the iWAT of DIO mice (Figure 5.3). To determine if this phe-

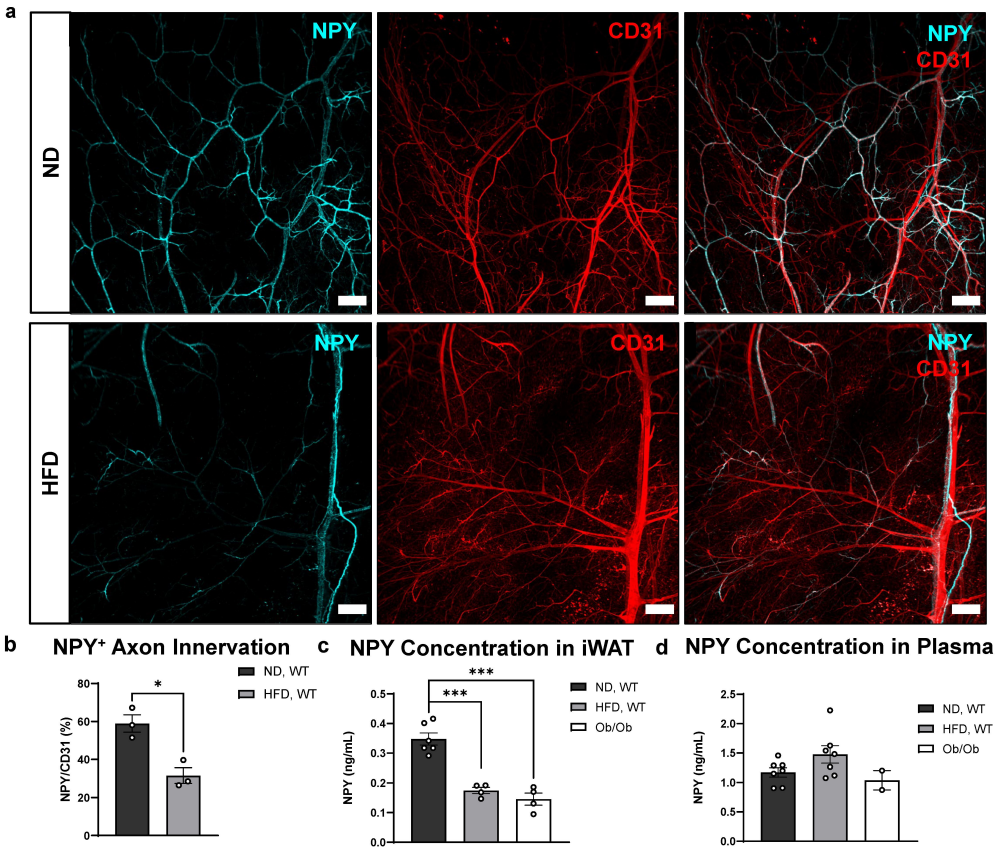


Figure 5.2: **High-fat diet-induced obesity (DIO) depletes NPY$^+$ innervation.** (a) Light-sheet images of cleared iWAT of normal diet (ND)-treated and high-fat diet (HFD)-treated 17-week-old male WT mice stained with anti-NPY (cyan) and anti-CD31 (red). Scale bar=500μm. (b) NPY$^+$ innervation calculated as the ratio of NPY to CD31 quantified based on images as in (a) (n=3 mice, P=0.0112). (c-d) The concentration of NPY in (c) iWAT (n=5&4&4 mice) and (d) blood plasma of ND and HFD-treated 17-week-old male WT mice, and ND-treated Ob/Ob 17-week-old male mice (n=6&7&2 mice). P=0.0002 for both comparisons. All values are expressed as mean $\pm$ SEM. Statistical comparisons were made using 2-tailed Student T-tests, *p<0.05, **p<0.01, ***p<0.001, ****p<0.0001.

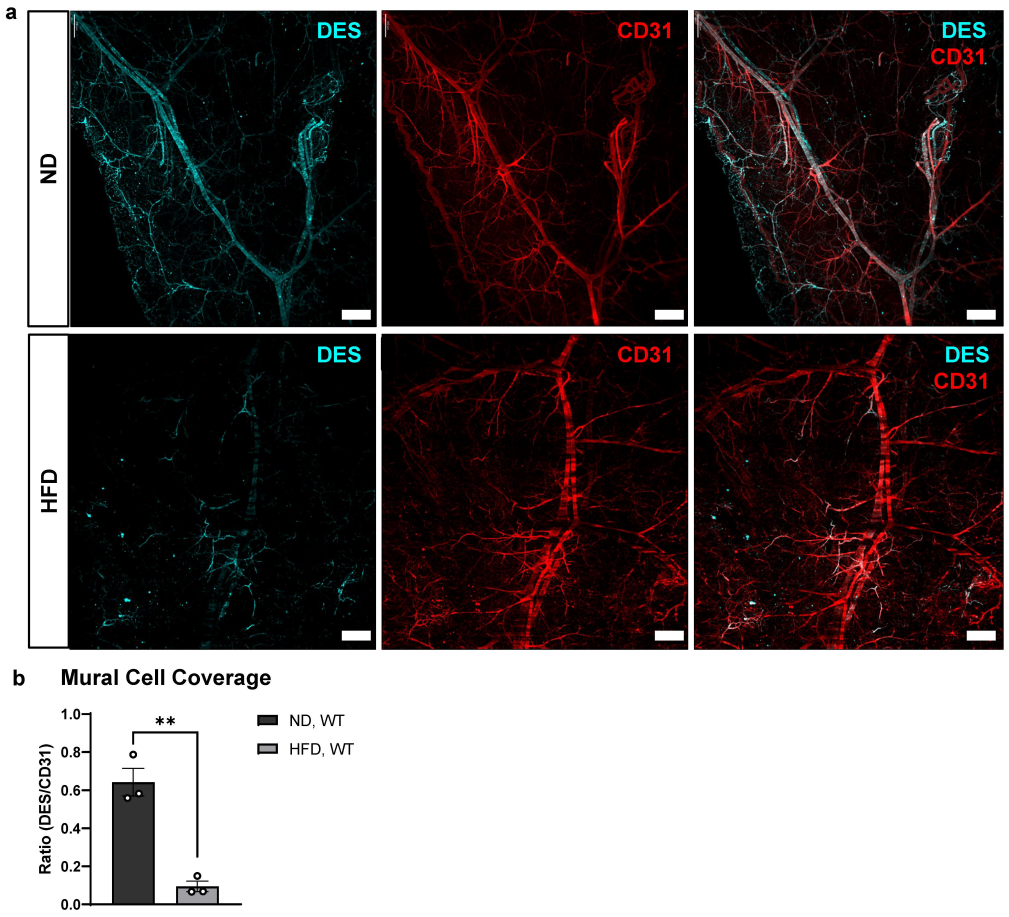


Figure 5.3: **DIO depletes mural cells in iWAT.** (a) Light-sheet images of cleared iWAT of ND- and HFD-treated 17-week-old male WT stained with anti-DES (cyan) and anti-CD31 (red). Scale bar=500μm. (b) Mural cell coverage was calculated as the ratio of DES$^+$ cells to CD31$^+$ cells quantified based on images as in (a) (n=3 mice, P=0.0021).

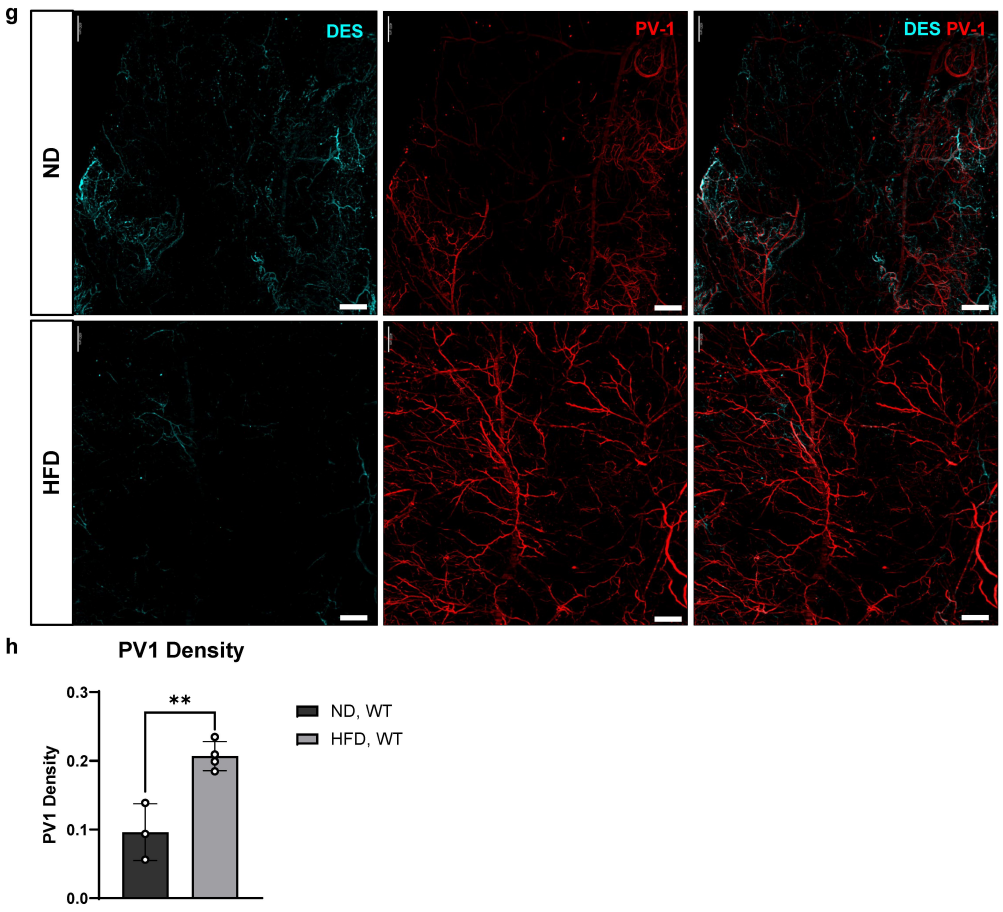


Figure 5.4: **DIO increases vascular leakiness in iWAT.**(a) Light-sheet images of iWATs of ND- and HFD-treated 17-week-old male mice stained with anti-DES (cyan) and anti-PV1 (red). Scale bar=500μm. (b) PV-1 density was quantified based on images as in (a) (n=3&4 mice, P=0.0053). All values are expressed as mean $\pm$ SEM. Statistical comparisons were made using 2-tailed Student T-tests, *p<0.05, **p<0.01, ***p<0.001, ****p<0.0001.

nomenon is related to NPY levels, we immunolabelled sympathetic ganglia for DES to ascertain if the mural cell coverage changes when the NPY levels are unaffected. We observed no significant difference in mural cell coverage of ganglionic vasculature between DIO mice and lean mice (Figure 5.5c&Figure 5.6), confirming that mural cell coverage positively correlates with local NPY level.

5.3.4 Discussion

Previous research indicates that sympathetic innervation in adipose tissue is decreased by obesity (P. Wang et al., 2020), here we show that consistently, NPY^+ innervation is also depleted by obesity. Relevant to NPY^+ axon depletion, mural cell coverage and vascular leakiness were also decreased. This phenomenon implies a positive correlation between NPY and mural cell coverage, supporting my previous finding that NPY sustains mural cells. The data shown in previous chapters let me hypothesize that the role of sympathetic-neuron-derived NPY is to maintain energy and immunometabolic homeostasis by sustaining mural cells as a source of thermogenic adipocytes as well as the protector of vascular integrity (Figure 5.7).

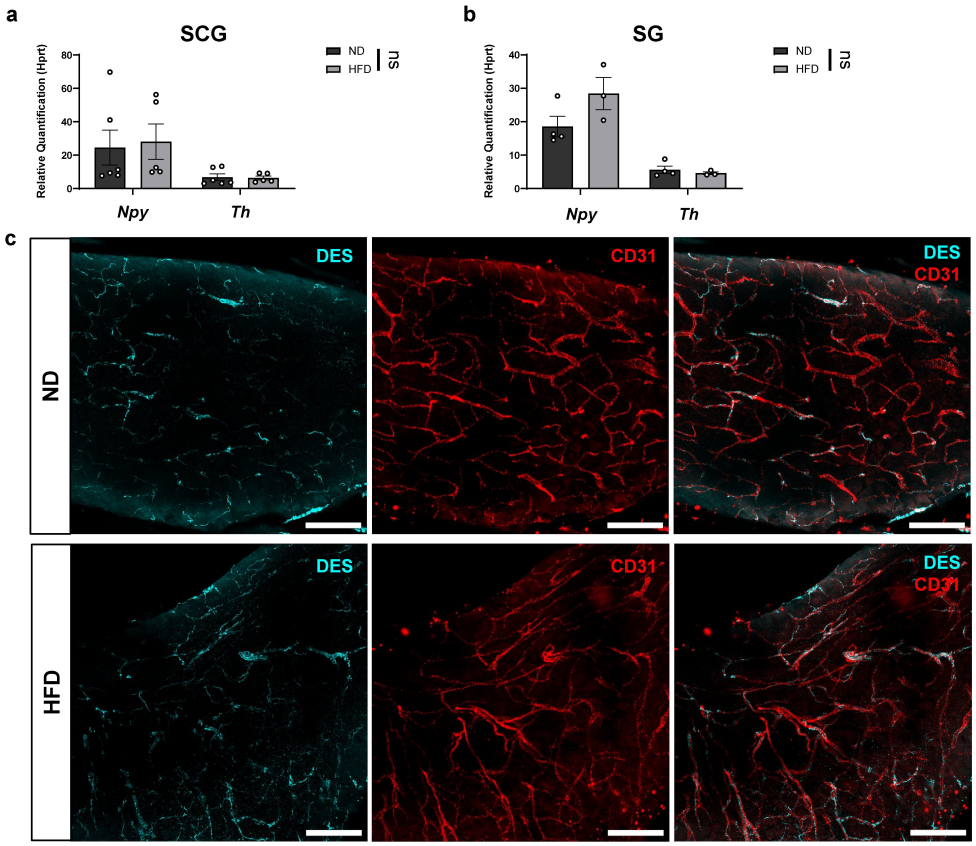


Figure 5.5: **DIO does not affect ganglionic NPY or SCG mural cell coverage.** (a-b) The expression of Npy and Th in the (a) superior cervical ganglia (SCG, n=6&5) and (b) stellate ganglia (SG, n=4&3) of ND- and HFD-treated 17-week-old WT male mice. (c) The images of cleared SCG and of ND- and HFD-treated 17-week-old WT male mice stained with anti-DES (cyan) and anti-CD31 (red) antibodies. Scale bar=100μm. All values are expressed as mean $\pm$ SEM. Statistical comparisons were made using 2-tailed Student T-tests, *p<0.05, **p<0.01, ***p<0.001, ****p<0.0001.

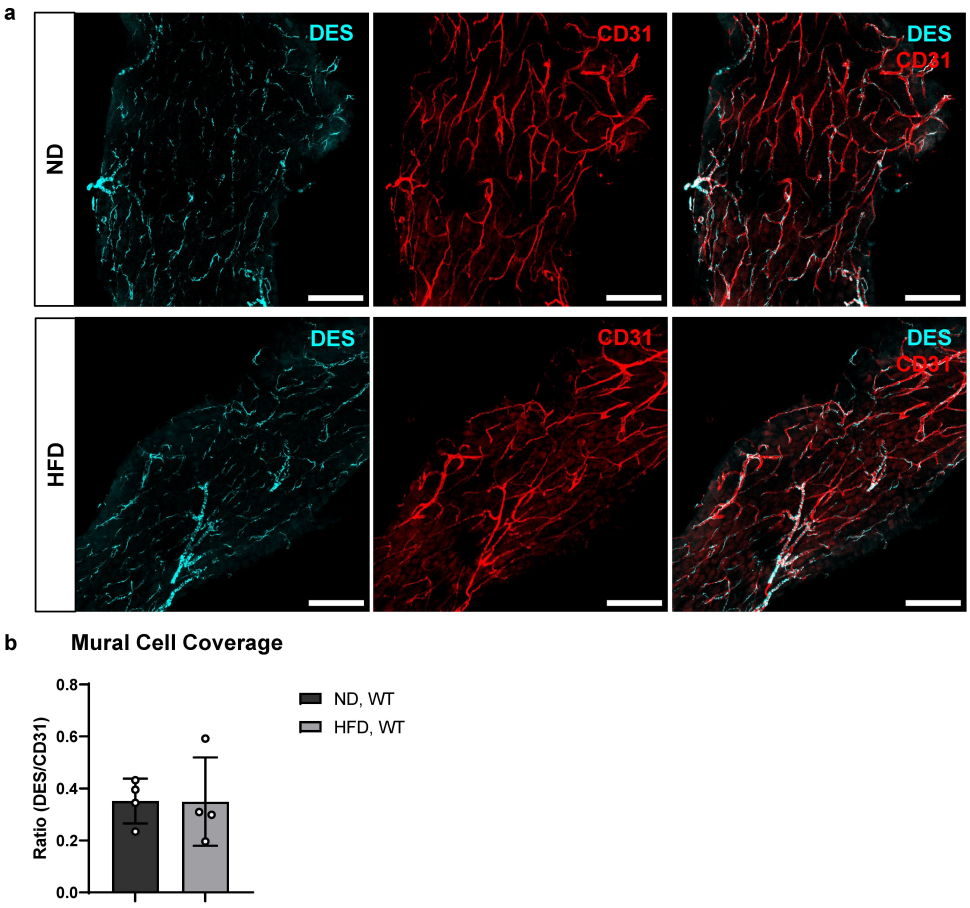


Figure 5.6: DIO does not affect mural cell coverage in SG. (a) The images of cleared SG of ND- and HFD-treated 17-week-old WT male mice stained with anti-DES (cyan) and anti-CD31 (red) antibodies. Scale bar=100μm. (e) The quantification of mural cell coverage in SG (n=4). All values are expressed as mean $\pm$ SEM. Statistical comparisons were made using 2-tailed Student T-tests, *p<0.05, **p<0.01, ***p<0.001, ****p<0.0001.

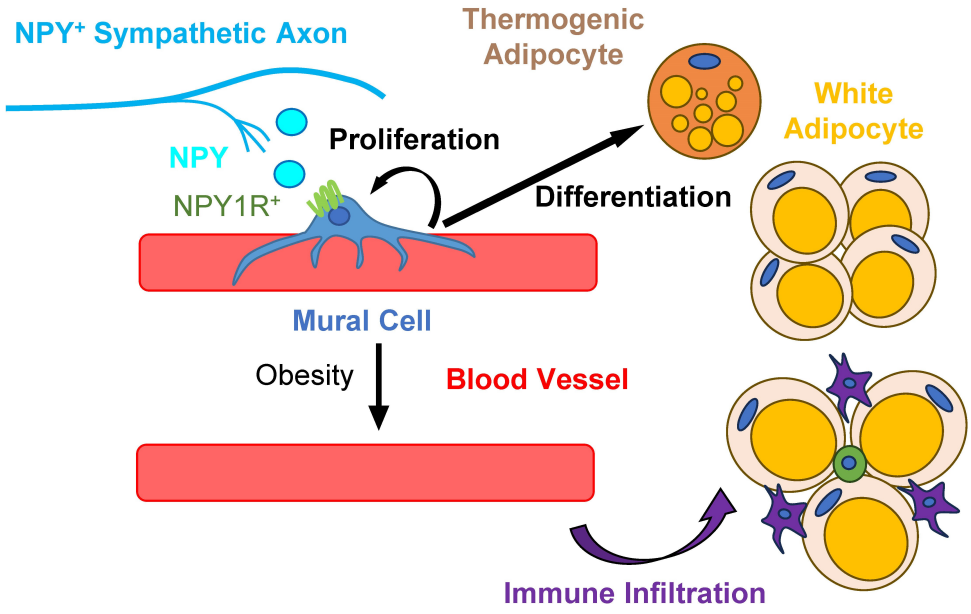


Figure 5.7: **Sympthetic-neuron-derived NPY maintains thermogenesis and vascular integrity by sustaining mural cells.**

6 | Sympathetic-Neuron-Derived NPY and Immunometabolic Homeostasis

6.1 Introduction

6.1.1 TH and NPY collocalisation

NPY exists in the periphery SNS and the adrenergic gland (LUNDBERG et al., 1982; Renshaw & Hinson, 2001). In the central nervous system, NPY can be found in the Arc of the hypothalamus, while NPY is not colocalised with TH in the hypothalamus (X. Zhang & van den Pol, 2016). Based on these findings, generating a mouse model with NPY ablated from the SNS by crossing Th^{Cre} mice with $Npy^{flox/flox}$ mice will not affect NPY in the hypothalamus, but it is unknown whether it will affect systemic NPY level. To verify the specificity of this mouse model, I checked the NPY level in the hypothalamus and blood plasma.

6.1.2 Thermogenesis and adipose tissue inflammation

Thermogenic adipocytes can generate heat using the UCP1-dependent and independent pathways and are important for maintaining energy homeostasis. Thermogenesis is affected by the progenitor of thermogenic adipocytes: energy expenditure (EE) and whole-body metabolism can be greatly affected if the progenitors are abrogated (Oguri et al., 2020). Adipose tissue will develop chronic inflammation in the obese state (Xu et al., 2003; Weisberg et al., 2003), and increased levels of cytokines and infiltrated immune cells can also affect thermogenesis: increased SAMs in obesity can degrade NE, an important neurotransmitter for thermogenesis and lipolysis (Pirzgalska et al., 2017; W. Zeng et al., 2015); pro-inflammatory

cytokines including IL1 and TNFα can suppress thermogenesis and the neogenesis of thermogenic adipocytes (Goto et al., 2016; Valladares et al., 2001; Estève et al., 2015). Since mural cells are a source of thermogenic adipocytes and can maintain vascular integrity, and NPY is important for sustaining mural cells, I hypothesize that the loss of NPY from the SNS will deplete mural cells, causing decreased thermogenesis and increased adipose tissue inflammation, which will result in decreased EE, cold tolerance and obesity.

6.2 Result

6.2.1 Th^{Cre};$Npy^{flox/flox}$ mouse model removes NPY from SNS efficiently and specifically

The idea to generate a mouse model where NPY is deleted from the SNS by crossing Th^{Cre} with $Npy^{flox/flox}$ mice is reasonable because TH and NPY do not colocalise in the hypothalamus (X. Zhang & van den Pol, 2016), which is also testified by immunolabelling the hypothalamus for TH and NPY (Figure 6.1b&d). The dopaminergic TH^+ neurons in the ventral tegmental area (VTA) do not have NPY as well (Figure 6.1a%c). Consistent with the lack of NPY/TH colocalisation in the hypothalamus, Th^{Cre};$Npy^{flox/flox}$ mice do not have altered levels of NPY in the hypothalamus, with *Cre* being expressed (Figure 6.1e). We also found that Th^{Cre};$Npy^{flox/flox}$ mice have the same NPY concentration in the blood plasma as WT mice, confirming that NPY-conditional knockout using Th^{Cre} does not affect the systemic NPY level (Figure 6.1f).

To verify that NPY is successfully removed from the SNS, I tested *Npy* expression in SCG and SG and found the expression was decreased (Figure 6.2a-b). By immunolabelling cleared iBAT and iWAT, I demonstrated that NPY^+ axons are

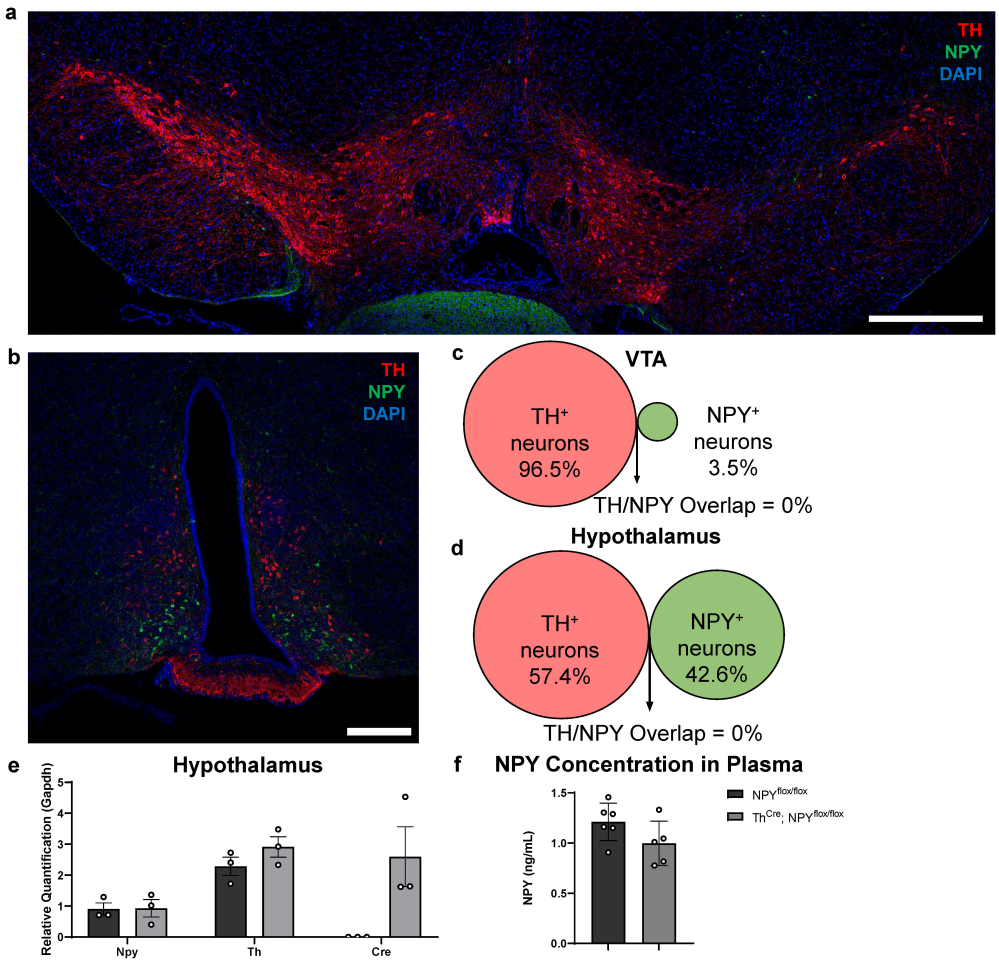


Figure 6.1: **Ablating NPY from sympathetic neurons using Th^{Cre};$Npy^{flox/flox}$ mice does not affect NPY levels in VTA, hypothalamus or plasma.** (a&c) Confocal image showing a slice of (a) ventral tegmental area (VTA, Scale bar=500μm) and (c) arcuate nucleus (Arc, Scale bar=200μm) of the hypothalamus of an NPY-GFP mouse stained with anti-TH (red), anti-GFP (green), and DAPI (blue). (b&d) Quantification of TH/NPY-GFP overlap in (b) VTA and (d) hypothalamus (n=3 mice). (e) The expression of *Npy, Th*, and *Cre* in the hypothalamus of 12-week-old Th^{Cre};$Npy^{flox/flox}$ and $Npy^{flox/flox}$ male mice (n=3). (f) NPY concentration in the blood plasma of 12-week-old Th^{Cre};$Npy^{flox/flox}$ and $Npy^{flox/flox}$ male mice (n=6&5). All values are expressed as mean $\pm$ SEM.

depleted in the adipose tissues of Th^{Cre};$Npy^{flox/flox}$ mice (Figure 6.2), while the TH^{+} sympathetic innervation was not changed (Figure 6.2c-f).

6.2.2 Loss of SNS-derived NPY depletes mural cells and increases immune infiltration in adipose tissues

To test the hypothesis that sympathetic-neuron-derived NPY is required to sustain mural cells *in vivo*, Using this mouse model, we demonstrated that the loss of NPY in sympathetic neurons downregulated mural cell markers in the iBAT of ND-treated mice (Figure 6.3c) and depleted mural cells from the iBAT and iWAT (Figure 6.3a-b). Since mural cells are required for vascular integrity (Daneman, Zhou, Kebede, & Barres, 2010), we observed increased vascular leakiness in both iBAT and iWAT of Th^{Cre};$Npy^{flox/flox}$ mice, as demonstrated by PV1-staining (Figure 6.3a-b). Consistent with the fact that increased vascular leakiness can increase immune infiltration into the adipose tissues, higher levels of cytokine genes including *Tnf* and *Il6* are expressed in the iBAT of Th^{Cre};$Npy^{flox/flox}$ mice (Figure 6.3d).

Using cell cytometry, I also showed that there are fewer mural cells and more infiltrated immune cells in the adipose tissues of ND-treated Th^{Cre};$Npy^{flox/flox}$ mice (Figure 6.4a-b). In HFD-treated Th^{Cre};$Npy^{flox/flox}$ mice, fewer mural cells exist in their adipose tissues (Figure 6.4c-e).

With the help of Professor Licio's lab members, We further evaluated vascular leakiness in epididymal WATs using an intravital method by intravenous (i.v.) injection of Dextran-70kDa. The same amount of Dextran was injected into the vasculature of Th^{Cre};$Npy^{flox/flox}$ and $Npy^{flox/flox}$ mice (Figure 6.5a-b&d). Increased vascular leakiness in Th^{Cre};$Npy^{flox/flox}$ mice was revealed by the leak of Dextran-70kDa into the parenchyma (Figure 6.5c), while blood flow remained unchanged

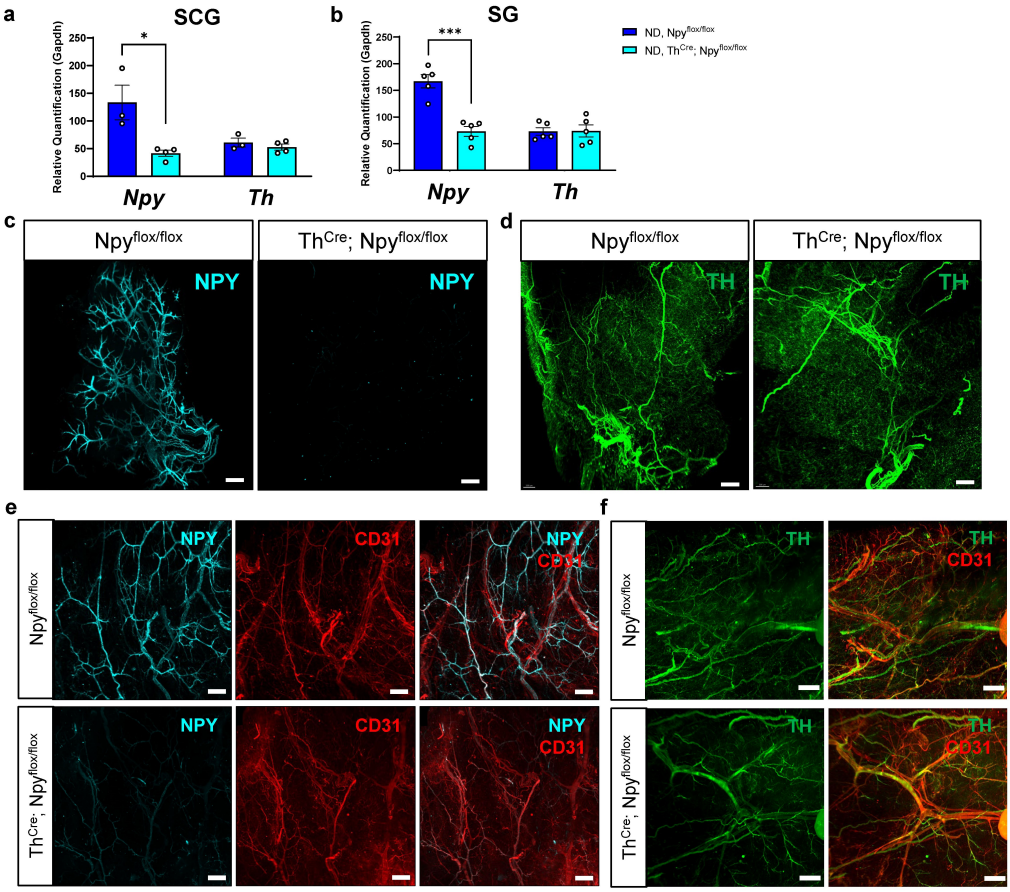


Figure 6.2: **Th^{Cre};Npy$^{flox/flox}$ mice have depleted NPY from the sympathetic nervous system and unchanged sympathetic innervation.** (a-b) The expression of *Npy* and *Th* in (a) SCG (n=3&4 mice) and (b) SG (n=5 mice) of 12-week-old Th^{Cre};Npy$^{flox/flox}$ and Npy$^{flox/flox}$ male mice.(c-d) Light-sheet image of cleared iBAT of 12-week-old Th^{Cre};Npy$^{flox/flox}$ and Npy$^{flox/flox}$ male mice stained with (c) anti-NPY (cyan), scale bar=500μm, or (d) anti-TH (green), scale bar=200μm. (e-f) The image of cleared iWAT of 12-week-old Th^{Cre};Npy$^{flox/flox}$ and Npy$^{flox/flox}$ male mice stained with (e) anti-NPY (cyan) or (f) anti-TH (green) and anti-CD31 (red). Scale bar=500μm. All values are expressed as mean $\pm$ SEM. Statistical comparisons were made using 2-tailed Student T-tests, *p<0.05, ***p<0.001.

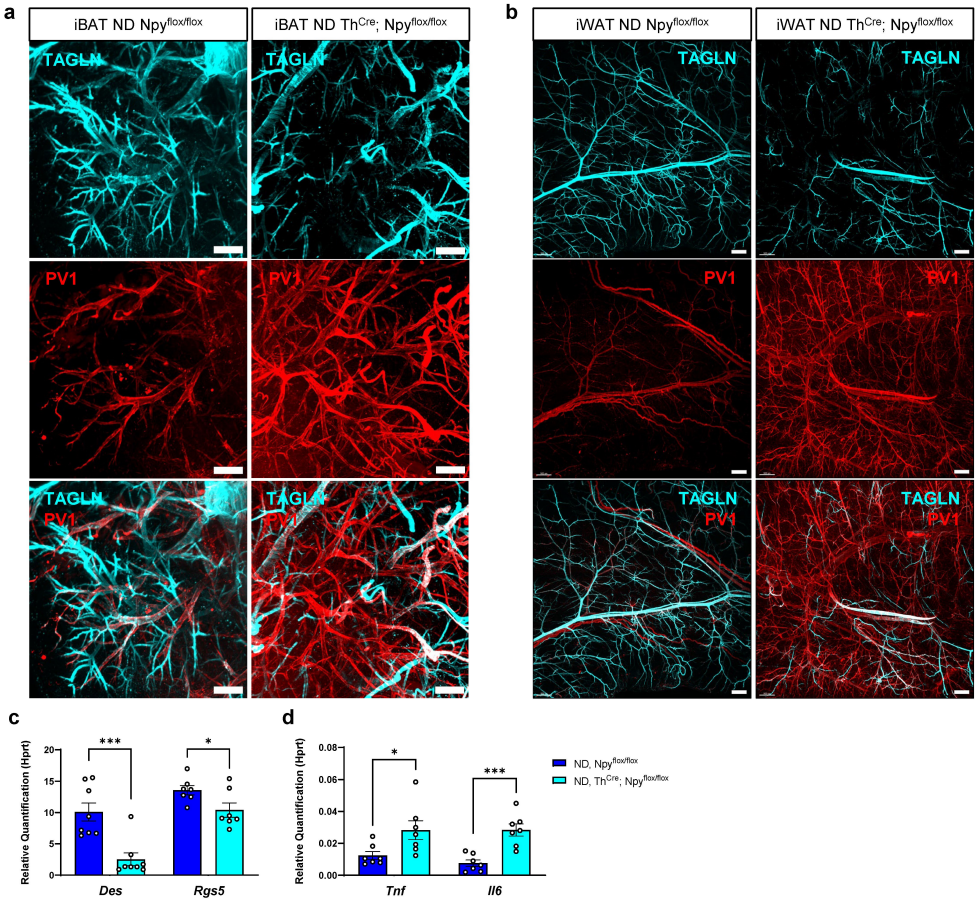


Figure 6.3: **Loss of NPY from sympathetic neurons depletes mural cells and increases vascular leakiness in both iBAT and iWAT.** (a-b) Light-sheet image of cleared (a) iBAT of 15-week-old ND-treated mice (scale bar=200μm) and (b) iWAT of 30-week-old ND-treated mice (scale bar=500μm) stained with anti-PV1 (red) and anti-TAGLN (cyan). (c-d) The expression levels of (c) mural cell markers *Des* (n=8 mice), *Rgs5* (n=7 mice), and (d) pro-inflammatory genes *Tnf* (n=7 mice), and *Il6* (n=7 mice) in the iBATs of ND-treated 12-week-old male Th^{Cre};$Npy^{flox/flox}$ and $Npy^{flox/flox}$ mice. All values are expressed as mean $\pm$ SEM. Statistical comparisons were made using 2-tailed Student T-tests, $^{*}p<0.05$, $^{***}p<0.001$.

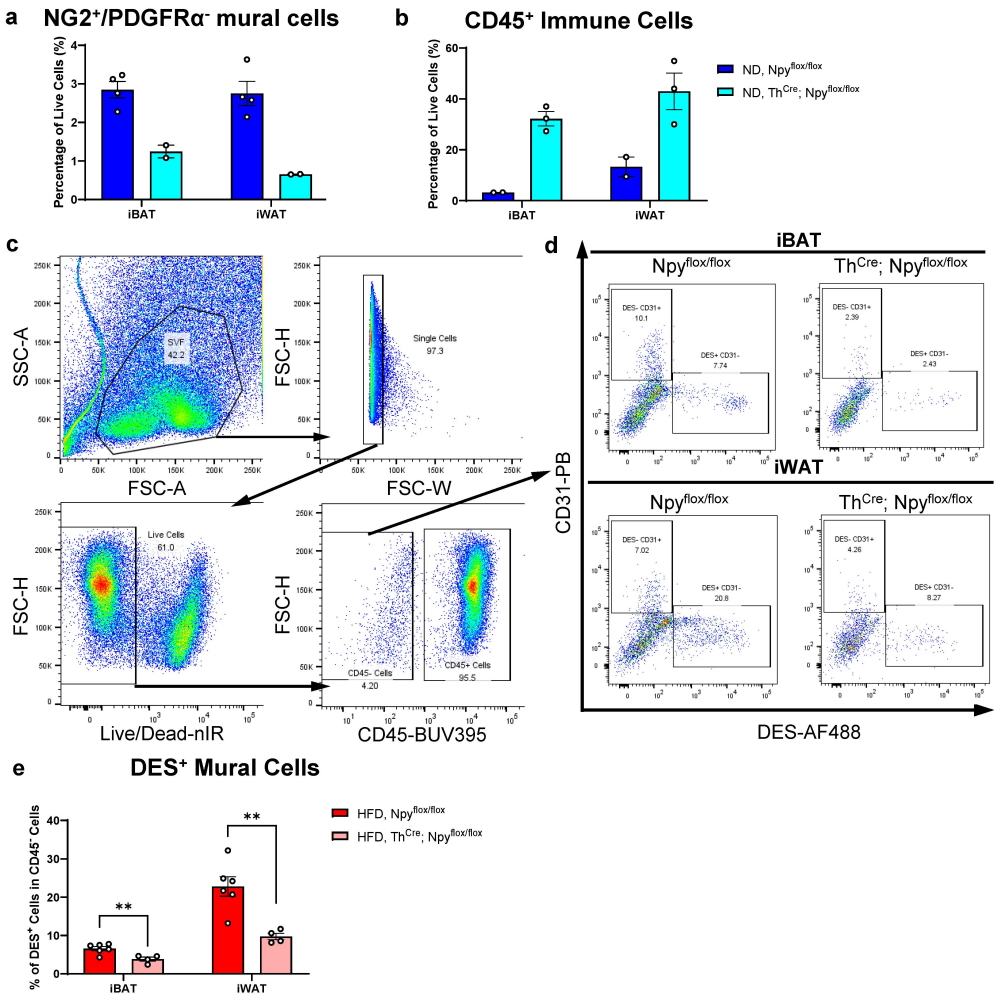


Figure 6.4: **Loss of sympathetic NPY causes mural cell loss and immune infiltration.** (a-b) The percentage of (a) PDGFRα^- /NG2$^+$ mural cells (n=4&2 mice) and (d) CD45$^+$ immune cells (n=2&3 mice) in iBATs and iWATs of 30-week-old, ND-treated mice measured by flow cytometry. (c) The gating strategy of flow cytometry to quantify the percentage of CD45$^+$ immune cells DES$^+$ mural cells. (d) The representative flow cytometry analysis of the percentage of mural cells (DES$^+$) in the iBAT (top) and iWAT (bottom) of HFD-treated male Th^{Cre};Npy$^{flox/flox}$ and Npy$^{flox/flox}$ mice. (e) The percentage of DES+ mural cells in iBATs and iWATs of 17-week-old, HFD-treated mice was measured by flow cytometry (n=4 mice). All values are expressed as mean $\pm$ SEM. Statistical comparisons were made using 2-tailed Student T-tests, $^{**}p<0.01$.

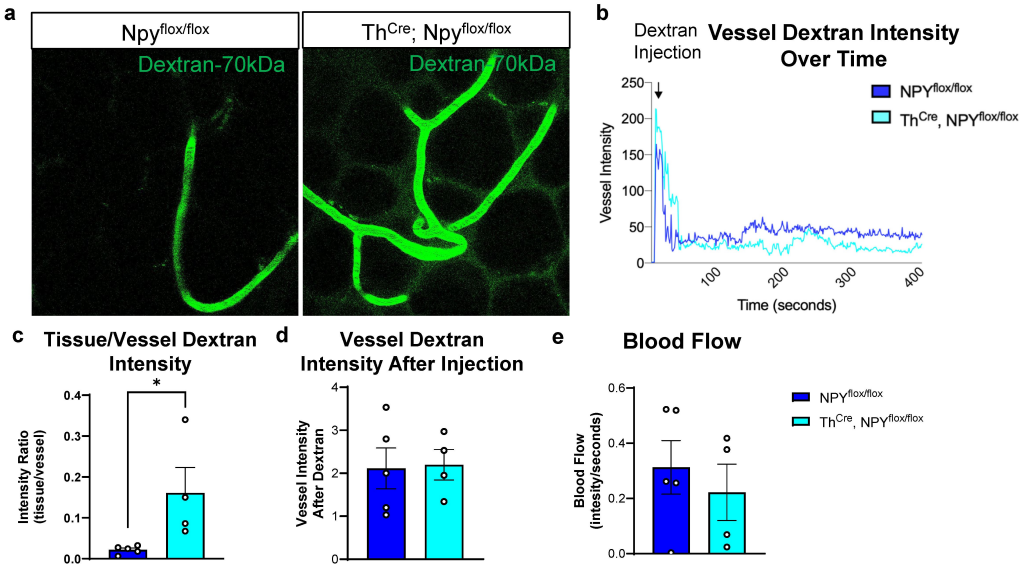


Figure 6.5: **The loss of sympathetic NPY increases vascular leakiness revealed by Dextran injection.** (a) Intravital microscopy of epididymal WATs of 23-week-old male Th^{Cre};$Npy^{flox/flox}$ and $Npy^{flox/flox}$ mice 12 minutes after i.v. injection of 70kDa Dextran at the orbital plexus. (b) Dextran intensity in vessels over time was measured with a 2-photon microscope. The arrow indicates the time when Dextran was injected. (c) The fluorescence intensity ratio between tissue parenchyma and the vessel was calculated based on images as (a) (n=5&4 mice). (d) Dextran intensity in the vessels of eWAT right after i.v. injection (n=5&4 mice). (e) Blood flow was calculated using the average of the raw intensity of Dextran inside the artery over 100 seconds right after the stabilization of the Dextran signal following administration (n=5&4 mice). All values are expressed as mean ± SEM. Statistical comparisons were made using 2-tailed Student T-tests, $^{*}p<0.05$.

(Figure 6.5e). These observations confirmed that NPY is required to sustain mural cells in adipose tissue and prevent immune infiltration.

6.2.3 Loss of SNS-derived NPY whitens BAT, reduces its thermogenic ability, and lowers energy expenditure (EE)

To test the hypothesis that NPY locally sourced from sympathetic axons in adipose tissues preserves the mural cell pool and is required for energy homeostasis,

we characterised the metabolism of Th^{Cre};$Npy^{flox/flox}$ mice. We discovered that ND-treated lean Th^{Cre};$Npy^{flox/flox}$ mice had whitened iBAT (Figure 6.6a), and their iBATs were dysfunctional in thermogenesis as shown by lower levels of thermogenic genes (Figure 6.6b). Consistent with this, Th^{Cre};$Npy^{flox/flox}$ mice have lower daily energy expenditure (EE) (Figure 6.6c-d). The decreased EE was not caused by the lower amount of muscles or local motor activity since these were unchanged in Th^{Cre};$Npy^{flox/flox}$ mice (Figure 6.6e-f). To directly show thermogenesis, mice were fasted for 14 hours and their iBAT temperatures were recorded (Figure 6.6g). The result indicates that Th^{Cre};$Npy^{flox/flox}$ mice displayed lower iBAT temperature and lost less weight during a 14-hour fast, indicative of energy conservation (Figure 6.6h-i).

Lower cold tolerance of Th^{Cre};$Npy^{flox/flox}$ mice was also demonstrated by the cold-challenge experiment (Figure 6.7a). After 8-hour cold exposure, Th^{Cre};$Npy^{flox/flox}$ mice displayed lower rectal temperature (Figure 6.7b) and downregulated thermogenic genes in iBAT and *Prdm16* in iWAT (Figure 6.7c-d) compared with their WT littermates.

All the data above demonstrate that the loss of NPY from sympathetic neurons negatively affects beiging and thermogenesis, and decreases EE and cold tolerance, indicating the importance of sympathetic-neuron-derived NPY in energy homeostasis.

6.2.4 Loss of SNS-derived NPY leads to adult-onset obesity and makes mice more susceptible to obesity without changing food consumption

Using a metabolic cage, we also found that Th^{Cre};$Npy^{flox/flox}$ mice have higher respiratory exchange ratio (RER), indicating that these mice have a defective ability

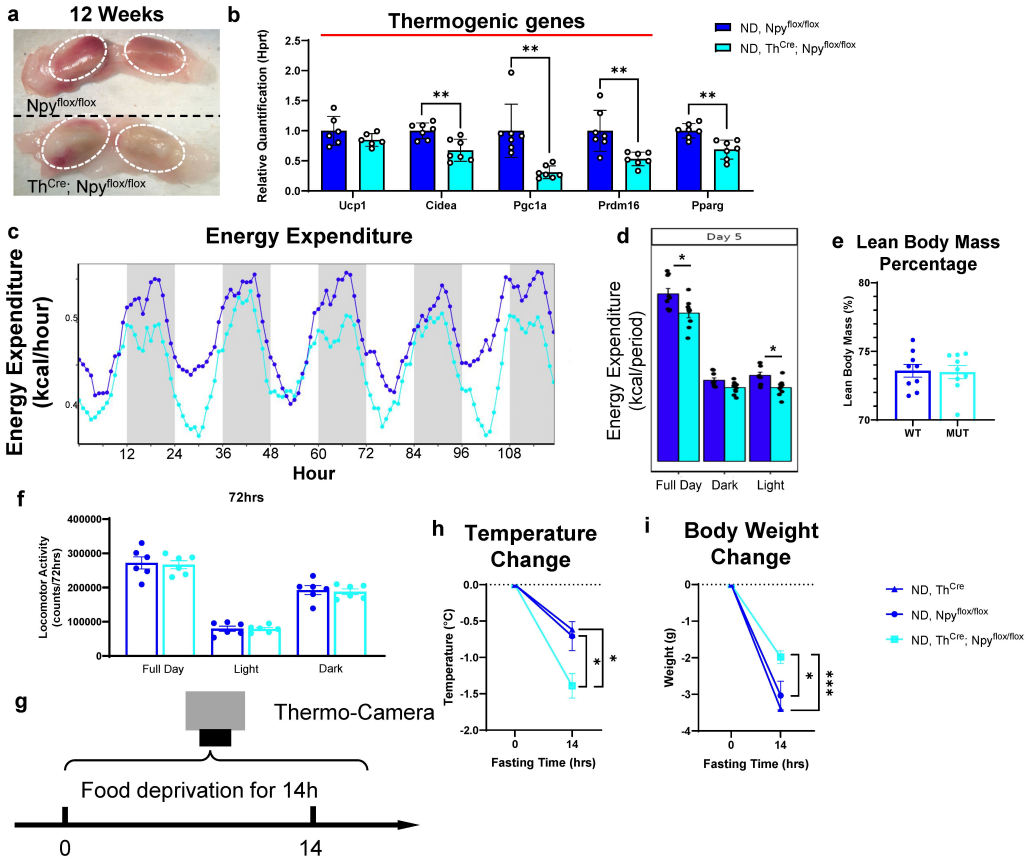


Figure 6.6: **Loss of sympathetic NPY whitens iBATs and decreases thermogenesis and EE.** (a) iBATs dissected from ND-treated male $Npy^{flox/flox}$ and Th^{Cre};$Npy^{flox/flox}$ mice. Dashed lines encircle the lobes of iBATs. (b) Expression of *Ucp1*, *Cidea* (P=0.0024), *Pgc1a* (P=0.0018), *Prdm16* (P=0.0048), and *Pparg* (P=0.0012) in the iBATs of ND-treated 12-week-old male Th^{Cre};$Npy^{flox/flox}$ and $Npy^{flox/flox}$ mice (n=6 mice for *Ucp1*; n=7 mice for other genes). (c) Daily energy expenditure of 7-week-old male Th^{Cre};$Npy^{flox/flox}$ and $Npy^{flox/flox}$ mice was measured using an indirect calorimetry system (n=9 mice). (d) The quantification of daily energy expenditure (EE) (n=9 mice). (e) The percentage of lean body weight (LBM) of 8-week-old male mice was measured by MiniSpec MRI (n=9). (f) The locomotor activity was measured using a Multitake cage (n=6 mice). (g) Schematic of food deprivation and thermo-imaging. (h-i) Changes in (h) iBAT temperature and (e) body weights of 12-week-old mice after a 14-hour fast (n=6 for Th^{Cre};$Npy^{flox/flox}$ mice and n=3 for Th^{Cre} and $Npy^{flox/flox}$ mice). All values are expressed as mean ± SEM. Statistical comparisons were made using 2-tailed Student T-tests, $^{*}p<0.05$, $^{**}p<0.01$, $^{***}p<0.001$.

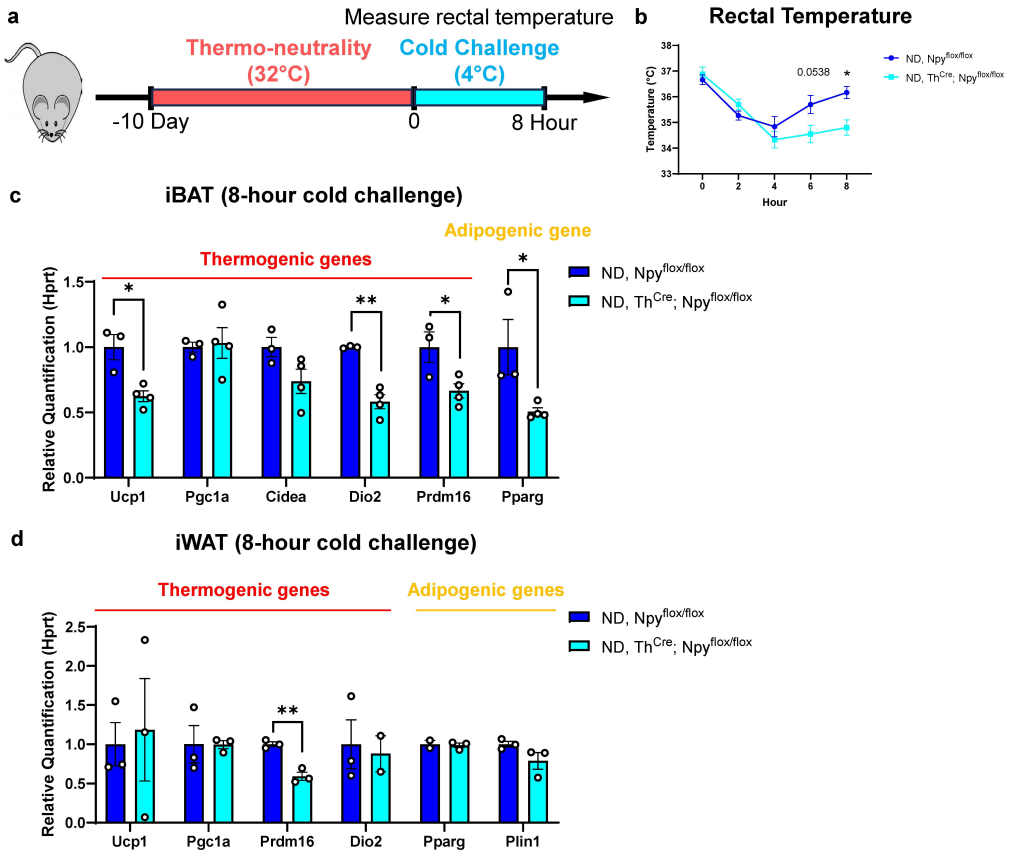


Figure 6.7: **Loss of sympathetic NPY causes decreased cold tolerance.** (a) Schematic of cold-challenging mice and recording rectal temperature. (b) Rectal temperature of 20-week-old $Npy^{flox/flox}$ and Th^{Cre};$Npy^{flox/flox}$ mice under cold exposure recorded using a rectal probe every hour (n=3&4 mice). (c-d) The expression of thermogenic and adipogenic genes in (c) iBATs (n=3&4 mice) and (d) iWATs (n=3 mice) of cold-challenged $Npy^{flox/flox}$ and Th^{Cre};$Npy^{flox/flox}$ mice. All values are expressed as mean ± SEM. Statistical comparisons were made using 2-tailed Student T-tests, $^{*}p<0.05$, $^{**}p<0.01$.

to use lipids for thermogenesis (Figure 6.8a-b). This finding lets me hypothesize that the loss of sympathetic NPY may affect fat depots and obesity. To test this hypothesis, I recorded the body weights of tissue weights of Th^{Cre};$Npy^{flox/flox}$ mice, and found that ND-treated Th^{Cre};$Npy^{flox/flox}$ mice developed adult-onset obesity at 30 weeks (Figure 6.8c), with heavier adipose depots compared with WT mice (Figure 6.8d-f). When on a HFD, Th^{Cre};$Npy^{flox/flox}$ mice became obese earlier and faster than WT mice, without increasing food intake (Figure 6.8g-h). Additionally, HFD-treated Th^{Cre};$Npy^{flox/flox}$ mice had significantly heavier adipose depots (Figure 6.8i), and their iBATs contained larger lipid droplets on average (Figure 6.9).

Lastly, the metabolic phenotypes were consistent across genders, as HFD-treated female Th^{Cre};$Npy^{flox/flox}$ mice also had heavier body weights, WATs, and iBATs compared with Npyflox/flox control mice (Figure 6.10).

6.2.5 Loss of NPY from the hindbrain does not affect thermogenesis or body weight.

It has been reported that NPY also exists in the hindbrain (J. Chen et al., 2020). To verify that the phenotypes of Th^{Cre};$Npy^{flox/flox}$ mice were not due to altered NPY in the hindbrain, I collaborated with Professor Cheng Zhan and generated a mouse model in which NPY is specifically abrogated from the hindbrain by injecting AAV-CRE into the hindbrain of $NPY^{flox/flox}$ mice ($NPY^{flox/flox}$;AAV-CRE mouse, Figure 6.11a). The body and tissue weight of the mice were recorded, and thermogenesis was recorded by measuring iBAT temperature after a 14-hour fast (Figure 6.11b). The results demonstrated that NPY was ablated from the hindbrain of $NPY^{flox/flox}$;AAV-CRE mice (Figure 6.11c) and the loss of NPY from the hindbrain does not affect either body and tissue weight or thermogenesis (Figure

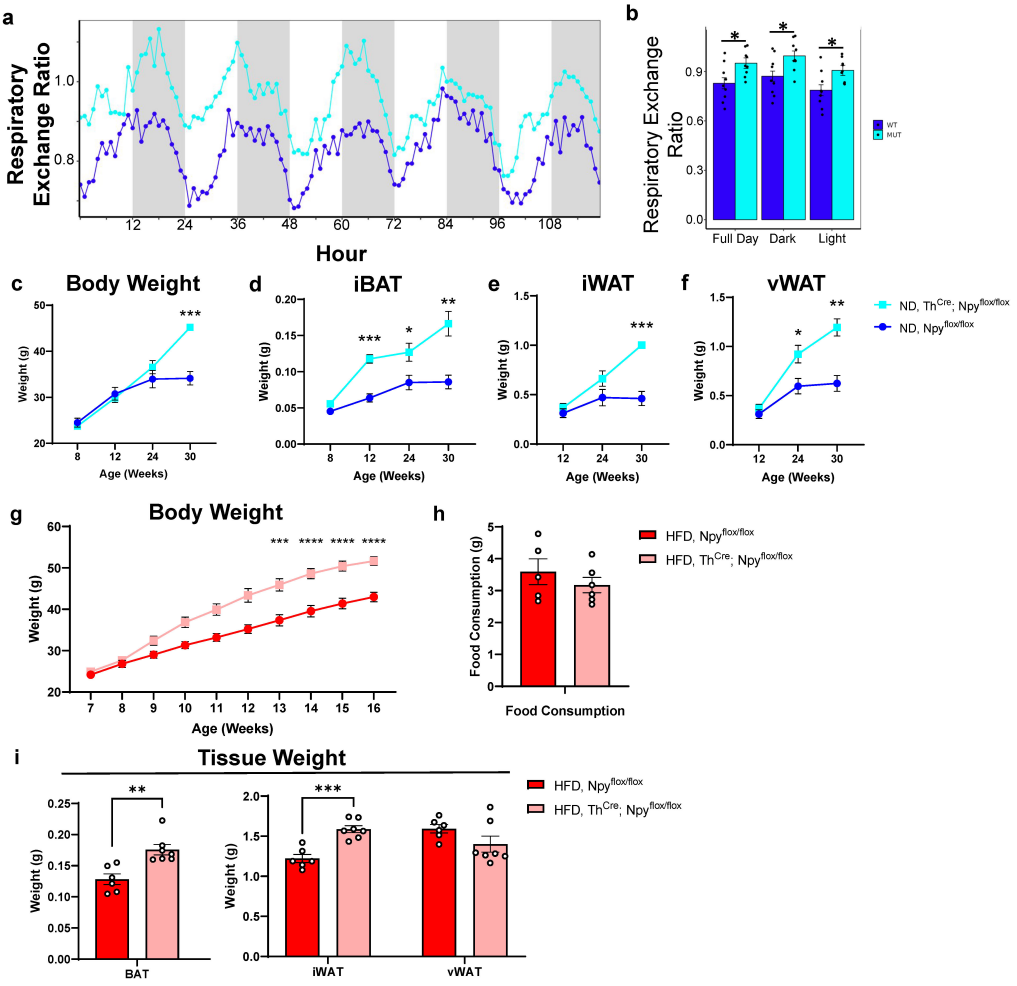


Figure 6.8: **Loss of Sympathetic NPY increases RER, causes adult-onset obesity, and makes mice susceptible to DIO.** (a) Respiratory exchange ratio (RER) of 8-week-old mice recorded using a metabolic cage. (b) The quantification of (a) (n=9 mice). (c-f) (c) Body weight, weights of (d) iBATs, (e) iWATs, and (f) vWATs of ND-treated male Th^{Cre};$Npy^{flox/flox}$ and $Npy^{flox/flox}$ mice (n=4). (g-h) (g) Weekly body weights (n=8) and (h) averaged daily food consumption (n=4&6 cages) of male HFD-treated Th^{Cre};$Npy^{flox/flox}$ and $Npy^{flox/flox}$ mice. (i) Weights of iBATs (n=5&6 mice), (m) iWATs (n=6&7 mice), and vWATs (n=6&7 mice) of HFD-treated 17-week-old male Th^{Cre};$Npy^{flox/flox}$ and $Npy^{flox/flox}$ mice. All values are expressed as mean ± SEM. Statistical comparisons were made using 2-tailed Student T-tests, $^{*}p<0.05$, $^{**}p<0.01$.

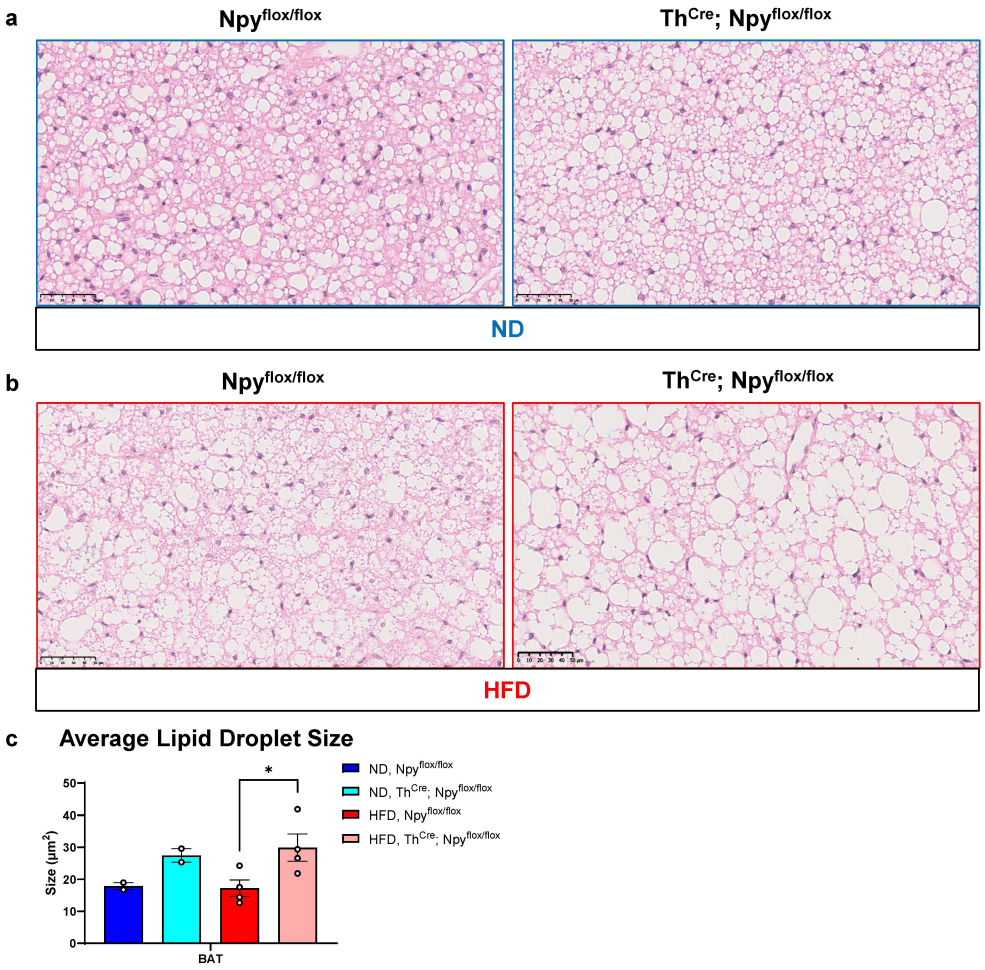


Figure 6.9: **Loss of sympathetic NPY results in bigger adipocyte size.** (a-b) Histological staining of iBATs of (a) ND- (top) and (b) HFD- (bottom) treated 17-week-old male Th^{Cre};$Npy^{flox/flox}$ and $Npy^{flox/flox}$ mice. Scale bar=50μm. (b) The average adipocyte size in the iBATs of ND- and HFD-treated male Th^{Cre};$Npy^{flox/flox}$ and $Npy^{flox/flox}$ mice (n=2 for ND-treated mice, n=4 for HFD-treated mice). All values are expressed as mean $\pm$ SEM. Statistical comparisons were made using 2-tailed Student T-tests, $^{*}p<0.05$.

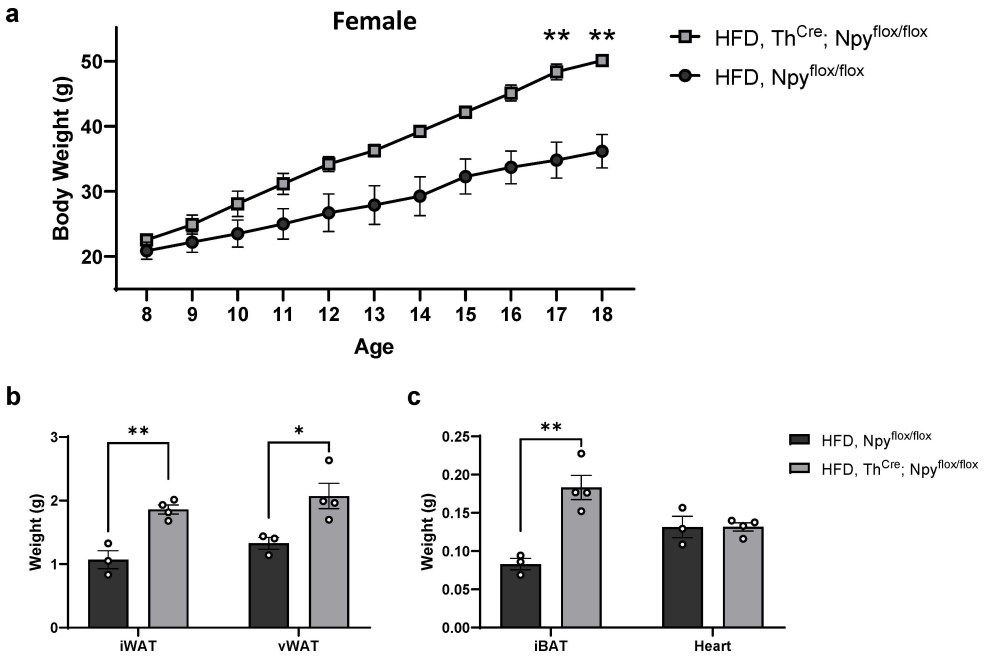


Figure 6.10: **Metabolic phenotype of female Th^{Cre};$Npy^{flox/flox}$ mice is similar to that of males.** (a) The weekly body weights of female Th^{Cre};$Npy^{flox/flox}$ and WT mice treated with high-fat diet (HFD) (n=4). (b-c) The weights of (b) iWAT and vWATs, and (c) iBAT and hearts of HFD-treated 18-week-old female Th^{Cre};$Npy^{flox/flox}$ and $Npy^{flox/flox}$ mice (n=3&4). All values are expressed as mean $\pm$ SEM. Statistical comparisons were made using 2-tailed Student T-tests, $^{*}p<0.05$, $^{**}p<0.01$.

6.11d-g).

6.3 Discussion

In previous chapters, I revealed the NPY-mural cell interactions that sustain mural cells and maintain their identity and ability to differentiate into thermogenic adipocytes. To discover the significance of NPY^{+} axons *in vivo*, I generated the mouse model where NPY is deleted from sympathetic neurons to determine how the loss of sympathetic NPY affects adipose tissue metabolism. First, I confirmed that the mouse model deleted NPY from the SNS without affecting the systemic or CNS NPY level. Then, I found that the loss of sympathetic NPY depletes mural cells resulting in vascular leakiness and immune infiltration, which is consistent with the *in vitro* results. Based on metabolic phenotypes of Th^{Cre};$Npy^{flox/flox}$ mice, I found that NPY derived from the SNS is vital for maintaining thermogenesis and EE, and the loss of sympathetic NPY will disrupt energy homeostasis in terms of reducing EE, resulting in decreased cold tolerance and increased fat depots. The effect of NPY-cKO might be due to a combination of the loss of thermogenic adipocyte progenitors and increased adipose tissue inflammation, which can also negatively affect thermogenesis. Although I have confirmed that the phenotypes I observed in NPY-cKO mice were not caused by plasma NPY or NPY depletion from the hindbrain, it is uncertain whether the phenotypes were affected by NPY depletion from sympathetic axons innervating other peripheral tissues or organs. Still, I uncovered the role of periphery SNS-derived NPY in protecting against obesity without affecting food intake, which is the opposite of CNS-derived NPY. This discovery is consistent with previous reports that the loss of NPY receptors results in late-onset obesity (Naveilhan et al., 1999; Pedrazzini et al., 1998; Nguyen et al., 2012) and able to explain why the NPY mutation in humans is more

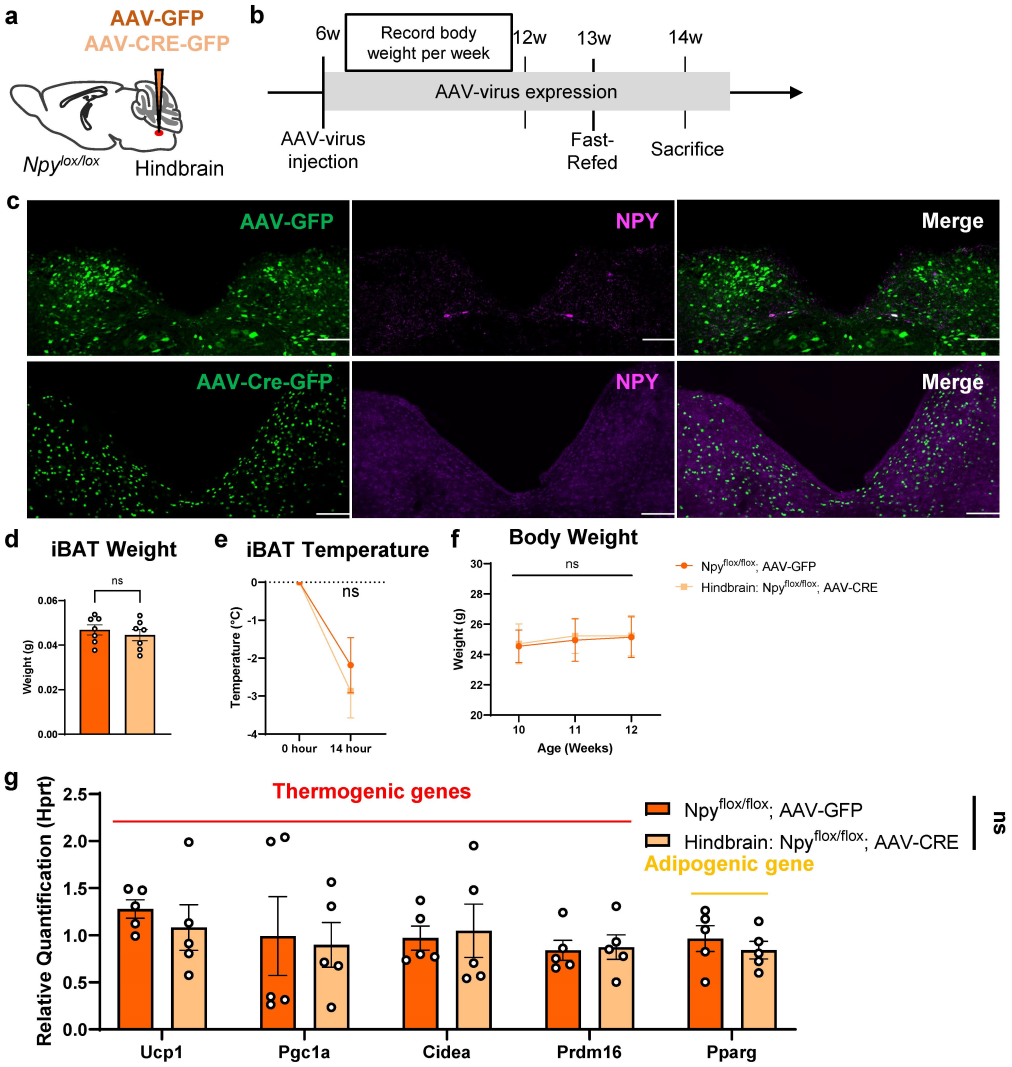


Figure 6.11: **Ablating NPY from the hindbrain does not affect body weight, BAT weight or thermogenesis.** (a) Schematic of knocking out NPY in the hindbrain by AAV injection. (b) Schematic of metabolic phenotyping of mice with NPY knocked out in the hindbrain (Hindbrain: $Npy^{flox/flox}$;AAV-CRE-GFP) and WT ($Npy^{flox/flox}$;AAV-GFP) mice. (c) Confocal images of the sliced hindbrain stained with anti-NPY (magenta). Scale bar=100μm. (d) iBAT weight of 14-week-old ND-treated male Hindbrain: $Npy^{flox/flox}$;AAV-CRE-GFP and WT mice (n=7). (e) iBAT temperature change after a 14-hour fast (n=7). (f) Weekly body weight of ND-treated male Hindbrain: $Npy^{flox/flox}$;AAV-CRE-GFP and WT mice (n=7). (g) The expression levels of thermogenic and adipogenic genes in the iBAT of RT-housed ND-treated male Hindbrain: $Npy^{flox/flox}$; AAV-CRE-GFP and WT mice (n=5). All values are expressed as mean $\pm$ SEM.

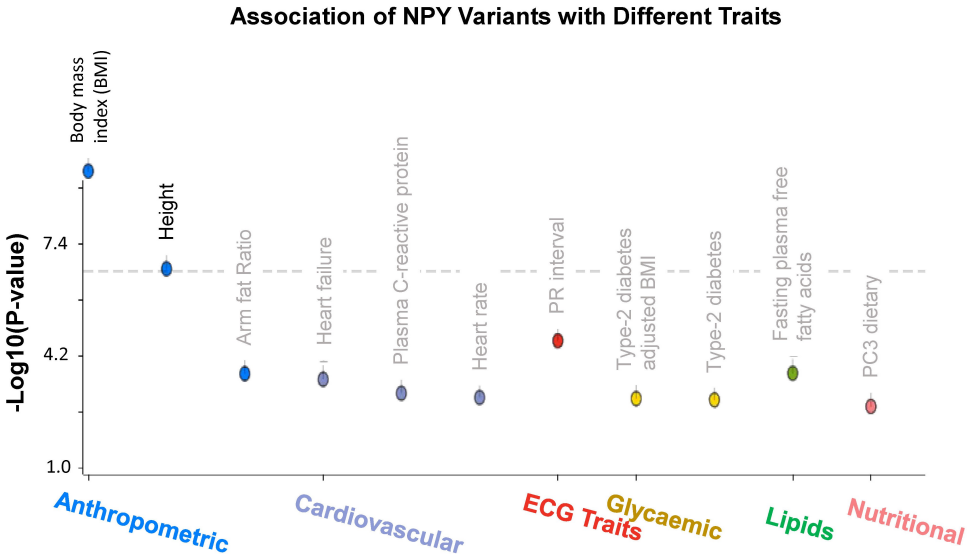


Figure 6.12: **NPY mutation correlates with BMI but not an unhealthy diet.**

relevant to BMI but not an unhealthy diet (Figure 6.12, (Dornbos et al., 2022)).

7 | Conclusion and Discussion

7.1 Main findings of my research

This thesis analysed sympathetic neuron-derived NPY and its functions in maintaining the immunometabolic homeostasis of adipose tissue. The main findings of this research include:

- NPY^+ axons are about one-third of all labelled sympathetic axons in adipose tissues and preferentially innervate the 5^{th} to 7^{th} orders of arteriole branches.
- Neuronal axons are the only source of NPY in adipose tissues, and no other types of cells including macrophages express *Npy*.
- Mural cells are the only group of cells highly expressing *Npy1r* in adipose tissue, and $NPY1R^+$ mural cells are progenitors of thermogenic adipocytes. NPY targets mural cells, promotes their proliferation, and sustains their role as progenitors of thermogenic adipocytes.
- DIO decreases NPY^+ innervations and NPY concentration in adipose tissue. It also depletes mural cells, resulting in increased vascular leakiness.
- DIO does not affect NPY levels or mural cell coverage in the SCG or stellate ganglia.
- Loss of NPY from sympathetic axons whitens iBATs, makes iBATs bigger, and decreases their capability of thermogenesis, resulting in decreased EE, cold intolerance, and adult-onset obesity.
- Loss of NPY from sympathetic axons makes mice more susceptible to DIO without changing daily food consumption.

- The phenotypes observed in NPY-cKO mice are not due to altered plasma or hypothalamus NPY or NPY depletion from the hindbrain.

7.2 Source of NPY in adipose tissues

In Chapter 3, I provided the anatomical maps of NPY^{+} axons in adipose tissue, showing that they preferentially innervate small arterioles where mural cells are located. Additionally, the NPY staining is exclusively axonal without labelling any other types of cells, which negates the previous conclusion that NPY exists in other cells including white adipocytes (Yang et al., 2008), fibroblasts (Killough et al., 2010), and macrophages (Singer et al., 2013). Recently published scRNA-Seq datasets of the stromal-vascular fraction (SVF) of murine iWAT and iBAT (Shamsi et al., 2021; Henriques et al., 2020) also favour that NPY is not detected in any non-neuron cells in the SVF including macrophages (Figure 3.3a-d), which means that NPY is only sourced from neurons or plasma in the adipose tissue. Consistently, using qPCR, I did not detect Npy expression in sorted ATMs from $Cx3cr1^{GFP/+}$ reporter mice, despite the positivity of the *Adgre1* (F4/80) control (Figure 3.3e-f).

7.3 Analysis of peripheral NPY in adipose tissue

Thermogenic adipocytes both in WAT and iBAT (Long et al., 2014; Shamsi et al., 2021; Oguri et al., 2020) are subject to the influence of NE released from adjacent sympathetic nerve terminals. These autonomic nerves co-release NPY (LUNDBERG et al., 1982; Lundberg et al., 1990; Kluge et al., 2021), but its function in the development and activity of thermogenic adipocytes was insofar unknown.

Three previous studies have implicated NPY in directing lipogenic actions in white adipocytes, which favoured the growth of white adipose mass (Rosmaninho-Salgado et al., 2012; Yang et al., 2008; Kuo et al., 2007). However, some of these studies are not replicated here (Rosmaninho-Salgado et al., 2012; Yang et al., 2008), and others are not supported by modern evidence provided by our imaging data and several single-cell sequencing datasets (Kuo et al., 2007). Specifically, we show in our supplementary data that NPY neither directly promotes adipogenesis (Rosmaninho-Salgado et al., 2012) nor the proliferation of 3T3-L1 preadipocytes (Yang et al., 2008). Thus, the evidence disfavours a pro-obesity role for peripheral NPY, contradicting the current perception. Other published data imply an anti-obesity role for peripheral NPY: in humans, mutations in NPY have been linked to high BMI but not to dietary patterns (Dornbos et al., 2022; *Common metabolic disease knowledge portal*, n.d.) (Figure 6.12); in mice, the loss of NPY receptors leads to late-onset obesity without increases in food intake (Naveilhan et al., 1999; Pedrazzini et al., 1998; Nguyen et al., 2012). Taken together, the experimental evidence points to the role of NPY in body weight homeostasis independent of regulating appetite.

Consistent with recent studies showing that sympathetic axons within adipose tissues retract and degenerate with the onset of obesity (W. Zeng et al., 2015; P. Wang et al., 2020), my data in Chapter 5 show that the axonal source of NPY, locally, within these tissues is also obliterated, and this, again, refutes a direct adipogenic role of peripheral NPY. Moreover, several modern datasets omit NPY receptors in adipocytes or immune cells, whereas *Npy1r* expression is robustly detected in mural cells, identifying these cells as the postsynaptic targets of NPY^{+} innervation within adipose tissues. We show that NPY sustains mural cells which are a source of thermogenic adipocytes by promoting their proliferation *in vitro*. *In vivo*, NPY sourced from sympathetic neurons is necessary for supporting mural

cells and the normal development of thermogenic adipocytes. Conditional knockout of NPY (NPY-cKO) in sympathetic neurons depletes mural cells and whitens brown fat before the onset of obesity, rendering this tissue hypertrophic and with reduced thermogenic ability. These NPY-cKO mice have reduced thermogenic ability, lower energy expenditure, show cold intolerance, develop late-onset obesity on a regular chow diet and quickly develop obesity when fed a high-fat diet, without eating more. This metabolic phenotype matches that of whole-body NPY receptors knockout14-16, which also develop late-onset obesity on a regular chow diet even though they eat slightly less.

Although I have confirmed that the phenotypes of NPY-cKO mice are not caused by changed plasma NPY, hypothalamic NPY, or depleted NPY from the hindbrain (Chapter 6), factors including NPY depletion from sympathetic innervation of other tissue or increased immune infiltration might also affect these phenotypes. More precise mouse tools that can locally deplete NPY should be developed to help us improve our understanding of the functions of NPY in adipose tissue.

7.4 Mural cell as a source of thermogenic adipocytes

Mural cells are contractile cells that wrap the vasculature to regulate the diameter of vessels(Almaça, Weitz, Rodriguez-Diaz, Pereira, & Caicedo, 2018) and have been described as a source of thermogenic adipocytes (Long et al., 2014; Shamsi et al., 2021). However, there are also papers claiming that PDGFRα^+ adipogenic fibroblasts are the only source of thermogenic adipocytes (Cattaneo et al., 2020). Since different progenitors might contribute to different thermogenic adipocytes at different stages: MYF5$^+$ progenitors generate brown adipocytes during the embryonic development stage; PDGFRα^+ progenitors generate thermogenic adipocytes in neonates; thermogenic adipocytes in adults are derived from

white adipocytes or MYH11$^+$/NPY1R$^+$ mural cells (Angueira et al., 2021), this discrepancy might be because different ways were used to induce the generation of thermogenic adipocytes at different stages *in vivo*: cold challenge v.s. ADRβ3 agonism; neonate v.s. adulthood. More efforts should be put into deciphering how different progenitors generate thermogenic adipocytes and what factors contribute to their differentiation *in vivo*.

7.5 NPY and other physiological processes

I have shown that sympathetic neuron-derived NPY is vital for maintaining adipose tissue immunometabolic homeostasis, which further questions whether NPY controls other physiological processes such as host defence or the development of atherosclerosis. These are relevant to NPY because NPY targets mural cells, which can regulate vascular permeability and immune infiltration, and these factors can affect the recruitment of immune cells to primary and secondary lymphatic organs or macrophages to atherosclerosis plaques. Relevant phenomena have been observed in recent studies (Yu et al., 2022), but detailed mechanisms still need figuring out.

7.6 The protective functions of thermogenic adipocytes

Thermogenic adipocytes generate heat in response to NE, but it is not clear whether they have a broader effect on physiological homeostasis. Previous studies indicate that the depletion of thermogenic adipocytes results in hyperglycaemia, and transplant of BAT to the abdominal cavity improves insulin tolerance (Lowell et al., 1993; Stanford et al., 2012). Thermogenic adipocytes can also affect different physiological processes using secretory factors that regulate inflammation (IL-6,

(Kristóf et al., 2019)), vasculature (VEGFA, (K. Sun et al., 2012)), and innervations in adipose tissue (NGF1, (Nisoli, Tonello, Benarese, Liberini, & Carruba, 1996)). Further research needs to be carried out to determine how these factors shape the overall microenvironment in adipose tissues, and how the BAT microenvironment affects physiological and pathological processes such as inflammation and aging.

7.7 Conclusion and future directions

NPY targets mural cells in adipose tissues, promotes their proliferation, and maintains their identity and ability to differentiate into thermogenic adipocytes. I clarify that central and peripheral sources of NPY have antipode roles in body weight homeostasis. The biological mechanism described in this study is a possible explanation for why mutations of the appetite-stimulating NPY are paradoxically associated with high BMI in humans (*Common metabolic disease knowledge portal*, n.d.) (Figure 6.12) and highlights that energy dissipation may be more important than appetite in some individuals via the mechanism we herein identify.

To better understand the mechanism, NPY secretion patterns should be analysed using *in vivo* sensors (H. Wang et al., 2023), which may explain the functional differences between NPY and NE. The factors and mechanisms mediating the neogenesis of thermogenic adipocytes should also be studied at developmental and adult stages, which might solve the contradictions concerning their progenitors. Since NPY exists in sympathetic axons innervating other tissue, efforts can be made to determine NPY functions in lymphatic organs or the cardiovascular system to find out whether it contributes to host defence or vascular functions. Following this path, other neuron transmitters in sympathetic or sensory nerves can be studied in different tissues at physiological or pathological conditions. The

endocrine or paracrine capacity of thermogenic adipocytes is also worth studying, as it might point to the role of thermogenic adipocytes beyond generating heat and emphasize their potential protective functions.

Bibliography

Abumrad, N. A., Cabodevilla, A. G., Samovski, D., Pietka, T., Basu, D., & Goldberg, I. J. (2021). Endothelial cell receptors in tissue lipid uptake and metabolism. *Circulation research*, *128*(3), 433–450.

Almaça, J., Weitz, J., Rodriguez-Diaz, R., Pereira, E., & Caicedo, A. (2018). The pericyte of the pancreatic islet regulates capillary diameter and local blood flow. *Cell metabolism*, *27*(3), 630–644.

Angueira, A. R., Sakers, A. P., Holman, C. D., Cheng, L., Arbocco, M. N., Shamsi, F., ... others (2021). Defining the lineage of thermogenic perivascular adipose tissue. *Nature metabolism*, *3*(4), 469–484.

Aponte, Y., Atasoy, D., & Sternson, S. M. (2011). Agrp neurons are sufficient to orchestrate feeding behavior rapidly and without training. *Nature neuroscience*, *14*(3), 351–355.

Armulik, A., Abramsson, A., & Betsholtz, C. (2005). Endothelial/pericyte interactions. *Circulation research*, *97*(6), 512–523.

Armulik, A., Genové, G., & Betsholtz, C. (2011). Pericytes: developmental, physiological, and pathological perspectives, problems, and promises. *Developmental cell*, *21*(2), 193–215.

Attwell, D., Mishra, A., Hall, C. N., OFarrell, F. M., & Dalkara, T. (2016). What is a pericyte. *Journal of Cerebral Blood Flow & Metabolism*, *36*(2), 451–455.

Bae, H., Hong, K. Y., Lee, C.-k., Jang, C., Lee, S.-J., Choe, K., ... Koh, G. Y. (2020). Angiopoietin-2–integrin $\alpha 5 \beta 1$ signaling enhances vascular fatty acid transport and prevents ectopic lipid-induced insulin resistance. *Nature communications*, *11*(1), 2980.

Balthasar, N., Dalgaard, L. T., Lee, C. E., Yu, J., Funahashi, H., Williams, T., ...

others (2005). Divergence of melanocortin pathways in the control of food intake and energy expenditure. *Cell*, *123*(3), 493–505.

Berry, R., & Rodeheffer, M. S. (2013). Characterization of the adipocyte cellular lineage in vivo. *Nature cell biology*, *15*(3), 302–308.

Boeni-Schnetzler, M., Boller, S., Debray, S., Bouzakri, K., Meier, D. T., Prazak, R., ... others (2009). Free fatty acids induce a proinflammatory response in islets via the abundantly expressed interleukin-1 receptor i. *Endocrinology*, *150*(12), 5218–5229.

Bolte, S., & Cordelières, F. P. (2006). A guided tour into subcellular colocalization analysis in light microscopy. *Journal of microscopy*, *224*(3), 213–232.

Bonet, M., Ribot, J., Felipe, F., & Palou, A. (2003). Vitamin a and the regulation of fat reserves. *Cellular and Molecular Life Sciences CMLS*, *60*, 1311–1321.

Brestoff, J. R., Kim, B. S., Saenz, S. A., Stine, R. R., Monticelli, L. A., Sonnenberg, G. F., ... others (2015). Group 2 innate lymphoid cells promote beiging of white adipose tissue and limit obesity. *Nature*, *519*(7542), 242–246.

Buechler, M. B., Pradhan, R. N., Krishnamurty, A. T., Cox, C., Calviello, A. K., Wang, A. W., ... others (2021). Cross-tissue organization of the fibroblast lineage. *Nature*, *593*(7860), 575–579.

Buechler, M. B., & Turley, S. J. (2018). A short field guide to fibroblast function in immunity. In *Seminars in immunology* (Vol. 35, pp. 48–58).

Callaghan, B. C., Reynolds, E., Banerjee, M., Chant, E., Villegas-Umana, E., & Feldman, E. L. (2020). Central obesity is associated with neuropathy in the severely obese. In *Mayo clinic proceedings* (Vol. 95, pp. 1342–1353).

Cannon, B., Nedergaard, J., Lundberg, J. M., Hökfelt, T., Terenius, L., & Goldstein, M. (1986). Neuropeptide tyrosine (npy) is co-stored with nora-

drenaline in vascular but not in parenchymal sympathetic nerves of brown adipose tissue. *Experimental cell research*, *164*(2), 546–550.

Cano, G., Passerin, A. M., Schiltz, J. C., Card, J. P., Morrison, S. F., & Sved, A. F. (2003). Anatomical substrates for the central control of sympathetic outflow to interscapular adipose tissue during cold exposure. *Journal of Comparative Neurology*, *460*(3), 303–326.

Cantu, R. C., & Goodman, H. M. (1967). Effects of denervation and fasting on white adipose tissue. *American Journal of Physiology-Legacy Content*, *212*(1), 207–212.

Cao, W., Daniel, K. W., Robidoux, J., Puigserver, P., Medvedev, A. V., Bai, X., ... Collins, S. (2004). p38 mitogen-activated protein kinase is the central regulator of cyclic amp-dependent transcription of the brown fat uncoupling protein 1 gene. *Molecular and cellular biology*, *24*(7), 3057–3067.

Cardoso, F., Klein Wolterink, R. G., Godinho-Silva, C., Domingues, R. G., Ribeiro, H., Da Silva, J. A., ... Veiga-Fernandes, H. (2021). Neuro-mesenchymal units control ilc2 and obesity via a brain–adipose circuit. *Nature*, *597*(7876), 410–414.

Carloni, S., Bertocchi, A., Mancinelli, S., Bellini, M., Erreni, M., Borreca, A., ... others (2021). Identification of a choroid plexus vascular barrier closing during intestinal inflammation. *Science*, *374*(6566), 439–448.

Carpéné, C., Bousquet-mélou, A., Galitzky, J., Berlan, M., & Lafontan, M. (1998). Lipolytic effects of β1-, β2-, and β3-adrenergic agonists in white adipose tissue of mammals. *Annals of the New York Academy of Sciences*, *839*(1), 186–189.

Carr, M. J., Toma, J. S., Johnston, A. P., Steadman, P. E., Yuzwa, S. A., Mahmud, N., ... Miller, F. D. (2019). Mesenchymal precursor cells in adult nerves contribute to mammalian tissue repair and regeneration. *Cell stem cell*,

24(2), 240–256.

Castan, I., Valet, P., Larrouy, D., Voisin, T., Remaury, A., Daviaud, D., ... Lafontan, M. (1993). Distribution of pyy receptors in human fat cells: an antilipolytic system alongside the alpha 2-adrenergic system. *American Journal of Physiology-Endocrinology and Metabolism*, *265*(1), E74–E80.

Cattaneo, P., Mukherjee, D., Spinozzi, S., Zhang, L., Larcher, V., Stallcup, W. B., ... others (2020). Parallel lineage-tracing studies establish fibroblasts as the prevailing in vivo adipocyte progenitor. *Cell reports*, *30*(2), 571–582.

Chen, J., Cheng, M., Wang, L., Zhang, L., Xu, D., Cao, P., ... Zhan, C. (2020). A vagal-nts neural pathway that stimulates feeding. *Current Biology*, *30*(20), 3986–3998.

Chen, Q., Lai, S. M., Xu, S., Tan, Y., Leong, K., Liu, D., ... others (2021). Resident macrophages restrain pathological adipose tissue remodeling and protect vascular integrity in obese mice. *EMBO reports*, *22*(8), e52835.

Cheng, S., Massaro, J. M., Fox, C. S., Larson, M. G., Keyes, M. J., McCabe, E. L., ... others (2010). Adiposity, cardiometabolic risk, and vitamin d status: the framingham heart study. *Diabetes*, *59*(1), 242–248.

Chi, J., Crane, A., Wu, Z., & Cohen, P. (2018). Adipo-clear: a tissue clearing method for three-dimensional imaging of adipose tissue. *JoVE (Journal of Visualized Experiments)*(137), e58271.

Chi, J., Lin, Z., Barr, W., Crane, A., Zhu, X. G., & Cohen, P. (2021). Early postnatal interactions between beige adipocytes and sympathetic neurites regulate innervation of subcutaneous fat. *Elife*, *10*, e64693.

Chi, J., Wu, Z., Choi, C. H. J., Nguyen, L., Tegegne, S., Ackerman, S. E., ... Cohen, P. (2018). Three-dimensional adipose tissue imaging reveals regional variation in beige fat biogenesis and prdm16-dependent sympathetic neurite density. *Cell metabolism*, *27*(1), 226–236.

Chmelař, J., Chatzigeorgiou, A., Chung, K.-J., Prucnal, M., Voehringer, D., Roers, A., & Chavakis, T. (2016). No role for mast cells in obesity-related metabolic dysregulation. *Frontiers in immunology*, *7*, 524.

Cho, K. W., Morris, D. L., DelProposto, J. L., Geletka, L., Zamarron, B., Martinez-Santibanez, G., ... Lumeng, C. N. (2014). An mhc ii-dependent activation loop between adipose tissue macrophages and cd4+ t cells controls obesity-induced inflammation. *Cell reports*, *9*(2), 605–617.

Cho, K. W., Zamarron, B. F., Muir, L. A., Singer, K., Porsche, C. E., DelProposto, J. B., ... Lumeng, C. N. (2016). Adipose tissue dendritic cells are independent contributors to obesity-induced inflammation and insulin resistance. *The Journal of Immunology*, *197*(9), 3650–3661.

Chui, P. C., Guan, H.-P., Lehrke, M., Lazar, M. A., et al. (2005). Pparγ regulates adipocyte cholesterol metabolism via oxidized ldl receptor 1. *The Journal of clinical investigation*, *115*(8), 2244–2256.

Cipolletta, D., Cohen, P., Spiegelman, B. M., Benoist, C., & Mathis, D. (2015). Appearance and disappearance of the mrna signature characteristic of treg cells in visceral adipose tissue: age, diet, and pparγ effects. *Proceedings of the National Academy of Sciences*, *112*(2), 482–487.

Coats, B. R., Schoenfelt, K. Q., Barbosa-Lorenzi, V. C., Peris, E., Cui, C., Hoffman, A., ... others (2017). Metabolically activated adipose tissue macrophages perform detrimental and beneficial functions during diet-induced obesity. *Cell reports*, *20*(13), 3149–3161.

Common metabolic disease knowledge portal. (n.d.). Retrieved from https://hugeamp.org/gene.html?gene=NPY

Cone, R. D. (2005). Anatomy and regulation of the central melanocortin system. *Nature neuroscience*, *8*(5), 571–578.

Cook, D. G., Mendall, M. A., Whincup, P. H., Carey, I. M., Ballam, L., Mor-

ris, J. E., ... Strachan, D. P. (2000). C-reactive protein concentration in children: relationship to adiposity and other cardiovascular risk factors. *Atherosclerosis*, *149*(1), 139–150.

Cowley, M. A., Smart, J. L., Rubinstein, M., Cerdán, M. G., Diano, S., Horvath, T. L., ... Low, M. J. (2001). Leptin activates anorexigenic pomc neurons through a neural network in the arcuate nucleus. *Nature*, *411*(6836), 480–484.

Cox, N., Crozet, L., Holtman, I. R., Loyher, P.-L., Lazarov, T., White, J. B., ... others (2021). Diet-regulated production of pdgfcc by macrophages controls energy storage. *Science*, *373*(6550), eabe9383.

Daneman, R., Zhou, L., Kebede, A. A., & Barres, B. A. (2010). Pericytes are required for blood–brain barrier integrity during embryogenesis. *Nature*, *468*(7323), 562–566.

Davis, S., Aldrich, T. H., Jones, P. F., Acheson, A., Compton, D. L., Jain, V., ... others (1996). Isolation of angiopoietin-1, a ligand for the tie2 receptor, by secretion-trap expression cloning. *Cell*, *87*(7), 1161–1169.

Dieudonne, M., Pecquery, R., Leneveu, M., & Giudicelli, Y. (2000). Opposite effects of androgens and estrogens on adipogenesis in rat preadipocytes: evidence for sex and site-related specificities and possible involvement of insulin-like growth factor 1 receptor and peroxisome proliferator-activated receptorγ 2. *Endocrinology*, *141*(2), 649–656.

Dornbos, P., Singh, P., Jang, D.-K., Mahajan, A., Biddinger, S. B., Rotter, J. I., ... Flannick, J. (2022). Evaluating human genetic support for hypothesized metabolic disease genes. *Cell metabolism*, *34*(5), 661–666.

Dumont, D., Gradwohl, G., Fong, G., Auerbach, R., & Breitman, M. (1993). The endothelial-specific receptor tyrosine kinase, tek, is a member of a new subfamily of receptors. *Oncogene*, *8*(5), 1293–1301.

Ejaz, A., LoGerfo, F. W., Khabbaz, K., & Pradhan, L. (2011). Expression of neuropeptide y, substance p, and their receptors in the right atrium of diabetic patients. *Clinical and Translational Science*, *4*(5), 346–350.

Elias, I., Franckhauser, S., Ferré, T., Vilà, L., Tafuro, S., Muñoz, S., ... others (2012). Adipose tissue overexpression of vascular endothelial growth factor protects against diet-induced obesity and insulin resistance. *Diabetes*, *61*(7), 1801–1813.

Emont, M. P., Jacobs, C., Essene, A. L., Pant, D., Tenen, D., Colleluori, G., ... others (2022). A single-cell atlas of human and mouse white adipose tissue. *Nature*, *603*(7903), 926–933.

Engström Ruud, L., Pereira, M. M., de Solis, A. J., Fenselau, H., & Brüning, J. C. (2020). Npy mediates the rapid feeding and glucose metabolism regulatory functions of agrp neurons. *Nature communications*, *11*(1), 442.

Estève, D., Boulet, N., Volat, F., Zakaroff-Girard, A., Ledoux, S., Coupaye, M., ... others (2015). Human white and brite adipogenesis is supported by msca1 and is impaired by immune cells. *Stem cells*, *33*(4), 1277–1291.

Feingold, K. R., Soued, M., Staprans, I., Gavin, L. A., Donahue, M. E., Huang, B.-J., ... others (1989). Effect of tumor necrosis factor (tnf) on lipid metabolism in the diabetic rat. evidence that inhibition of adipose tissue lipoprotein lipase activity is not required for tnf-induced hyperlipidemia. *The Journal of clinical investigation*, *83*(4), 1116–1121.

Félix, I., Jokela, H., Karhula, J., Kotaja, N., Savontaus, E., Salmi, M., & Rantakari, P. (2021). Single-cell proteomics reveals the defined heterogeneity of resident macrophages in white adipose tissue. *Frontiers in immunology*, *12*, 719979.

Figueiredo, A. M., Villacampa, P., Diéguez-Hurtado, R., José Lozano, J., Kobialka, P., Cortazar, A. R., ... others (2020). Phosphoinositide 3-kinase–

regulated pericyte maturation governs vascular remodeling. *Circulation*, *142*(7), 688–704.

Fischer, K., Ruiz, H. H., Jhun, K., Finan, B., Oberlin, D. J., Van Der Heide, V., ... others (2017). Alternatively activated macrophages do not synthesize catecholamines or contribute to adipose tissue adaptive thermogenesis. *Nature medicine*, *23*(5), 623–630.

Folkman, J. (2002). Role of angiogenesis in tumor growth and metastasis. In *Seminars in oncology* (Vol. 29, pp. 15–18).

Folkman, J., & D'Amore, P. A. (1996). Blood vessel formation: what is its molecular basis? *Cell*, *87*(7), 1153–1155.

Foster, M. T., Song, C. K., & Bartness, T. J. (2010). Hypothalamic paraventricular nucleus lesion involvement in the sympathetic control of lipid mobilization. *Obesity*, *18*(4), 682–689.

Frohnert, B. I., Hui, T. Y., & Bernlohr, D. A. (1999). Identification of a functional peroxisome proliferator-responsive element in the murine fatty acid transport protein gene. *Journal of Biological Chemistry*, *274*(7), 3970–3977.

Furlan, A., La Manno, G., Lübke, M., Häring, M., Abdo, H., Hochgerner, H., ... others (2016). Visceral motor neuron diversity delineates a cellular basis for nipple-and pilo-erection muscle control. *Nature neuroscience*, *19*(10), 1331–1340.

Garrity, R., Arora, N., Haque, M. A., Weis, D., Trinh, R. T., Neerukonda, S. V., ... others (2023). Fibroblast-derived pi16 sustains inflammatory pain via regulation of cd206+ myeloid cells. *Brain, behavior, and immunity*, *112*, 220–234.

Glentis, A., Gurchenkov, V., & Vignjevic, D. M. (2014). Assembly, heterogeneity, and breaching of the basement membranes. *Cell adhesion & migration*, *8*(3), 236–245.

Gogg, S., Nerstedt, A., Boren, J., & Smith, U. (2019). Human adipose tissue microvascular endothelial cells secrete pparγ ligands and regulate adipose tissue lipid uptake. *Jci Insight*, *4*(5).

Goto, T., Naknukool, S., Yoshitake, R., Hanafusa, Y., Tokiwa, S., Li, Y., ... others (2016). Proinflammatory cytokine interleukin-1β suppresses cold-induced thermogenesis in adipocytes. *Cytokine*, *77*, 107–114.

Granneman, J. G., Moore, H.-P. H., Granneman, R. L., Greenberg, A. S., Obin, M. S., & Zhu, Z. (2007). Analysis of lipolytic protein trafficking and interactions in adipocytes. *Journal of Biological Chemistry*, *282*(8), 5726–5735.

Grundemar, L., Jonas, S., Mörner, N., Högestätt, E. D., Wahlestedt, C., & Håkanson, R. (1992). Characterization of vascular neuropeptide y receptors. *British journal of pharmacology*, *105*(1), 45–50.

Guan, L., van der Heijden, G. W., Bortvin, A., & Greenberg, M. M. (2011). Intracellular detection of cytosine incorporation in genomic dna by using 5-ethynyl-2-deoxycytidine. *ChemBioChem*, *12*(14), 2184–2190.

Guzik, T. J., Skiba, D. S., Touyz, R. M., & Harrison, D. G. (2017). The role of infiltrating immune cells in dysfunctional adipose tissue. *Cardiovascular research*, *113*(9), 1009–1023.

Haberman, E. R., Sarker, G., Arús, B. A., Ziegler, K. A., Meunier, S., Martínez-Sánchez, N., ... others (2024). Immunomodulatory leptin receptor+ sympathetic perineurial barrier cells protect against obesity by facilitating brown adipose tissue thermogenesis. *Immunity*, *57*(1), 141–152.

Haemmerle, G., Lass, A., Zimmermann, R., Gorkiewicz, G., Meyer, C., Rozman, J., ... others (2006). Defective lipolysis and altered energy metabolism in mice lacking adipose triglyceride lipase. *Science*, *312*(5774), 734–737.

Hallmann, R., Mayer, D., Berg, E., Broermann, R., & Butcher, E. (1995). Novel mouse endothelial cell surface marker is suppressed during differentiation

of the blood brain barrier. *Developmental dynamics*, *202*(4), 325–332.

Hao, Y., Hao, S., Andersen-Nissen, E., Mauck, W. M., Zheng, S., Butler, A., ... others (2021). Integrated analysis of multimodal single-cell data. *Cell*, *184*(13), 3573–3587.

Henning, R. J. (2021). Obesity and obesity-induced inflammatory disease contribute to atherosclerosis: a review of the pathophysiology and treatment of obesity. *American journal of cardiovascular disease*, *11*(4), 504.

Henriques, F., Bedard, A. H., Guilherme, A., Kelly, M., Chi, J., Zhang, P., ... others (2020). Single-cell rna profiling reveals adipocyte to macrophage signaling sufficient to enhance thermogenesis. *Cell reports*, *32*(5).

Hepler, C., Shan, B., Zhang, Q., Henry, G. H., Shao, M., Vishvanath, L., ... others (2018). Identification of functionally distinct fibro-inflammatory and adipogenic stromal subpopulations in visceral adipose tissue of adult mice. *Elife*, *7*, e39636.

Holm, C., Kirchgessner, T. G., Svenson, K. L., Fredrikson, G., Nilsson, S., Miller, C. G., ... others (1988). Hormone-sensitive lipase: sequence, expression, and chromosomal localization to 19 cent-q13. 3. *Science*, *241*(4872), 1503–1506.

Hong, S. H., Kim, B., Lee, D.-S., Yu, K., Lee, K.-S., et al. (2018). Neuropeptide y mitigates er stress–induced neuronal cell death by activating the pi3k–xbp1 pathway. *European Journal of Cell Biology*, *97*(5), 339–348.

Hosaka, K., Yang, Y., Seki, T., Fischer, C., Dubey, O., Fredlund, E., ... others (2016). Pericyte–fibroblast transition promotes tumor growth and metastasis. *Proceedings of the National Academy of Sciences*, *113*(38), E5618–E5627.

Hotamisligil, G. S., Shargill, N. S., & Spiegelman, B. M. (1993). Adipose expression of tumor necrosis factor-α: direct role in obesity-linked insulin

resistance. *Science*, *259*(5091), 87–91.

Houstis, N., Rosen, E. D., & Lander, E. S. (2006). Reactive oxygen species have a causal role in multiple forms of insulin resistance. *Nature*, *440*(7086), 944–948.

Huesing, C., Zhang, R., Gummadi, S., Lee, N., Qualls-Creekmore, E., Yu, S., ... others (2022). Organization of sympathetic innervation of interscapular brown adipose tissue in the mouse. *Journal of Comparative Neurology*, *530*(9), 1363–1378.

Ikeda, K., Kang, Q., Yoneshiro, T., Camporez, J. P., Maki, H., Homma, M., ... others (2017). Ucp1-independent signaling involving serca2b-mediated calcium cycling regulates beige fat thermogenesis and systemic glucose homeostasis. *Nature medicine*, *23*(12), 1454–1465.

Ikeda, K., Maretich, P., & Kajimura, S. (2018). The common and distinct features of brown and beige adipocytes. *Trends in Endocrinology & Metabolism*, *29*(3), 191–200.

Imtiyaz, H. Z., & Simon, M. C. (2010). Hypoxia-inducible factors as essential regulators of inflammation. *Diverse Effects of Hypoxia on Tumor Progression*, 105–120.

Jackerott, M., & Larsson, L.-I. (1997). Immunocytochemical localization of the npy/pyy y1 receptor in enteric neurons, endothelial cells, and endocrine-like cells of the rat intestinal tract. *Journal of Histochemistry & Cytochemistry*, *45*(12), 1643–1650.

Jaitin, D. A., Adlung, L., Thaiss, C. A., Weiner, A., Li, B., Descamps, H., ... others (2019). Lipid-associated macrophages control metabolic homeostasis in a trem2-dependent manner. *Cell*, *178*(3), 686–698.

Jansen, A., Wessendorf, M., & Loewy, A. (1995). Transneuronal labeling of cns neuropeptide and monoamine neurons after pseudorabies virus injections

into the stellate ganglion. *Brain research*, *683*(1), 1–24.

Jiang, H., Ding, X., Cao, Y., Wang, H., & Zeng, W. (2017). Dense intra-adipose sympathetic arborizations are essential for cold-induced beiging of mouse white adipose tissue. *Cell metabolism*, *26*(4), 686–692.

Kalucka, J., de Rooij, L. P., Goveia, J., Rohlenova, K., Dumas, S. J., Meta, E., ... others (2020). Single-cell transcriptome atlas of murine endothelial cells. *Cell*, *180*(4), 764–779.

Kanda, T., Brown, J. D., Orasanu, G., Vogel, S., Gonzalez, F. J., Sartoretto, J., ... others (2008). Pparγ in the endothelium regulates metabolic responses to high-fat diet in mice. *The Journal of clinical investigation*, *119*(1).

Killough, S., Lundy, F., & Irwin, C. (2010). Dental pulp fibroblasts express neuropeptide y y1 receptor but not neuropeptide y. *International Endodontic Journal*, *43*(10), 835–842.

Kim, D., Grath, A., Lu, Y. W., Chung, K., Winkelman, M., Schwarz, J. J., & Dai, G. (2023). Sox17 mediates adult arterial endothelial cell adaptation to hemodynamics. *Biomaterials*, *293*, 121946.

Kitamura, T., Kitamura, Y., Kuroda, S., Hino, Y., Ando, M., Kotani, K., ... others (1999). Insulin-induced phosphorylation and activation of cyclic nucleotide phosphodiesterase 3b by the serine-threonine kinase akt. *Molecular and cellular biology*, *19*(9), 6286–6296.

Klein, S., Wadden, T., & Sugerman, H. J. (2002). Aga technical review on obesity. *Gastroenterology*, *123*(3), 882–932.

Kluge, N., Dacey, M., Hadaya, J., Shivkumar, K., Chan, S.-A., Ardell, J. L., & Smith, C. (2021). Rapid measurement of cardiac neuropeptide dynamics by capacitive immunoprobe in the porcine heart. *American Journal of Physiology-Heart and Circulatory Physiology*, *320*(1), H66–H76.

Koh, Y. J., Koh, B. I., Kim, H., Joo, H. J., Jin, H. K., Jeon, J., ... others (2011).

Stromal vascular fraction from adipose tissue forms profound vascular network through the dynamic reassembly of blood endothelial cells. *Arteriosclerosis, thrombosis, and vascular biology*, *31*(5), 1141–1150.

Kolodin, D., van Panhuys, N., Li, C., Magnuson, A. M., Cipolletta, D., Miller, C. M., ... Mathis, D. (2015). Antigen-and cytokine-driven accumulation of regulatory t cells in visceral adipose tissue of lean mice. *Cell metabolism*, *21*(4), 543–557.

Koutnikova, H., Cock, T.-A., Watanabe, M., Houten, S. M., Champy, M.-F., Dierich, A., & Auwerx, J. (2003). Compensation by the muscle limits the metabolic consequences of lipodystrophy in pparγ hypomorphic mice. *Proceedings of the National Academy of Sciences*, *100*(24), 14457–14462.

Kristóf, E., Klusóczki, Á., Veress, R., Shaw, A., Combi, Z. S., Varga, K., ... others (2019). Interleukin-6 released from differentiating human beige adipocytes improves browning. *Experimental cell research*, *377*(1-2), 47–55.

Krueger, M., & Bechmann, I. (2010). Cns pericytes: concepts, misconceptions, and a way out. *Glia*, *58*(1), 1–10.

Kumari, M., Heeren, J., & Scheja, L. (2018). Regulation of immunometabolism in adipose tissue. In *Seminars in immunopathology* (Vol. 40, pp. 189–202).

Kuo, L. E., Kitlinska, J. B., Tilan, J. U., Li, L., Baker, S. B., Johnson, M. D., ... others (2007). Neuropeptide y acts directly in the periphery on fat tissue and mediates stress-induced obesity and metabolic syndrome. *Nature medicine*, *13*(7), 803–811.

Lass, A., Zimmermann, R., Haemmerle, G., Riederer, M., Schoiswohl, G., Schweiger, M., ... Zechner, R. (2006). Adipose triglyceride lipase-mediated lipolysis of cellular fat stores is activated by cgi-58 and defective in chanarin-dorfman syndrome. *Cell metabolism*, *3*(5), 309–319.

Lee, B.-C., Kim, M.-S., Pae, M., Yamamoto, Y., Eberlé, D., Shimada, T., ... oth-

ers (2016). Adipose natural killer cells regulate adipose tissue macrophages to promote insulin resistance in obesity. *Cell metabolism*, *23*(4), 685–698.

Lee, M.-W., Odegaard, J. I., Mukundan, L., Qiu, Y., Molofsky, A. B., Nussbaum, J. C., ... Chawla, A. (2015). Activated type 2 innate lymphoid cells regulate beige fat biogenesis. *Cell*, *160*(1), 74–87.

Lee, Y.-H., Petkova, A. P., Mottillo, E. P., & Granneman, J. G. (2012). In vivo identification of bipotential adipocyte progenitors recruited by β3-adrenoceptor activation and high-fat feeding. *Cell metabolism*, *15*(4), 480–491.

Lefterova, M. I., Zhang, Y., Steger, D. J., Schupp, M., Schug, J., Cristancho, A., ... others (2008). Pparγ and c/ebp factors orchestrate adipocyte biology via adjacent binding on a genome-wide scale. *Genes & development*, *22*(21), 2941–2952.

Levéen, P., Pekny, M., Gebre-Medhin, S., Swolin, B., Larsson, E., & Betsholtz, C. (1994). Mice deficient for pdgf b show renal, cardiovascular, and hematological abnormalities. *Genes & development*, *8*(16), 1875–1887.

Li, F., Lan, Y., Wang, Y., Wang, J., Yang, G., Meng, F., ... Yang, X. (2011). Endothelial smad4 maintains cerebrovascular integrity by activating n-cadherin through cooperation with notch. *Developmental cell*, *20*(3), 291–302.

Li, L., Miano, J. M., Cserjesi, P., & Olson, E. N. (1996). Sm22α, a marker of adult smooth muscle, is expressed in multiple myogenic lineages during embryogenesis. *Circulation research*, *78*(2), 188–195.

Lindahl, P., Johansson, B. R., Leveen, P., & Betsholtz, C. (1997). Pericyte loss and microaneurysm formation in pdgf-b-deficient mice. *Science*, *277*(5323), 242–245.

Lindblom, P., Gerhardt, H., Liebner, S., Abramsson, A., Enge, M., Hellström,

M., ... others (2003). Endothelial pdgf-b retention is required for proper investment of pericytes in the microvessel wall. *Genes & development*, *17*(15), 1835–1840.

Lindhorst, A., Raulien, N., Wieghofer, P., Eilers, J., Rossi, F. M., Bechmann, I., & Gericke, M. (2021). Adipocyte death triggers a pro-inflammatory response and induces metabolic activation of resident macrophages. *Cell death & disease*, *12*(6), 579.

Long, J. Z., Svensson, K. J., Tsai, L., Zeng, X., Roh, H. C., Kong, X., ... others (2014). A smooth muscle-like origin for beige adipocytes. *Cell metabolism*, *19*(5), 810–820.

Lowell, B. B., S-Susulic, V., Hamann, A., Lawitts, J. A., Himms-Hagen, J., Boyer, B. B., ... Flier, J. S. (1993). Development of obesity in transgenic mice after genetic ablation of brown adipose tissue. *Nature*, *366*(6457), 740–742.

Lundberg, J., Franco-Cereceda, A., Hemsen, A., Lacroix, J., & Pernow, J. (1990). Pharmacology of noradrenaline and neuropeptide tyrosine (npy)-mediated sympathetic cotransmission. *Fundamental & clinical pharmacology*, *4*(4), 373–391.

LUNDBERG, J. M., TERENIUS, L., HÖKFELT, T., MARTLING, C. R., TATEMOTO, K., MUTT, V., ... GOLDSTEIN, M. (1982). Neuropeptide y (npy)-like immunoreactivity in peripheral noradrenergic neurons and effects of npy on sympathetic function. *Acta Physiologica Scandinavica*, *116*(4), 477–480.

Lundell, I., Blomqvist, A. G., Berglund, M. M., Schober, D. A., Johnson, D., Statnick, M. A., ... Larhammar, D. (1995). Cloning of a human receptor of the npy receptor family with high affinity for pancreatic polypeptide and peptide yy. *Journal of Biological Chemistry*, *270*(49), 29123–29128.

Madsen, L., Petersen, R. K., & Kristiansen, K. (2005). Regulation of adipocyte

differentiation and function by polyunsaturated fatty acids. *Biochimica et Biophysica Acta (BBA)-Molecular Basis of Disease*, *1740*(2), 266–286.

Maningat, A. L., & Munakomi, S. (2023). Neuroanatomy, superior cervical ganglion. In *Statpearls [internet]*. StatPearls Publishing.

Marsh, D. J., Hollopeter, G., Kafer, K. E., & Palmiter, R. D. (1998). Role of the y5 neuropeptide y receptor in feeding and obesity. *Nature medicine*, *4*(6), 718–721.

Masliukov, P. M., Moiseev, K., Emanuilov, A. I., Anikina, T. A., Zverev, A. A., & Nozdrachev, A. D. (2016). Development of neuropeptide y-mediated heart innervation in rats. *Neuropeptides*, *55*, 47–54.

Molofsky, A. B., Nussbaum, J. C., Liang, H.-E., Van Dyken, S. J., Cheng, L. E., Mohapatra, A., ... Locksley, R. M. (2013). Innate lymphoid type 2 cells sustain visceral adipose tissue eosinophils and alternatively activated macrophages. *Journal of Experimental Medicine*, *210*(3), 535–549.

Muhl, L., Genové, G., Leptidis, S., Liu, J., He, L., Mocci, G., ... others (2020). Single-cell analysis uncovers fibroblast heterogeneity and criteria for fibroblast and mural cell identification and discrimination. *Nature communications*, *11*(1), 3953.

Nakamura, K., Matsumura, K., Hübschle, T., Nakamura, Y., Hioki, H., Fujiyama, F., ... others (2004). Identification of sympathetic premotor neurons in medullary raphe regions mediating fever and other thermoregulatory functions. *Journal of Neuroscience*, *24*(23), 5370–5380.

Naveilhan, P., Hassani, H., Canals, J. M., Ekstrand, A. J., Larefalk, Å., Chhajlani, V., ... others (1999). Normal feeding behavior, body weight and leptin response require the neuropeptide y y2 receptor. *Nature medicine*, *5*(10), 1188–1193.

Nehls, V., Denzer, K., & Drenckhahn, D. (1992). Pericyte involvement in capillary

sprouting during angiogenesis in situ. *Cell and tissue research*, *270*, 469–474.

Nguyen, A. D., Mitchell, N. F., Lin, S., Macia, L., Yulyaningsih, E., Baldock, P. A., ... others (2012). Y1 and y5 receptors are both required for the regulation of food intake and energy homeostasis in mice. *PloS one*, *7*(6), e40191.

Nishimura, S., Manabe, I., Nagasaki, M., Eto, K., Yamashita, H., Ohsugi, M., ... others (2009). Cd8+ effector t cells contribute to macrophage recruitment and adipose tissue inflammation in obesity. *Nature medicine*, *15*(8), 914–920.

Nisoli, E., Tonello, C., Benarese, M., Liberini, P., & Carruba, M. (1996). Expression of nerve growth factor in brown adipose tissue: implications for thermogenesis and obesity. *Endocrinology*, *137*(2), 495–503.

Nunes, S., Maijub, J., Krishnan, L., Ramakrishnan, V., Clayton, L., Williams, S., ... Boyd, N. (2013). Generation of a functional liver tissue mimic using adipose stromal vascular fraction cell-derived vasculatures. *Scientific reports*, *3*(1), 2141.

Oguri, Y., Shinoda, K., Kim, H., Alba, D. L., Bolus, W. R., Wang, Q., ... others (2020). Cd81 controls beige fat progenitor cell growth and energy balance via fak signaling. *Cell*, *182*(3), 563–577.

Oldfield, B. J., Giles, M., Watson, A., Anderson, C., Colvill, L., & McKinley, M. J. (2002). The neurochemical characterisation of hypothalamic pathways projecting polysynaptically to brown adipose tissue in the rat. *Neuroscience*, *110*(3), 515–526.

Onogi, Y., Wada, T., Kamiya, C., Inata, K., Matsuzawa, T., Inaba, Y., ... others (2017). Pdgfrβ regulates adipose tissue expansion and glucose metabolism via vascular remodeling in diet-induced obesity. *Diabetes*, *66*(4), 1008–

1021.

Paik, S., Kim, J. K., Silwal, P., Sasakawa, C., & Jo, E.-K. (2021). An update on the regulatory mechanisms of nlrp3 inflammasome activation. *Cellular & molecular immunology*, *18*(5), 1141–1160.

Park, C., Kim, J., Ko, S.-B., Choi, Y. K., Jeong, H., Woo, H., ... others (2022). Structural basis of neuropeptide y signaling through y1 receptor. *Nature communications*, *13*(1), 853.

Parker-Duffen, J. L., Nakamura, K., Silver, M., Kikuchi, R., Tigges, U., Yoshida, S., ... Walsh, K. (2013). T-cadherin is essential for adiponectin-mediated revascularization. *Journal of Biological Chemistry*, *288*(34), 24886–24897.

Parlee, S. D., Lentz, S. I., Mori, H., & MacDougald, O. A. (2014). Quantifying size and number of adipocytes in adipose tissue. In *Methods in enzymology* (Vol. 537, pp. 93–122). Elsevier.

Pedrazzini, T., Seydoux, J., Künstner, P., Aubert, J.-F., Grouzmann, E., Beermann, F., & Brunner, H. R. (1998). Cardiovascular response, feeding behavior and locomotor activity in mice lacking the npy y1 receptor. *Nature medicine*, *4*(6), 722–726.

Pellieux, C., Sauthier, T., Domenighetti, A., Marsh, D. J., Palmiter, R. D., Brunner, H.-R., & Pedrazzini, T. (2000). Neuropeptide y (npy) potentiates phenylephrine-induced mitogen-activated protein kinase activation in primary cardiomyocytes via npy y5 receptors. *Proceedings of the National Academy of Sciences*, *97*(4), 1595–1600.

Pirzgalska, R. M., Seixas, E., Seidman, J. S., Link, V. M., Sánchez, N. M., Mahú, I., ... others (2017). Sympathetic neuron–associated macrophages contribute to obesity by importing and metabolizing norepinephrine. *Nature medicine*, *23*(11), 1309–1318.

Pons, J., Kitlinska, J., Jacques, D., Perreault, C., Nader, M., Everhart, L., ...

Zukowska, Z. (2008). Interactions of multiple signaling pathways in neuropeptide y-mediated bimodal vascular smooth muscle cell growth. *Canadian journal of physiology and pharmacology*, *86*(7), 438–448.

Rana, B. M., Jou, E., Barlow, J. L., Rodriguez-Rodriguez, N., Walker, J. A., Knox, C., ... others (2019). A stromal cell niche sustains ilc2-mediated type-2 conditioning in adipose tissue. *Journal of Experimental Medicine*, *216*(9), 1999–2009.

Rehman, S., & Dimri, M. (2018). Biochemistry, g protein coupled receptors.

Renier, N., Wu, Z., Simon, D. J., Yang, J., Ariel, P., & Tessier-Lavigne, M. (2014). idisco: a simple, rapid method to immunolabel large tissue samples for volume imaging. *Cell*, *159*(4), 896–910.

Renshaw, D., & Hinson, J. (2001). Neuropeptide y and the adrenal gland: a review. *Peptides*, *22*(3), 429–438.

Ricard, N., Bailly, S., Guignabert, C., & Simons, M. (2021). The quiescent endothelium: signalling pathways regulating organ-specific endothelial normalcy. *Nature Reviews Cardiology*, *18*(8), 565–580.

Rocha, V. Z., Folco, E. J., Sukhova, G., Shimizu, K., Gotsman, I., Vernon, A. H., & Libby, P. (2008). Interferon-γ, a th1 cytokine, regulates fat inflammation: a role for adaptive immunity in obesity. *Circulation research*, *103*(5), 467–476.

Romano, M., Fanelli, G., Tan, N., Nova-Lamperti, E., McGregor, R., Lechler, R. I., ... Scottà, C. (2018). Expanded regulatory t cells induce alternatively activated monocytes with a reduced capacity to expand t helper-17 cells. *Frontiers in immunology*, *9*, 1625.

Ronaldson, P. T., DeMarco, K. M., Sanchez-Covarrubias, L., Solinsky, C. M., & Davis, T. P. (2009). Transforming growth factor-β signaling alters substrate permeability and tight junction protein expression at the blood-brain barrier

during inflammatory pain. *Journal of Cerebral Blood Flow & Metabolism*, *29*(6), 1084–1098.

Rose, S., Frye, R. E., Slattery, J., Wynne, R., Tippett, M., Pavliv, O., ... James, S. J. (2014). Oxidative stress induces mitochondrial dysfunction in a subset of autism lymphoblastoid cell lines in a well-matched case control cohort. *PloS one*, *9*(1), e85436.

Rosen, E. D., Hsu, C.-H., Wang, X., Sakai, S., Freeman, M. W., Gonzalez, F. J., & Spiegelman, B. M. (2002). C/ebpα induces adipogenesis through pparγ: a unified pathway. *Genes & development*, *16*(1), 22–26.

Rosen, E. D., Sarraf, P., Troy, A. E., Bradwin, G., Moore, K., Milstone, D. S., ... Mortensen, R. M. (1999). Pparγ is required for the differentiation of adipose tissue in vivo and in vitro. *Molecular cell*, *4*(4), 611–617.

Rosmaninho-Salgado, J., Cortez, V., Estrada, M., Santana, M. M., Gonçalves, A., Marques, A. P., & Cavadas, C. (2012). Intracellular mechanisms coupled to npy y2 and y5 receptor activation and lipid accumulation in murine adipocytes. *Neuropeptides*, *46*(6), 359–366.

Sakers, A., De Siqueira, M. K., Seale, P., & Villanueva, C. J. (2022). Adipose-tissue plasticity in health and disease. *Cell*, *185*(3), 419–446.

Sanders, M. A., Madoux, F., Mladenovic, L., Zhang, H., Ye, X., Angrish, M., ... others (2015). Endogenous and synthetic abhd5 ligands regulate abhd5-perilipin interactions and lipolysis in fat and muscle. *Cell metabolism*, *22*(5), 851–860.

Sárvári, A. K., Van Hauwaert, E. L., Markussen, L. K., Gammelmark, E., Marcher, A.-B., Ebbesen, M. F., ... Mandrup, S. (2021). Plasticity of epididymal adipose tissue in response to diet-induced obesity at single-nucleus resolution. *Cell metabolism*, *33*(2), 437–453.

Sato, Y., & Rifkin, D. B. (1989). Inhibition of endothelial cell movement by per-

icytes and smooth muscle cells: activation of a latent transforming growth factor-beta 1-like molecule by plasmin during co-culture. *The Journal of cell biology*, *109*(1), 309–315.

Schindelin, J., Arganda-Carreras, I., Frise, E., Kaynig, V., Longair, M., Pietzsch, T., ... others (2012). Fiji: an open-source platform for biological-image analysis. *Nature methods*, *9*(7), 676–682.

Schoonjans, K., Peinado-Onsurbe, J., Lefebvre, A.-M., Heyman, R. A., Briggs, M., Deeb, S., ... Auwerx, J. (1996). Pparalpha and ppargamma activators direct a distinct tissue-specific transcriptional response via a ppre in the lipoprotein lipase gene. *The EMBO journal*, *15*(19), 5336–5348.

Schulz, C., Perdiguero, E. G., Chorro, L., Szabo-Rogers, H., Cagnard, N., Kierdorf, K., ... others (2012). A lineage of myeloid cells independent of myb and hematopoietic stem cells. *Science*, *336*(6077), 86–90.

Schupp, M., & Lazar, M. A. (2010). Endogenous ligands for nuclear receptors: digging deeper. *Journal of Biological Chemistry*, *285*(52), 40409–40415.

Scott-Solomon, E., Boehm, E., & Kuruvilla, R. (2021). The sympathetic nervous system in development and disease. *Nature Reviews Neuroscience*, *22*(11), 685–702.

Seale, P., Bjork, B., Yang, W., Kajimura, S., Chin, S., Kuang, S., ... others (2008). Prdm16 controls a brown fat/skeletal muscle switch. *Nature*, *454*(7207), 961–967.

Shamsi, F., Piper, M., Ho, L.-L., Huang, T. L., Gupta, A., Streets, A., ... Tseng, Y.-H. (2021). Vascular smooth muscle-derived trpv1+ progenitors are a source of cold-induced thermogenic adipocytes [Journal Article]. *Nature metabolism*, *3*(4), 485-495.

Shapira, S. N., & Seale, P. (2019). Transcriptional control of brown and beige fat development and function. *Obesity*, *27*(1), 13–21.

Sheppard, D. (2006). Transforming growth factor β: a central modulator of pulmonary and airway inflammation and fibrosis. *Proceedings of the American Thoracic Society*, *3*(5), 413–417.

Shi, Y.-C., Lau, J., Lin, Z., Zhang, H., Zhai, L., Sperk, G., ... others (2013). Arcuate npy controls sympathetic output and bat function via a relay of tyrosine hydroxylase neurons in the pvn. *Cell metabolism*, *17*(2), 236–248.

Shields Jr, R. W. (1993). Functional anatomy of the autonomic nervous system. *Journal of clinical neurophysiology: official publication of the American Electroencephalographic Society*, *10*(1), 2–13.

Shimada, K., Ohno, Y., Okamatsu-Ogura, Y., Suzuki, M., Kamikawa, A., Terao, A., & Kimura, K. (2012). Neuropeptide y activates phosphorylation of erk and stat3 in stromal vascular cells from brown adipose tissue, but fails to affect thermogenic function of brown adipocytes. *Peptides*, *34*(2), 336–342.

Shimizu, I., Aprahamian, T., Kikuchi, R., Shimizu, A., Papanicolaou, K. N., MacLauchlan, S., ... others (2014). Vascular rarefaction mediates whitening of brown fat in obesity. *The Journal of clinical investigation*, *124*(5), 2099–2112.

Singer, K., Morris, D. L., Oatmen, K. E., Wang, T., DelProposto, J., Mergian, T., ... Lumeng, C. N. (2013). Neuropeptide y is produced by adipose tissue macrophages and regulates obesity-induced inflammation. *PloS one*, *8*(3), e57929.

Singhmar, P., Trinh, R. T. P., Ma, J., Huo, X., Peng, B., Heijnen, C. J., & Kavelaars, A. (2020). The fibroblast-derived protein pi16 controls neuropathic pain. *Proceedings of the National Academy of Sciences*, *117*(10), 5463–5471.

Sinha, S., Hoofnagle, M. H., Kingston, P. A., McCanna, M. E., & Owens, G. K.

(2004). Transforming growth factor-β1 signaling contributes to development of smooth muscle cells from embryonic stem cells. *American Journal of Physiology-Cell Physiology*, *287*(6), C1560–C1568.

Smas, C. M., Chen, L., Zhao, L., Latasa, M.-J., & Sul, H. S. (1999). Transcriptional repression of pref-1by glucocorticoids promotes 3t3-l1 adipocyte differentiation. *Journal of Biological Chemistry*, *274*(18), 12632–12641.

Spadoni, I., Zagato, E., Bertocchi, A., Paolinelli, R., Hot, E., Di Sabatino, A., ... others (2015). A gut-vascular barrier controls the systemic dissemination of bacteria. *Science*, *350*(6262), 830–834.

Stanford, K. I., Middelbeek, R. J., Townsend, K. L., An, D., Nygaard, E. B., Hitchcox, K. M., ... others (2012). Brown adipose tissue regulates glucose homeostasis and insulin sensitivity. *The Journal of clinical investigation*, *123*(1).

Stolarczyk, E., Vong, C. T., Perucha, E., Jackson, I., Cawthorne, M. A., Wargent, E. T., ... Howard, J. K. (2013). Improved insulin sensitivity despite increased visceral adiposity in mice deficient for the immune cell transcription factor t-bet. *Cell metabolism*, *17*(4), 520–533.

Sullivan, T., Rapp, M., Fan, X., Walzer, T., Dannenberg, A., Sun, J., ... others (2016). Adipose-resident group 1 innate lymphoid cells promote obesity-associated insulin resistance article adipose-resident group 1 innate lymphoid cells promote obesity-associated insulin resistance. *Immunity*, *45*, 428–441.

Sun, K., Asterholm, I. W., Kusminski, C. M., Bueno, A. C., Wang, Z. V., Pollard, J. W., ... Scherer, P. E. (2012). Dichotomous effects of vegf-a on adipose tissue dysfunction. *Proceedings of the national academy of sciences*, *109*(15), 5874–5879.

Sun, W., Dong, H., Balaz, M., Slyper, M., Drokhlyansky, E., Colleluori, G., ...

others (2020). snrna-seq reveals a subpopulation of adipocytes that regulates thermogenesis. *Nature*, *587*(7832), 98–102.

Sundberg, C., Kowanetz, M., Brown, L. F., Detmar, M., & Dvorak, H. F. (2002). Stable expression of angiopoietin-1 and other markers by cultured pericytes: phenotypic similarities to a subpopulation of cells in maturing vessels during later stages of angiogenesis in vivo. *Laboratory investigation*, *82*(4), 387–401.

Sung, H.-K., Doh, K.-O., Son, J. E., Park, J. G., Bae, Y., Choi, S., ... others (2013). Adipose vascular endothelial growth factor regulates metabolic homeostasis through angiogenesis. *Cell metabolism*, *17*(1), 61–72.

Syrovatkina, V., Alegre, K. O., Dey, R., & Huang, X.-Y. (2016). Regulation, signaling, and physiological functions of g-proteins. *Journal of molecular biology*, *428*(19), 3850–3868.

Sztalryd, C., Xu, G., Dorward, H., Tansey, J. T., Contreras, J. A., Kimmel, A. R., & Londos, C. (2003). Perilipin a is essential for the translocation of hormone-sensitive lipase during lipolytic activation. *The Journal of cell biology*, *161*(6), 1093–1103.

Tang, L., Shi, J., Yu, M., Shan, Y., Zhao, J., & Sheng, M. (2022). Isolation and characterization of peritoneal microvascular pericytes. *FEBS Open Bio*, *12*(4), 784–797.

Torres, G., Bitran, M., & Huidobro-Toro, J. P. (1992). Co-release of neuropeptide y (npy) and noradrenaline from the sympathetic nerve terminals supplying the rat vas deferens; influence of calcium and the stimulation intensity. *Neuroscience letters*, *148*(1-2), 39–42.

Uemura, M. T., Maki, T., Ihara, M., Lee, V. M., & Trojanowski, J. Q. (2020). Brain microvascular pericytes in vascular cognitive impairment and dementia. *Frontiers in aging neuroscience*, *12*, 80.

Vaiopoulos, A. G., Marinou, K., Christodoulides, C., & Koutsilieris, M. (2012). The role of adiponectin in human vascular physiology. *International journal of cardiology*, *155*(2), 188–193.

Valladares, A., Roncero, C., Benito, M., & Porras, A. (2001). Tnf-α inhibits ucp-1 expression in brown adipocytes via erks: opposite effect of p38mapk. *FEBS letters*, *493*(1), 6–11.

Vivier, E., Artis, D., Colonna, M., Diefenbach, A., Di Santo, J. P., Eberl, G., ... others (2018). Innate lymphoid cells: 10 years on. *Cell*, *174*(5), 1054–1066.

Wahlestedt, C., Yanaihara, N., & Håkanson, R. (1986). Evidence for different pre-and post-junctional receptors for neuropeptide y and related peptides. *Regulatory peptides*, *13*(3-4), 307–318.

Wang, H., Qian, T., Zhao, Y., Zhuo, Y., Wu, C., Osakada, T., ... others (2023). A tool kit of highly selective and sensitive genetically encoded neuropeptide sensors. *Science*, *382*(6672), eabq8173.

Wang, H. U., Chen, Z.-F., & Anderson, D. J. (1998). Molecular distinction and angiogenic interaction between embryonic arteries and veins revealed by ephrin-b2 and its receptor eph-b4. *Cell*, *93*(5), 741–753.

Wang, P., Loh, K. H., Wu, M., Morgan, D. A., Schneeberger, M., Yu, X., ... others (2020). A leptin–bdnf pathway regulating sympathetic innervation of adipose tissue. *Nature*, *583*(7818), 839–844.

Wang, Q. A., Tao, C., Gupta, R. K., & Scherer, P. E. (2013). Tracking adipogenesis during white adipose tissue development, expansion and regeneration. *Nature medicine*, *19*(10), 1338–1344.

Wang, Y., Leung, V. H., Zhang, Y., Nudell, V. S., Loud, M., Servin-Vences, M. R., ... others (2022). The role of somatosensory innervation of adipose tissues. *Nature*, *609*(7927), 569–574.

Wee, N. K., Sinder, B. P., Novak, S., Wang, X., Stoddard, C., Matthews, B. G., & Kalajzic, I. (2019). Skeletal phenotype of the neuropeptide y knockout mouse. *Neuropeptides*, *73*, 78–88.

Weisberg, S. P., McCann, D., Desai, M., Rosenbaum, M., Leibel, R. L., Ferrante, A. W., et al. (2003). Obesity is associated with macrophage accumulation in adipose tissue. *The Journal of clinical investigation*, *112*(12), 1796–1808.

Wu, D., Molofsky, A. B., Liang, H.-E., Ricardo-Gonzalez, R. R., Jouihan, H. A., Bando, J. K., ... Locksley, R. M. (2011). Eosinophils sustain adipose alternatively activated macrophages associated with glucose homeostasis. *Science*, *332*(6026), 243–247.

Xu, H., Barnes, G. T., Yang, Q., Tan, G., Yang, D., Chou, C. J., ... others (2003). Chronic inflammation in fat plays a crucial role in the development of obesity-related insulin resistance. *The Journal of clinical investigation*, *112*(12), 1821–1830.

Yan, C., Zeng, T., Lee, K., Nobis, M., Loh, K., Gou, L., ... others (2021). Peripheral-specific y1 receptor antagonism increases thermogenesis and protects against diet-induced obesity. *Nature communications*, *12*(1), 2622.

Yang, K., Guan, H., Arany, E., Hill, D. J., & Cao, X. (2008). Neuropeptide y is produced in visceral adipose tissue and promotes proliferation of adipocyte precursor cells via the y1 receptor. *The FASEB Journal*, *22*(7), 2452–2464.

Yu, J., Xiao, K., Chen, X., Deng, L., Zhang, L., Li, Y., ... others (2022). Neuron-derived neuropeptide y fine-tunes the splenic immune responses. *Neuron*, *110*(8), 1327–1339.

Zeng, H., He, X., Tuo, Q.-h., Liao, D.-f., Zhang, G.-q., & Chen, J.-x. (2016). Lps causes pericyte loss and microvascular dysfunction via disruption of sirt3/angiopoietins/tie-2 and hif-2α/notch3 pathways. *Scientific reports*, *6*(1), 20931.

Zeng, W., Pirzgalska, R. M., Pereira, M. M., Kubasova, N., Barateiro, A., Seixas, E., ... others (2015). Sympathetic neuro-adipose connections mediate leptin-driven lipolysis. *Cell*, *163*(1), 84–94.

Zeng, X., Ye, M., Resch, J. M., Jedrychowski, M. P., Hu, B., Lowell, B. B., ... Spiegelman, B. M. (2019). Innervation of thermogenic adipose tissue via a calsyntenin 3β–s100b axis. *Nature*, *569*(7755), 229–235.

Zhang, P., He, Y., Wu, S., Li, X., Lin, X., Gan, M., ... others (2022). Factors associated with white fat browning: New regulators of lipid metabolism. *International Journal of Molecular Sciences*, *23*(14), 7641.

Zhang, W., & Liu, H. T. (2002). Mapk signal pathways in the regulation of cell proliferation in mammalian cells. *Cell research*, *12*(1), 9–18.

Zhang, X., & van den Pol, A. N. (2016). Hypothalamic arcuate nucleus tyrosine hydroxylase neurons play orexigenic role in energy homeostasis. *Nature neuroscience*, *19*(10), 1341–1347.

Zhang, Y., Proenca, R., Maffei, M., Barone, M., Leopold, L., & Friedman, J. M. (1994). Positional cloning of the mouse obese gene and its human homologue. *Nature*, *372*(6505), 425–432.

Zhou, Y., Yu, X., Chen, H., Sjöberg, S., Roux, J., Zhang, L., ... others (2015). Leptin deficiency shifts mast cells toward anti-inflammatory actions and protects mice from obesity and diabetes by polarizing m2 macrophages. *Cell metabolism*, *22*(6), 1045–1058.

Zhu, L., Vranckx, R., Van Kien, P. K., Lalande, A., Boisset, N., Mathieu, F., ... others (2006). Mutations in myosin heavy chain 11 cause a syndrome associating thoracic aortic aneurysm/aortic dissection and patent ductus arteriosus. *Nature genetics*, *38*(3), 343–349.

Zhu, Y., Yao, L., Gallo-Ferraz, A. L., Bombassaro, B., Simões, M. R., Abe, I., ... others (2024). Sympathetic neuropeptide y protects from obesity by

sustaining thermogenic fat. *Nature*, 1–8.